**Master of Science Thesis** **October 16, 2020**

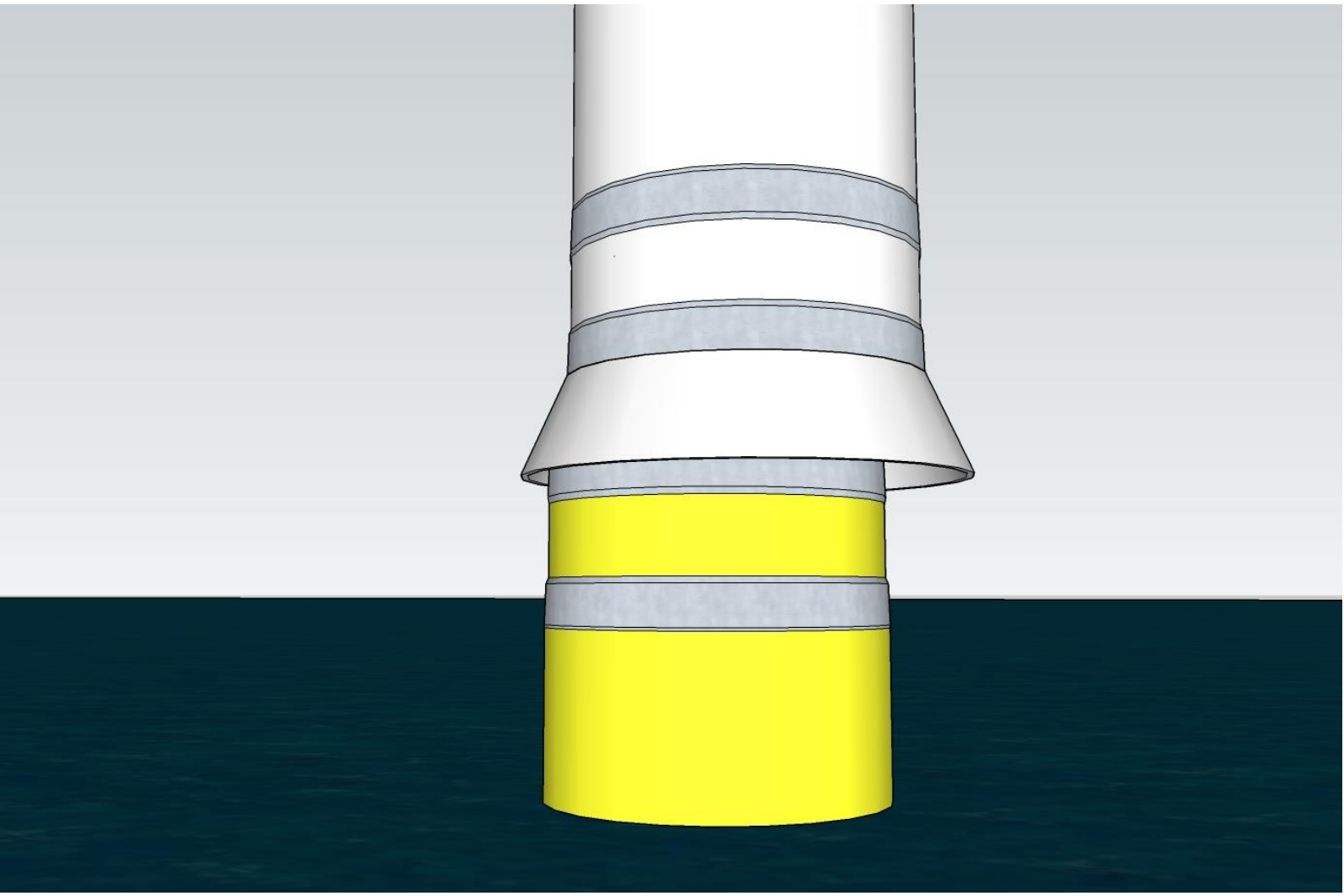

# Limits of Offshore Wind Turbine Installation with the Double Slip Joint

Offshore WTG Tower Lowering and Mating with a Double Slip Joint Connection Using Catchers and Tower Guidance. A Determination of Installation Limits and Exploration of Workability

Maarten van den Berg

KCI THE ENGINEERS.

TU Delft Delft University of Technology

# Limits of Offshore Wind Turbine Installation with the Double Slip Joint

*Offshore WTG Tower Lowering and Mating with a Double Slip Joint Connection Using Catchers and Tower Guidance. A Determination of Installation Limits and Exploration of Workability*

Master of Science Thesis

For obtaining the degree of Master of Science in

Offshore & Dredging Engineering at Delft University of Technology

Maarten van den Berg

October 16, 2020


| | | |
|---|---|---|
| Student number: | 4383389 | TU Delft |
| Supervision: | Prof. dr. A.V. Metrikine | TU Delft |
| | Dr. ir. B.C. Ummels | TU Delft |
| | Ir. K.B. van Gelder | KCI The Engineers |

# Acknowledgements

Put simply, performing this research was awesome and I was surrounded by great people. I therefore wish to express my deepest appreciation to the members of my graduation committee.

I am very thankful for the great support and guidance of the chairman of my graduation committee, Prof. dr. A.V. Metrikine. During the research, I received guidance that pushed the research to the next level, and I am thankful for the questions that sometimes served as a 'major diner plates' of food for thought.

I also heartfully thank Dr. ir. B.C. Ummels for his dedicated and truly passionate guidance and support. A deep understanding of scientific research and a professional, yet personal approach really helped along the 'graduation way', which sometimes was a 'rocky ride'.

I would like to thank ir. K.B. van Gelder very much for his thorough, professional, and reliable support and guidance. 'Team Double Slip Joint' was an absolute success and together, in our Covid-19 driven online meetings, the most interesting findings and creative ideas surfaced that really bolstered this research. Furthermore, I wish to thank KCI The Engineers in general for providing me the opportunity to perform this Double Slip Joint research project.

Last but not least, I hereby thank my family, girlfriend, and other relatives for their support. You were, are and will be great!

# Abstract

In current offshore wind turbine (WTG) tower installations, bolted flange connections are common. These connections are however reaching their limit due to the maximized size of the bolts. Also, bolted connections require the motions between the tower and foundation to be limited during installation, suggesting their workability of installation is low. The Double Slip Joint is a promising and innovative connection between a WTG tower and the support structure, which may remove or reduce these limitations. This research explores the motion and collision limits for WTG tower installation on a monopile (MP) foundation and focuses on the lowering and mating using two types guiding structures, or catchers: the vertical asymmetric catcher and the conical catcher. A first exploration of installation workability is provided as well.

A model is developed that simulates the lowering and catcher mating of a WTG tower with a MP. This model includes physical phenomena that affect the motion and collision behavior of the WTG tower. Specific attention is paid to collisions between the catcher and the MP. With the use of finite element analysis, a stiffening non-linearity is observed in the lumped contact element to describe collisions. It is found to be caused by the local deformation of the mating elements.

Furthermore, the simulation model calculates 3 degree of freedom in-plane motions numerically of the WTG tower in the time domain using Euler integration. Besides the aforementioned stiffening non-linearity in collisions, other important model features are a time and spatially variable wind load, aerodynamic damping, harmonic horizontal and vertical crane tip motions, crane operator induced crane tip motions and lifting line stiffness and damping characteristics.

The model simulates the WTG tower lowering and catcher mating and to determine the installation limits, installation requirements have been defined, aimed at preventing critical events. To be specific, installation requirements aim to prevent slack wires, axial impact, and plastic deformation of the catcher due to contact with the MP. It is also required that the side-lead angle (i.e. the lifting line angle with respect to the vertical) remains below a maximum allowable value.

Model simulations are performed for both jack-up and floating installation vessel crane tip excitation characteristics. This research indicates that in both cases, the conical catcher yields higher allowable wind velocities than the vertical asymmetric catcher during installation. This is supported by the findings that the conical catcher has higher allowable contact forces, requires less or no crane operator action during catcher mating and the side-lead angle varies less than with the vertical asymmetric catcher. Another important observation is that the installation limits are often reached through installation requirements related to the motions and collisions of the mating elements. This study shows that applying linear damping to the horizontal WTG tower bottom motions, achievable by (active) tugger winches, the allowable mean wind velocity in installation is increased and this research suggests that the workability of installation increases consequently.

The focus in this study is on motion and collision limits in installation as well as on installation requirements. It is recommended for future research to focus on workability and to analyze the entire system consisting of vessel, load, and foundation. As such, wind and waves are considered separately as a source of excitation and vessel-load interaction is incorporated. For 3D analyses, it is recommended to study the control of out-of-plane WTG tower bottom motions and potential inclined collision responses between the catcher and foundation.

# Contents

# List of Tables

# List of Figures

# Nomenclature

## Abbreviations

| *Abbreviation* | *Definition* | *Explanation* |
|---|---|---|
| *AHC* | Active heave compensation | |
| *DOF* | Degree of freedom | |
| *DP* | Dynamic positioning | |
| *DSJ* | Double Slip Joint | |
| *EB* | Euler-Bernoulli | |
| *FD* | Frequency domain | |
| *MP* | Monopile | |
| *OWT(s)* | Offshore Wind Turbine(s) | |
| *PHC* | Passive heave compensation | |
| *RAO* | Response amplitude operator | |
| *SWL* | Still water level | |
| *TD* | Time domain | |
| *TLP* | Tension leg platform | |
| *TP* | Transition piece | |
| *TRL* | Technical Readiness Level | |
| *TSPC* | Tri-suction Pile Caisson | |
| *ULS* | Ultimate Limit State | |
| *WTG(s)* | Wind turbine generator(s) | |

## List of Greek symbols

| *Symbol* | *Unit* | *Explanation* |
|---|---|---|
| $\alpha$ | rad | WTG tower angle to the vertical |
| $\dot{\alpha}$ | rad/s | Time derivative of WTG tower angle to the vertical |
| $\alpha_j$ | - | Phillips Constant in the Jonswap Spectrum |
| $\gamma^r$ | - | Peak enhancement factor in the Jonswap Spectrum |
| $\delta$ | - | Logarithmic decrement |
| $\zeta$ | - | Dimensionless damping |
| $\zeta_a$ | m | Incoming wave amplitude |
| $\Theta$ | rad | Vessel pitch angle |
| $\nu$ | $m^2/s$ | Kinematic viscosity |
| $\pi_i$ | - | Dimensionless parameters from Buckingham Pi-theorem |

| | | |
|---|---|---|
| $\rho$ | kg/m$^3$ | Density |
| $\sigma$ | - | Spectral width parameter |
| $\tau$ | s | Gust wavelet period |
| $\Phi$ | rad | Vessel roll angle |
| $\Psi$ | rad | Vessel yaw angle |
| $\omega$ | rad/s | Frequency |
| $\omega_p$ | rad/s | Peak frequency |

# List of Latin symbols

| *Symbol* | *Unit* | *Explanation* |
|---|---|---|
| $A$ | m/s | Wind gust amplitude |
| $\boldsymbol{A}(\omega)$ | kg | Ship added mass matrix (frequency dependent) |
| $A_{eff}$ | m$^2$ | Effective area |
| $\boldsymbol{B}(\omega)$ | kg/s | Ship hydrodynamic damping matrix (frequency dependent) |
| $\boldsymbol{B_{DP}}(\omega)$ | kg/s | Ship DP hydrodynamic damping matrix (frequency dependent) |
| $b$ | kg/s | Damping coefficient |
| $b_{crit}$ | kg/s | Critical damping coefficient |
| $C_D$ | - | Drag coefficient |
| $\boldsymbol{C}$ | kg/s$^2$ | Ship hydrostatic stiffness matrix (frequency independent) |
| $\boldsymbol{C_{DP}}$ | kg/s$^2$ | Ship DP hydrostatic stiffness matrix (frequency independent) |
| $D(z)$ | m | WTG tower diameter as a function of height |
| $dA$ | m$^2$ | Differential of area |
| $dz$ | m | Differential of height |
| $E$ | N/m$^2$ | Young's modulus |
| $F_w$ | N/m | Wind force per unit length |
| $\vec{F}(\omega)$ | N/m | First-order wave excitation force amplitude vector |
| $g$ | m/s$^2$ | Gravitational acceleration |
| $H_{\frac{1}{3}}$ | m | Significant wave height |
| $H_{\frac{1}{3},fd}$ | m | Significant wave height in fully developed sea |
| $H_{10}$ | m | Height of 10 m above still water level |
| $H_{CoG}$ | m | Height of the WTG tower center of gravity |
| $I^S$ | - | Crane coordinate system |
| $I^E$ | - | Inertial coordinate system |
| $k$ | N/m | Axial wire stiffness |
| $L$ | m | Wire length |
| $\boldsymbol{M}$ | kg | Ship mass matrix |
| $m_n$ | - | n-th spectral moment of wave spectrum |
| $q$ | N/m$^2$ | Air pressure |
| $q_i$ | N/m$^2$ | Independent physical variables from Buckingham Pi-theorem |
| $S_j$ | m$^2$s/rad | Jonswap spectrum |
| $t$ | s | Time |
| $U_{10}$ | m/s | Wind velocity at height of 10 m above SWL |

| | | |
|---|---|---|
| $U(t,z)$ | m/s | Wind velocity as a function of time and height |
| $\bar{u}$ | m/s | Average wind speed without gusts |
| $u(t,z)$ | m/s | Relative wind velocity as a function of time and height |
| $u_f$ | m/s | Friction velocity |
| $x$ | m | WTG tower horizontal displacement |
| $\dot{x}$ | m/s | WTG tower horizontal velocity |
| $\overrightarrow{x_a}$ | m | Ship motion amplitude vector |
| $x_a$ | m | Ship surge amplitude |
| $\overrightarrow{x_E}$ | m | 3 DOF crane tip motion vector |
| $X$ | m | Distance from lee shore |
| $X_{fetch}$ | m | Distance from lee shore marking boundary between fetch-limited and fully developed seas |
| $y_a$ | m | Ship sway amplitude |
| $z$ | m | Height coordinate |
| $z_a$ | m | Ship heave coordinate |
| $z_0$ | m | Surface roughness |

# 1

# Introduction

Section 1.1 provides the background of the offshore wind energy market and technology. Besides, it will emphasize the need for innovation in offshore wind turbine generator (WTG) installations and how the Double Slip Joint connection is a promising technology for achieving this necessary innovation. The following section describes how this research contributes to the aforementioned innovation. The problem description, research objectives, methodology and research scope are provided.

## 1.1 Background

In this section, the demographics and economics of offshore wind are first briefly touched upon. The second subsection provides a technical overview of offshore wind turbine generators, followed by an overview of vessel types used for installing offshore wind turbine generators in the third subsection. Technical challenges that arise from current developments are explained and the necessity for innovation are consequently emphasized.

### 1.1.1 Demographics and economics of offshore wind energy

With a global push of scaling down $CO_2$ emissions, offshore wind energy appears to be a viable and low-cost opportunity to achieve the decarbonization agenda goals. 40% of the world population lives in regions within 100 km of the shoreline and therefore, offshore wind means energy independency and deployment opportunities for many countries. Besides, in contrary to their land-based counterparts, offshore wind turbines pose no noise or visual pollution. Offshore wind turbines therefore yield economic and social advantages as the impact of land-based turbines is considerable on local residents as found by [1]. This research shows that noise pollution reduces house prices up to 6.69% whereas visual pollution for the more distant turbines reduces house prices by up to 3.15%. It should be noted however that only if offshore wind farms are built at least 26 miles offshore, they do not negatively affect property values, according to [2] and [3].

Offshore wind also tends to be faster and steadier than on land according to the American Geosciences Institute. This therefore yields a more reliable source of electrical power than land-based wind power. One of the key disadvantages is that subsea power cables and foundation and installation costs of offshore wind turbine generators or WTG's is higher compared to land-based turbines according to the Bureau of Ocean Energy Management. In order to increase competitiveness and reduce costs, the offshore wind energy market is constantly innovating.

This innovation has already proven to yield remarkable results in terms of cost reduction and therefore competitiveness. The Department for Business, Energy and Industrial Strategy (BEIS) predicts that for the United Kingdom, offshore wind prices could be cheaper than gas plants as soon as 2023 and reach price parity with onshore wind going into 2024. This is visualized in Figure 1.

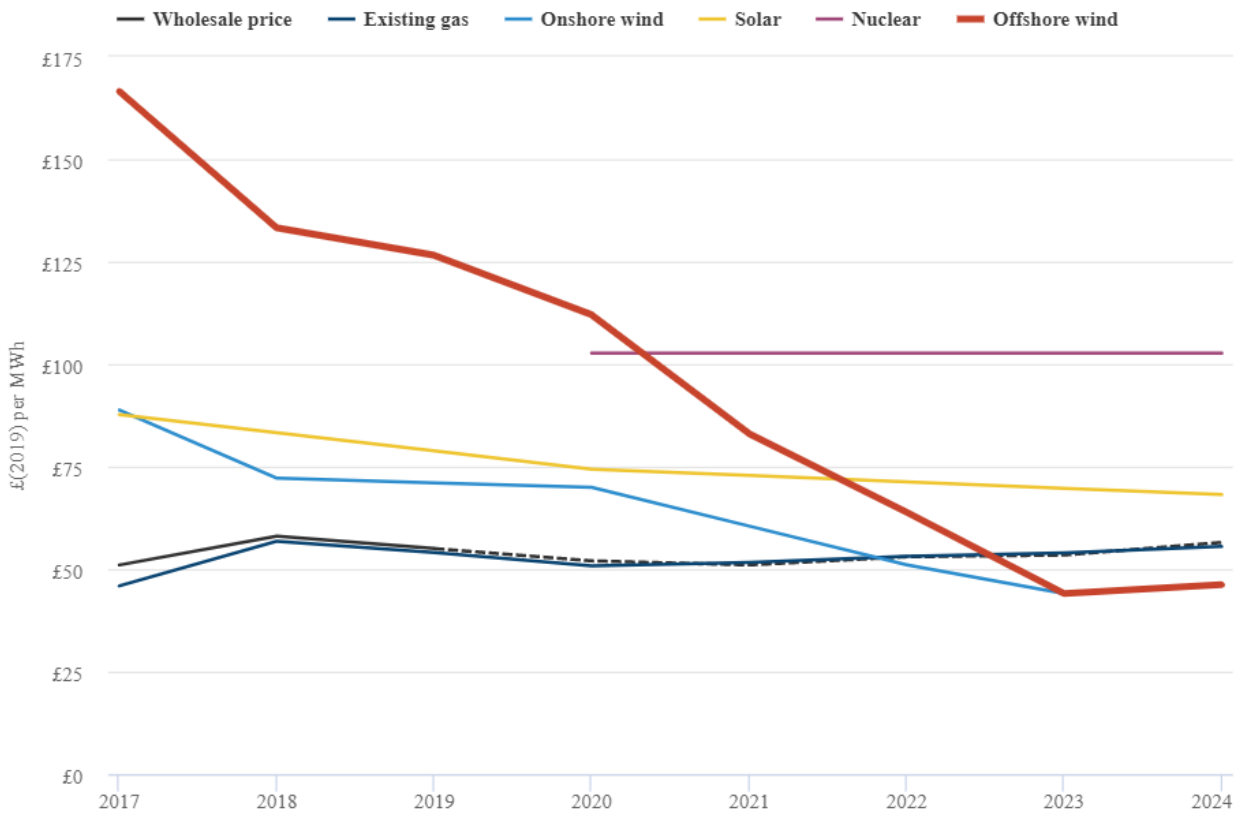


*Figure 1: Prices in Pound Sterling per MWh for various technologies in the UK (Source: BEIS)*

This promising economical trend is accompanied by a significant increase in global installed offshore wind energy capacity. This trend is widely expected to continue as [4] predicts a sevenfold increase of global installed offshore wind capacity by 2028. This is visualized in Figure 2.

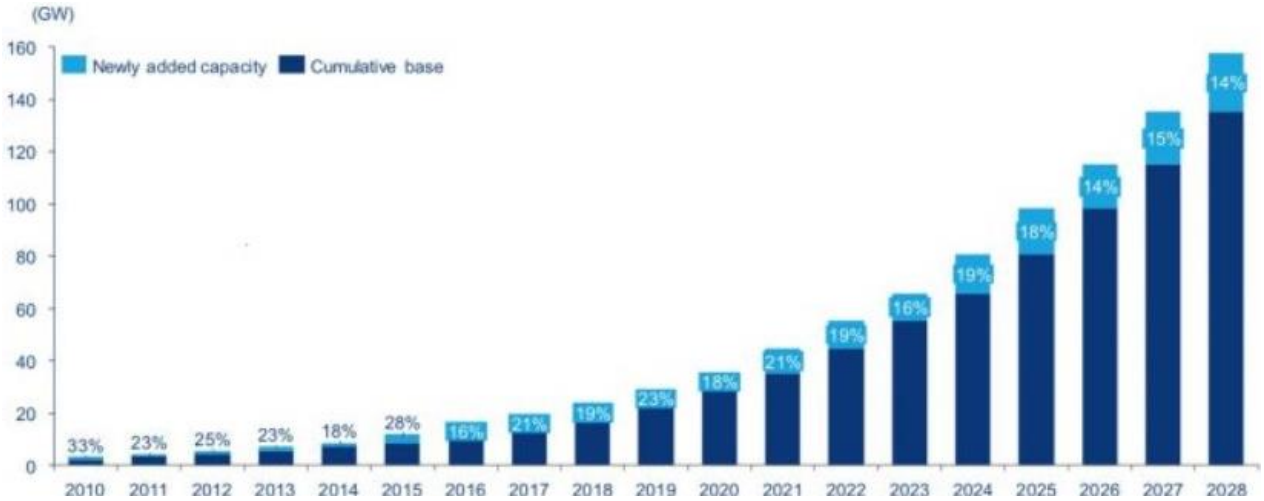


*Figure 2: Global offshore wind capacity (Source: Wood Mackenzie)*

### 1.1.2 Overview of offshore WTG support structure technology

Offshore wind turbines are either supported by a bottom-fixed or a floating support structure. The first and second paragraph of this subsection will provide an overview of both technologies respectively. The third paragraph explains the existing technologies regarding connections between the WTG tower and its support structure and the need for innovation in that field. The final paragraph introduces the Double Slip Joint or DSJ connection.

#### *1.1.2.1 Bottom fixed WTG support structures*

There are four main concepts of bottom fixed offshore wind turbine foundations, according to [5] and visualized in Figure 3. All concepts and their application are explained:

- The monopile or MP is the most commonly applied foundation and is basically a steel tube hammered or otherwise driven into the seabed. Dependent on design loads, water depth, soil conditions and environmental conditions, typically, 40% to 50% of the monopile length is embedded into the seabed [6]. A transition piece or TP is commonly used to connect the MP to the WTG. It is currently applied in water depths of up to 50m.
- A gravity-based foundation or GBF consists of a heavy concrete cone on the seabed with a cylinder on top extending above the sea level to support the WTG. [7] found that they are usually applied on high load-bearing capacity soils with water depths of up to 20 m. It should be noted however that the concept has not been applied since 2013.
- A tripod foundation for offshore wind turbines is fixed with piles through the foot the steel tripod-legs in the seabed as visualized in Figure 3. Initially, it was predicted that tripods would be applied for water depths between 25 and 50 m, according to [8]. However, as monopile technology impressively progressed over the last years, they now occupy these water depths and the tripod disappeared from the scene.
- A jacket structure consists of three or four main legs with K-, Z- or X- braces between the legs [9]. Steel piles are installed through the foots of the legs to fix the structure to the seabed. The structures are designed for a water depth of 30 – 60 m. After the monopile, the jacket structure is the most common support structure for offshore wind turbines in Europe as of 2017, according to WindEurope. However, with 315 units installed, this is a far cry of 3720 monopiles installed as of 2017.

Innovation has led to another foundation concept that gains momentum in the offshore wind energy market. Tri-suction Pile Caissons (TSPC) are currently being developed by SPT and KCI The Engineers. This foundation technology consists of three suction anchors with an MP in the middle. This foundation type allows for cheap installation, because it floats and can be towed to the installation site, where a small crane is needed for installation. It combines the low construction costs of an MP with the ability to be installed in deeper waters. It is therefore a cheaper alternative to the more expensive jacket foundations. Also, TSPC's allow for noise-free and vibration-free installation. This is a welcome feature as for monopile driving, it appears noises associated with this process are damaging to marine mammals, fish and invertebrates as shown by [10] and [11]. Although noise mitigation technology exists and is applied, the radius of responsiveness is still 12 km for marine mammals like seals and porpoises as found by [10] and [12]. Therefore, from an environmental perspective, there is a strong case for the Tri-suction Pile Caisson (TSPC). The Universal Foundation is another innovative foundation type that uses a clustered suction pile. This foundation technology consists of a pile with a single clustered suction bucket on the bottom. Both technologies are displayed in Figure 4.

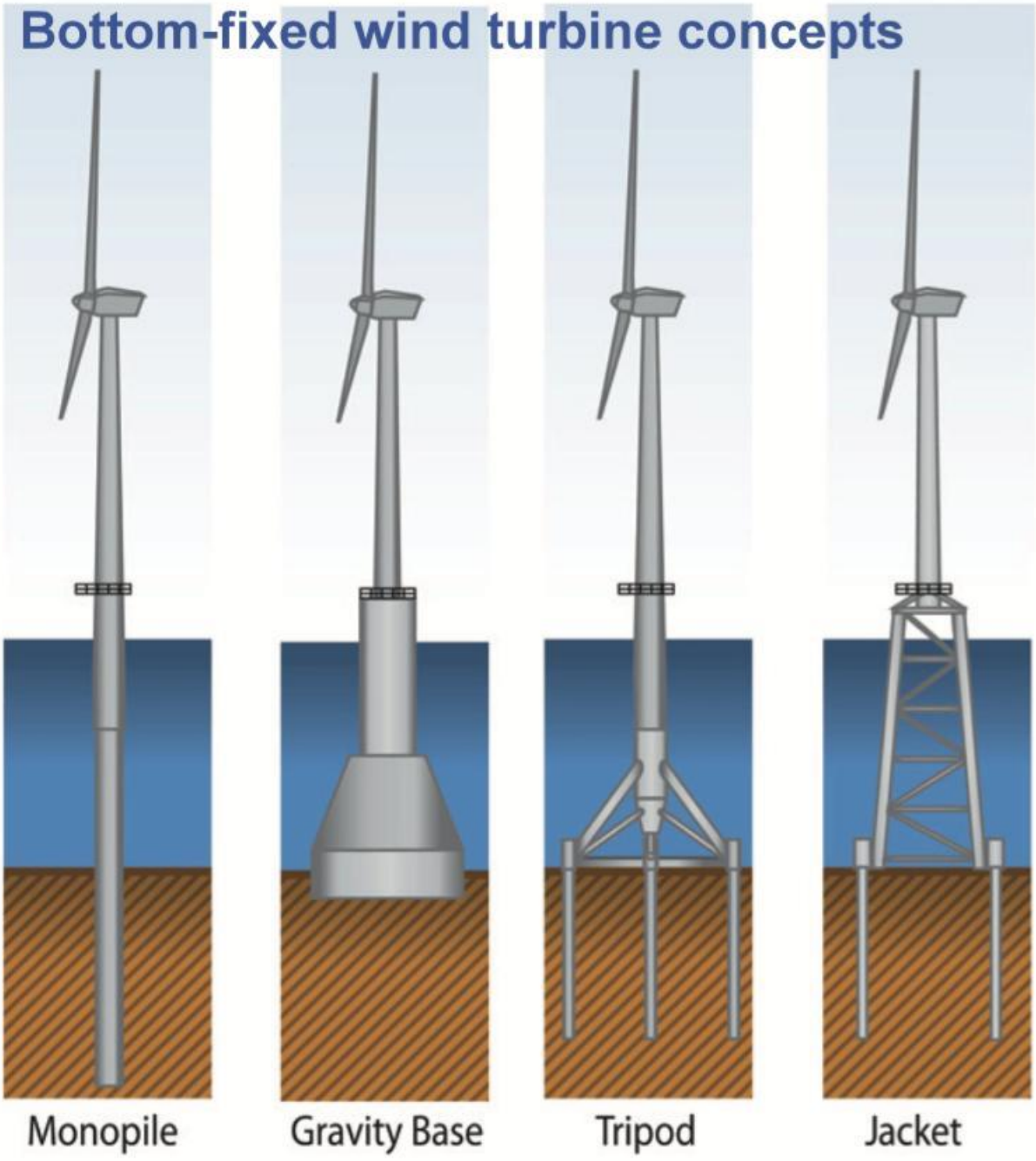


*Figure 3: Foundation types for bottom fixed offshore wind turbines (Source: Norwegian University of Science and Technology)*

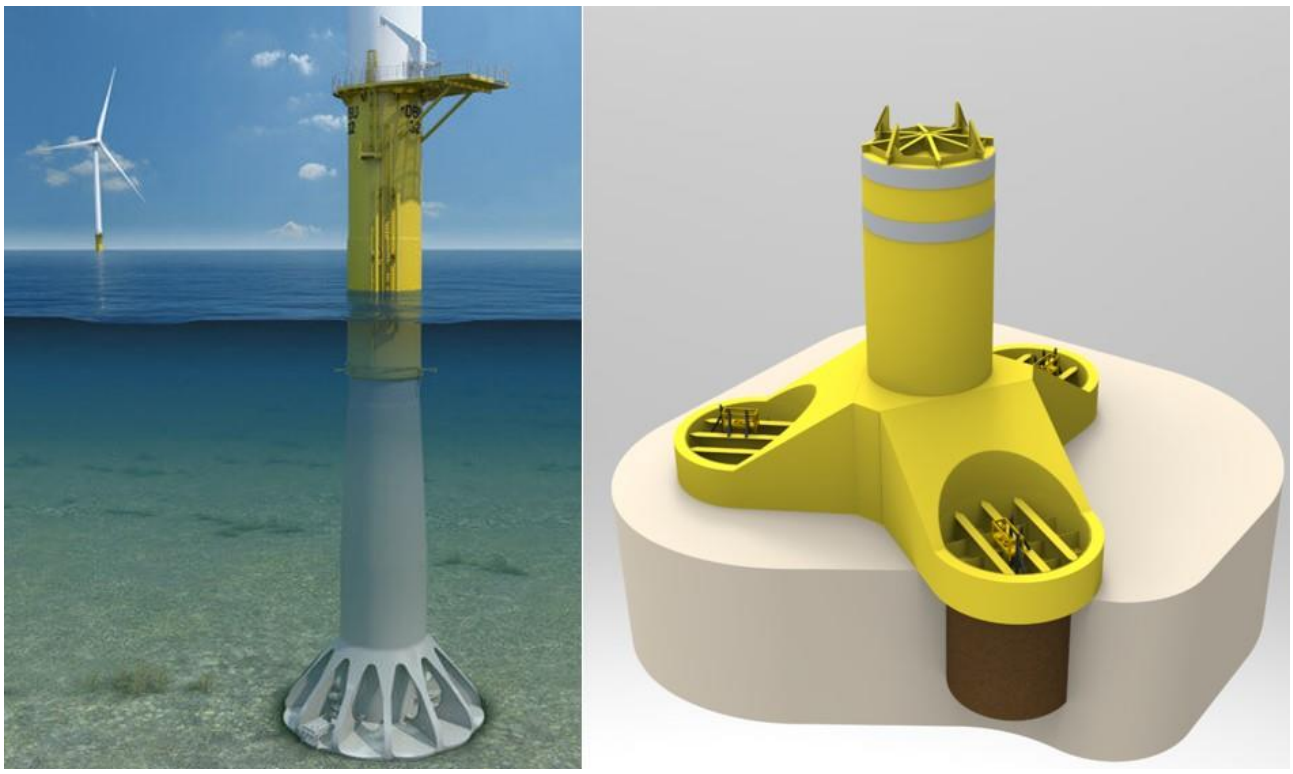

*Figure 4: Universal Foundation (left) with a monobucket in the soil (source: universalfoundation.com) and the Tri-suction Pile Caisson (right) with three suction buckets (source: SPT Offshore)*

The monopile foundation is clearly the most commonly applied foundation for bottom fixed WTGs. To this date, it outcompetes other foundation concepts and monopiles are placed in increasing water depths. However, research by [13] on the relationship between investment costs of wind farms and the corresponding water depth has shown an exponential increase in CAPEX with water depths for bottom fixed wind turbine foundations. From 50 m water depth and higher, floating wind becomes attractive financially.

#### *1.1.2.2 Floating WTG support structures*

There are three main floating WTG concepts in offshore floating wind, all of them being existing structures from the offshore floating oil and gas market. The three floating wind turbine concepts are the spar, the semi-submersible and the tension leg platform or TLP. Figure 5 depicts these three concepts on the left, middle and right respectively.

*Figure 5: Three main floating wind concepts (source: NREL, illustration by Josh Bauer)*

All three concepts attain their stability in different ways [14]. Below, these structures and their stability mechanisms are explained:

- The spar floating platform (left in Figure 5) is stable due to the ballasted submerged spar. The ballast in the bottom of the spar ensures a center of gravity below the center of buoyancy and therefore a strong stabilizing moment when the WTG is tilted out of its vertical orientation due to environmental loading. The mooring lines are meant for keeping the WTG in position in this concept and provide significant damping to the motions of the spar.
- The semi-submersible floater (middle in Figure 5) concept relies primarily on a large water plane area, ballasting and inertia for its stability. When the WTG pitches or gets tilted out of its vertical orientation, the part of the semi-submersible in the direction of the pitch is further submerged whereas the other side gets partly out of the water. This creates a buoyancy induced stabilizing moment to upright the WTG in its vertical orientation. Mooring lines are used for position keeping. Ballasting aims to reduce the effects of waves and swell as the mass increases together with the draft.
- The TLP or tension leg platform (right in Figure 5) relies on a totally different mechanism for stability. The relatively lightweight submerged structure is positively buoyant, meaning that the upward water pressure on the structure is higher than its own weight including the wind turbine weight. Mooring lines are attached to the legs of the TLP and provide the counteracting force against this positive buoyancy. The mooring lines are tensioned and pull the structure and the wind turbine generator in the vertical position and orientation.

Demographically, the potential for floating wind energy is great as the 66% of the total surface area of the planet consists of water with a depth of at least 200m and just 5% of water with a shallower depth, according to [15]. Also, some countries only have water depths of over 200m offshore and floating wind is their only option for harnessing offshore wind energy.

#### *1.1.2.3 Conventional connections between support structures and WTG and the need for innovation*

In the installation of an offshore WTG, the foundation is already in place and a connection, either with or without TP, has to be made. Conventional ways of making this connection is by either grouting or bolting. Both connections however have shown to have their limitations. For both types of connections an explanation is provided, and the corresponding limitations are shown.

- Grouted connections have been applied for decades in the oil and gas industry and were since 2002 widely applied in the first offshore wind turbines [16]. A cementitious grout is cast in the annulus between two structural elements, like for example an MP and TP. Due to the dynamic loading characteristics of a wind turbine and other effects, the axial capacity of the connection appeared insufficient [17]. This is supported by [18] who found that engineers have detected grouted connection failures since 2009 in 60% of the North Sea wind turbines. These turbines appeared to settle progressively over or into their foundations, with the grout wearing out progressively. Although catastrophe was avoided, effective solutions were provided. KCI the Engineers was one of the companies that provided an effective mitigation measure. However, grouted connections are nowadays no longer used in offshore wind as a stand-alone jointing solution. Based on its experiences with remedying grout connection issues, KCI developed the Double Slip Joint connection contributing to the industry's goal of both CAPEX and OPEX reduction. This technology is described in paragraph 1.1.2.4.
- Bolted connections on flanges also have weaknesses and are reaching their limits. [19] pointed out that most of the wind turbine collapses are caused by loose bolts. Apparently, some bolts loosen over time due to unproper installation (human error), or vibration induced wear in the bolts. For both grouted and bolted connections, safety monitoring during wind turbine operation is therefore required. It should be noted here that design limits for flanges and bolts are reached as bolted connections already involve the largest bolt size M72. Due to the increasing size of wind turbines, an increasing number of bolts is required to be used, increasing the tower diameter and/or requiring the use of the stronger T-flanges, which is undesirable offshore. This results in higher costs and risks,

and will possibly require expensive maintenance operations in case of bolts exposed to the offshore environment. Besides the technical shortcomings of bolted flange connections, they pose a significant safety hazard as well. Manpower is needed to fasten bolts immediately after landing the WTG on its support structure, meaning workers are present under a suspended load. Although potential solutions to the technical shortcomings are proposed, it still requires manpower to fasten the bolts. It is expensive both in terms of CAPEX and OPEX, time-consuming and still involves safety risks. Therefore, a connection that is maintenance free, does not require manpower and is immediately fastened would be a preferred solution both financially and from a safety hazard perspective.

Another significant shortcoming that both grouted and bolted connections face is that they are not immediately stable. Grout takes time to cure and bolts need to be fastened. Before that time, there is no stable connection. This limits the weather window for installation of a WTG as the critical event of a WTG tilting from its support structure due to environmental loadings has to be prevented. This is especially true for floating support structures. Floating support structures have far greater motions due to wave loads than bottom fixed structures and therefore a connection should be immediately stable.

One of the possible connections that does not require manpower to fasten and is immediately stable is the Slip Joint, which has in the past been applied in very small onshore wind turbines. [20] studied the connection and found that it is based on a geometrical fit, where the load transfer due to friction is low. Two coated steel conical sections with an angle of about 1° are put over each other form the connection. It is comparable to two inverted paper cups that are pushed together. The upper conical section is the bottom of the wind turbine and the lower conical section is the top of the support structure. A schematic representation of the conical sections is shown in Figure 6. The angle of the upper conical section is slightly smaller than the angle of the bottom conical section, resulting in the highest hoop stress at the bottom of the connection. With this connection type there is a reduction in equipment and personnel compared to conventional connections. The technology has been tested offshore in the Princess Amalia wind farm in the North Sea for a small bottom fixed wind turbine for a period of one year. The turbine tower was short in comparison to an oversized foundation and the Slip Joint connection was made above the water surface which means that dynamic loads have been below realistic loads by up to a factor of 3. Also, the contact surface area is large, resulting in low hoop stresses between the conical sections. Oxygen and water could enter between the elements and therefore, corrosion remains a risk. To counter this risk, a paste is applied on the ends of the Slip Joint connection in order to prevent water and oxygen from entering between the conical elements.

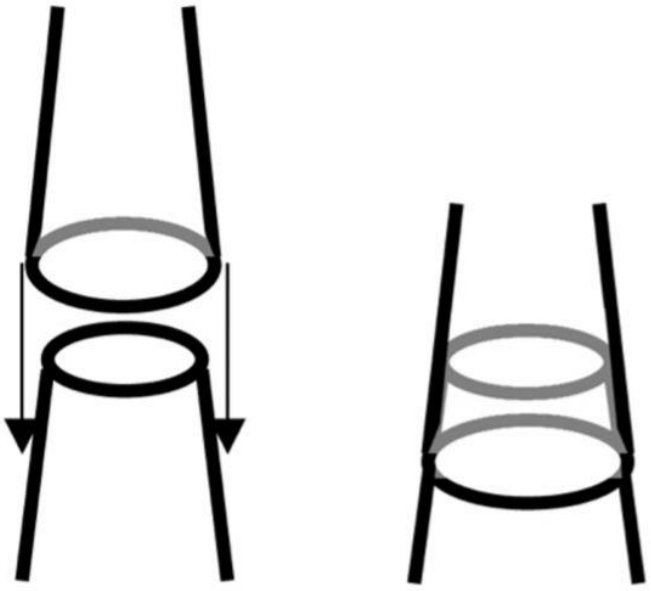

*Figure 6: Schematic representation of a Slip Joint connection [20]*

A Slip Joint connection is applied as an offshore demonstration in the Borssele V wind farm off the coast of the Netherlands. In the next paragraph, the Double Slip Joint connection will be explained. In paragraph 1.1.2.5, both technologies will be compared for utilization in the Borssele V wind farm.

#### *1.1.2.4 The Double Slip Joint connection*

A later version of the Slip Joint is the Double Slip Joint or DSJ. This is a connection type that is immediately stable, which consists of two sets of conical rings [21]. Figure 7 shows how these conical rings lock the wind

turbine fixed to the support structure. The reason for this more novel connection is increased predictability of settling behavior, more control over tolerances and reduced weight and costs.

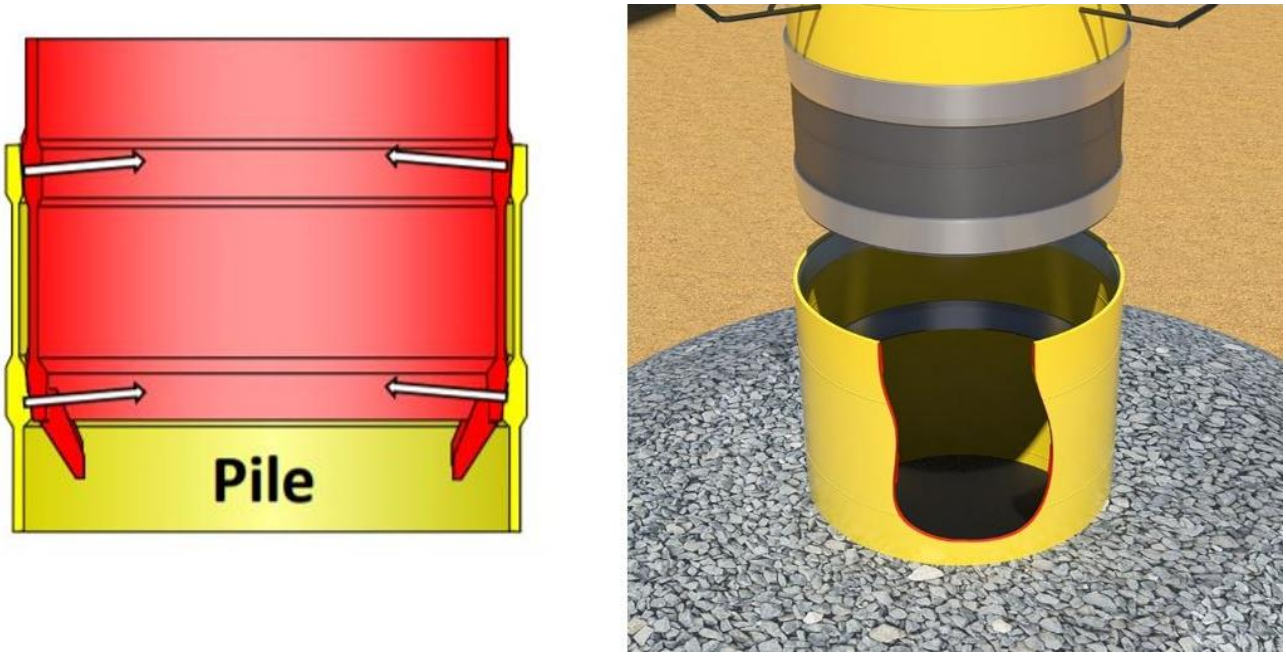


*Figure 7: The Double Slip Joint (source: KCI The Engineers)*

The conical rings have been tapered at an angle of about 2°. The self-weight and environmental loading induce settlement of the wind turbine into its support structure whereas the clamping pressure between the rings of the support structure and the rings of the wind turbine increase as found by [22]. The forces between the two structural elements are completely transferred by static friction and therefore, no wear occurs at the ring surfaces. Also due to the high hoop stress between the rings, the rings are completely interlocked with 100% steel on steel contact. Therefore, no water and oxygen enter the annulus between the 4 rings and no corrosion will occur. This benefit is not found at the slip joint connection as the hoop stresses are too small there to prevent air and water from entering the annulus.

A scaled WTG tower with DSJ connection with a diameter of 1.6 m has been tested extensively at the Dutch test institute WMC and the settling behavior of the connection is determined for different environmental load variations. A photo of the size of the heavy structure as tested at WMC is visualized in Figure 8 on the truck. Figure 9 shows an overview of the testing configuration with a photo (left) and a schematic overview (right). It appeared that due to the self-weight of the WTG, the DSJ connection could only settle further under environmental loading, making the connection stronger until settling stops. A Technical Readiness Level or TRL 6 is therefore obtained, marking the end of the development phase, and making the connection ready for an offshore demonstration. In preparation for an offshore demonstration, this thesis will investigate the motion and collision limits regarding installation of an offshore WTG tower with a DSJ connection on its support structure.


*Figure 8: 1.6 m diameter steel construction used for environmental loading tests to obtain the settling behavior of the DSJ connection*

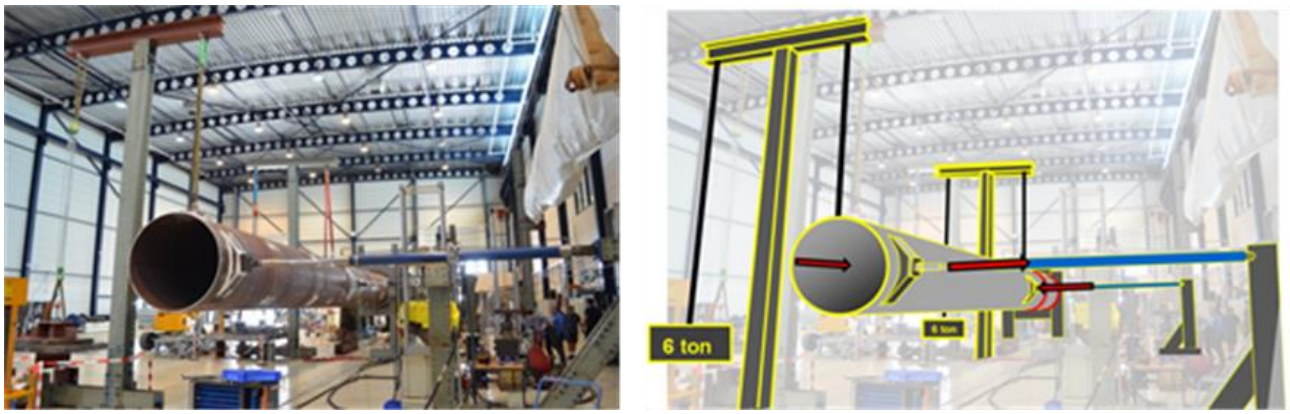


*Figure 9: Photo of the testing configuration (left) and a schematical overview of the loads exerted on the structure and the DSJ connection (right).*

#### *1.1.2.5 Borssele V wind farm demonstration*

A Slip Joint connection has been applied in the Borssele V wind farm as a demonstration. It will serve as an underwater connection between the MP and TP. A DSJ connection has also been designed for Borssele V in order to compare the differences in material weight and costs.

Figure 10 provides a clear overview of the situation. The soil is indicated in grey, whereas the water is blue. An underwater connection is made between the MP (lower structure) and the TP (upper structure). On the left in the figure, the structures are shown with a Slip Joint connection. On the right, the structures are shown with a DSJ connection. In this case, it is an inverted DSJ connection, which means that the TP slides over the MP. Dimensions are indicated in the figure.

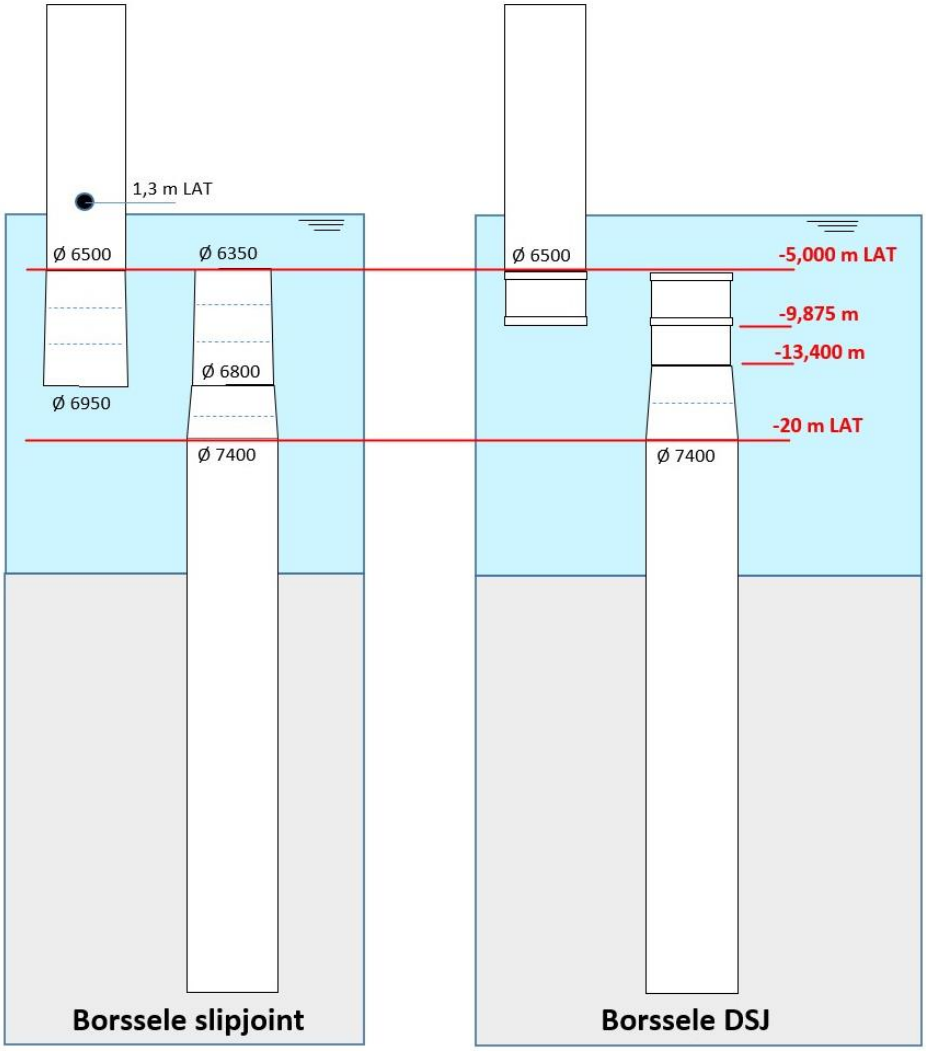


*Figure 10: Visualization of a Borssele V MP and TP whilst utilizing a Slip Joint (left) or Double Slip Joint or DSJ (right) as an underwater connection between the two structures.*

Comparing a Slip Joint and Double Slip Joint respectively, it appeared that a DSJ connection would have reduced steel weight with roughly 90 metric tons per WTG. This weight reduction is found between the red lines in Figure 10 and for this structural section, it indicates a reduction of 30 % in steel weight and a 30 % cost reduction.

### 1.1.3 Installation vessels used for installation of offshore wind turbines

Bottom fixed offshore wind turbines are usually installed by jack-up vessels or moored vessels, according to [23]. A jack-up vessel has jacket like legs that lifts the platform up above the sea water wave zone during installation. Figure 11 illustrates how a jack-up installation vessel performs the installation of an offshore wind turbine. During installation, the jack-up vessel is not subjected to wave loads and the motions of the vessel will therefore be small.

*Figure 11: Wind turbine installation using a jack-up vessel (source: jandenul.com)*

Currently, the largest jack-up vessel is named the Voltaire and is still under construction. The vessel that is set to be delivered in 2022 will have a lift capacity of 3000 tons and an operating depth of up to 80 m. However, for floating offshore wind farms that could be placed in water depths of considerably more than 100 m, installation is impossible with jack-up vessels.

Moored installation vessels are also used for installation of bottom fixed wind turbines. Passive motion compensation is achieved by taut or catenary mooring lines that obtain their restoring force from elasticity and self-weight respectively. However, mooring is a very time-consuming effort and the weather window for installing a wind turbine is small [23].

In deeper waters, floating offshore wind is viable, but jack-up vessels are obsolete as they don't reach the required depth to jack themselves up and install wind turbines. Also, installation possibilities using a moored installation vessel are very limited. The greater the water depth, the greater the excursions around the equilibrium position of the moored vessel. This means that for installing a wind turbine offshore, the weather window shrinks with increasing depth when using moored installation vessels. To overcome this problem installation vessels with dynamic positioning systems can be used.

Dynamic positioning or DP is a way of actively maintaining a vessel's position and orientation by using propellers and or thrusters. This technology is described in paragraph 2.1.3.2. This feature overcomes the problem that moored installation vessels have in greater water depths. These vessels have been successfully used in installation of offshore floating wind turbines. Figure 12 is a photo of a wind turbine being installed on a floating spar support structure in the Hywind floating offshore wind farm. A yoke was placed around the top section of the tower. This yoke was suspended by steel wire ropes in two cranes. It should be noted that in this particular installation, bolted flanges were used as a connection. Hydraulic clamping was used to stabilize the wind turbine after mating before bolting was performed. However, such installation is not economically viable for future projects as it requires very expensive installation vessels and very calm weather.

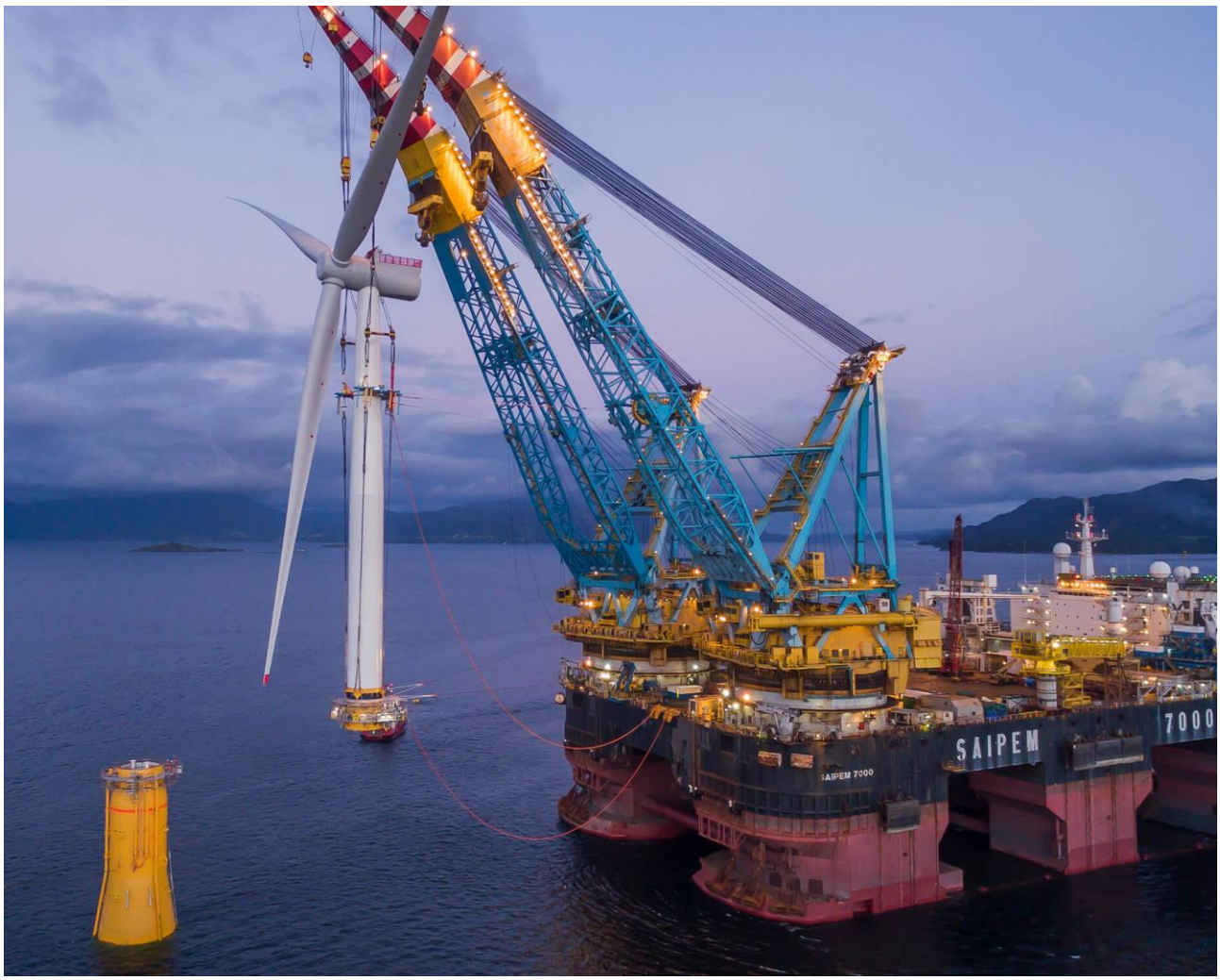


*Figure 12: Installation of a wind turbine on a floating spar support structure using a DP crane vessel (source: saipem.com)*

Dynamically positioned vessels are however subjected to wind and wave loading and the wind turbine will therefore be excited as a result of these motions. This is a challenge during installation as there is a limit on the relative motions during installation.

## 1.2 This Thesis

### 1.2.1 Problem description and research question

The Double Slip Joint is a promising innovation and it has been experimentally proven to be a strong, immediately stable and corrosion-free connection. The immediate stability hypothetically allows for higher installation limits and workability than grouted or bolted connections. However, this is not only determined by the connection type, but also by the catchers used, the installation vessel and the support structure.

Subsection 1.1.1 emphasized the need CAPEX and OPEX reduction in order to increase the financial competitiveness of offshore wind energy compared to other energy sources. Increasing the installation workability as a result of immediately stable connections would decrease the time needed for an installation vessel to be contracted and consequently the installation costs come down. A CAPEX reduction is consequently obtained. A maintenance-free connection also of course reduces OPEX compared to a connection that does require maintenance.

The installation workability depends on many factors and research to the subject is quite novel. This research aims to provide a first exploration into workability of installation using catchers and utilizing a Double Slip Joint connection. In this research, the focus is placed on the installation behavior and the motion and collision limits of the WTG tower during lowering and catcher mating with the MP. The main research question that this research project aims to find an answer to can be described as follows.

*"What are the allowable motion and collision limits during lowering and catcher mating in the installation of a WTG tower on a MP whilst utilizing a DSJ connection?"*

### 1.2.2 Objectives and Methodology

The ultimate goal of this research is to find the motion and collision limits of installation of a WTG tower using catchers on an MP. Motion and collision limits are based on installation requirements that are to be identified in this research. This primary objective can be subdivided and explained with several sub-objectives.

- During installation of a WTG tower on a monopile, collisions or impacts occur between the two structures. A physical description of the contact forces resulting from collisions is required. Also, it is required to assess the maximum allowable contact force. For this research, the collision behavior and maximum contact load will be determined for contact between the MP and the catcher on the bottom of the WTG tower.
- In order to obtain motion behavior of a WTG tower suspended by a crane of an offshore installation vessel, it is required to know the physical phenomena affecting these motions. It is therefore an objective to identify and quantify these effects. An example of a physical phenomenon in this case is the wind load acting on the WTG tower. The nacelle, hub and rotor are not considered in this research since the focus is on tower installation only.
- It is necessary to identify installation requirements that determine the allowable motion and collision limits of WTG tower installation onto its support structure. An example of such a requirement could be prevention of slack wires.
- An important research objective is to assess simulation model validity. In the research process, assumptions and simplifications are made that may limit the validity of outcomes and consequently, the validity has to be assessed in order to obtain reliable research outcomes.

The research method can be explained using Figure 13. Literature research is the basis of identifying and quantifying physical phenomena related to the installation. It should be noted here that although a literature-based assessment of collision dynamics is made, finite element analysis will also be performed to quantify contact forces and collision responses. Central in the research method are model simulations. The physical phenomena together with the variables are the model input. Model output is first checked for validity. As

mentioned in the final objective, due to simplifications and assumptions made, model output should be assessed for validity.

The identification and quantification of restrictive or critical events is important in determining the allowable limits of WTG motions with respect to the support structure. Literature research will be the basis of identification and quantification of these limits. If model output complies to both validity and installation requirements, the installation is successful for the variables used as input for that specific simulation.

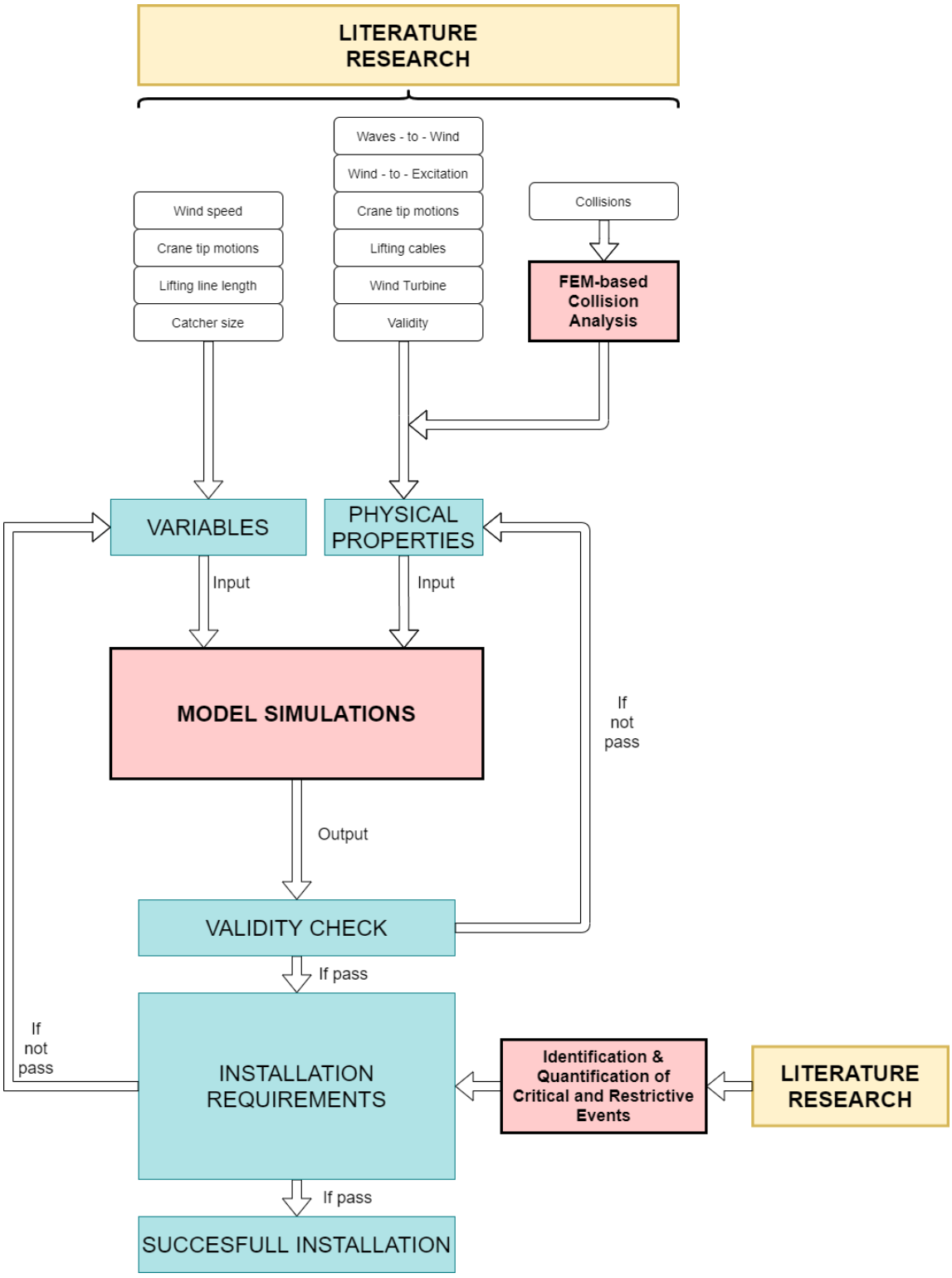


*Figure 13: Flow chart of research methodology*

### 1.2.3 Thesis scope and delineations

The main focus of this thesis is to find the allowable limits of motions and collisions in WTG tower installation onto an MP and as such, to provide a first exploration into workability of installation. The study covers the physical phenomena that affect the motion behavior of a WTG tower in installation and provides an accurate description of collision responses and impact forces occurring between the WTG tower catcher and an MP. The coverage of this study also includes quantification of installation limits, based on identification of installation requirements. All study results concern installation of a WTG tower on an MP where a DSJ connection is applied.

The study does not cover installation where other connections than the DSJ are applied. From an installation perspective, the research focuses on the situations where the WTG tower is already above the support structure, is being lowered and when the first few collisions are made. The research does not include installation phases prior to vertical alignment of WTG tower and support structure, nor does it include final settling behavior after the first few collisions.

This study is performed in 2D and focuses on in-plane motions and collisions of the WTG tower. This approach has been taken because the WTG tower, MP and Double Slip Joint connection are axisymmetric and therefore, their lateral (out of the axis of symmetry) collisions have identical responses. Also, based on OWT installation practices, it is shown out-of-plane motions of the WTG tower in are relatively easy to control. A further explanation and discussion of installation in 3D is given in section 5.5.

### 1.2.4 Thesis outline

Chapter 1 provided background information of offshore wind demographics and economics. It also introduced technologies that are currently used for support structures, connections, and installation vessels. Besides, it presents the necessity of innovation in the field of connections between OWT's and their support structures and introduced the Double Slip Joint as such innovation. It is also shown that currently, the weather window for installation is small, which leads to higher CAPEX due to long waiting times for installation vessels. In the second section of the first chapter, it is explained how this research will contribute to a solution for this problem by assessing motion and collision limits in installation. The problem description and research question are provided together with research objectives, methodology and a thesis scope.

Chapter 2 in this thesis report contains the findings of the literature research. Figure 13 shows that literature research is the basis of the model input and the identification and quantification of critical and restrictive events, as explained in subsection 1.2.2. Chapter 2 contains this literature-based assessment of physical phenomena and critical and restrictive events.

Chapter 3 describes the model development. This includes the finite element method-based analysis of collisions as mentioned in subsection 1.2.2. These results will be fed back into the model to accurately describe collision responses and impact loads.

Chapter 4 contains the validation and model updating of the simulation model. Since this research investigates motion and collision limits, this validation also focuses on both the WTG tower motions and collisions. The model updating focuses on changing the stiffness and damping in the contact element to incorporate the effects of flexibility of the WTG tower and MP.

Chapter 5 outlines the model simulation outcomes and answers the research question as stated in subsection 1.2.1. These results also yield conclusions with regards to the different catchers used in installation. Finally, the analyses serve as a first exploration into workability of installation.

# 2

# Theoretical Review

This chapter concerns the literature research findings regarding the physical phenomena and requirements for installation. In accordance to the research methodology and objectives as described in subsection 1.2.2 and the thesis outline described in 1.2.4, the physical phenomena will be the basis for model development and the requirements are pivotal in setting allowable motion and collision limits to the installation based on identification and quantification of restrictive and critical events. Section 2.1 describes the physical phenomena and section 2.2 continues with the requirements to the installation.

## 2.1 Physical Phenomena

Figure 13 shows that in this research, describing the physical phenomena related to the installation and mating of a WTG tower on its support structure is necessary in order to develop a model. In this section, all physical phenomena with respect to installation and mating are described based on literature research. The aforementioned figure also referred to the need of performing FEM analysis of collisions, but this is part of the model development and will be discussed in Chapter 3.

### 2.1.1 Contact-Impact

Contact-impact in this context refers to the collisions that take place between the WTG tower and its support structure during installation. These collisions can occur in the radial as well as the axial direction.

[24] studied the installation and mating of a transition piece or TP on a monopile or MP. The bottom of the TP contains catchers or finger guides as seen in Figure 14a and Figure 15a and b, aiming to guide the TP over the MP during installation. An example of a radial collision is seen in Figure 14b. The catchers of the TP impact with the MP in the horizontal plane and these collisions are represented by spring-dampers. Figure 15c shows an example of an axial collision between the TP and MP. This collision is also represented by a linear spring-damper.

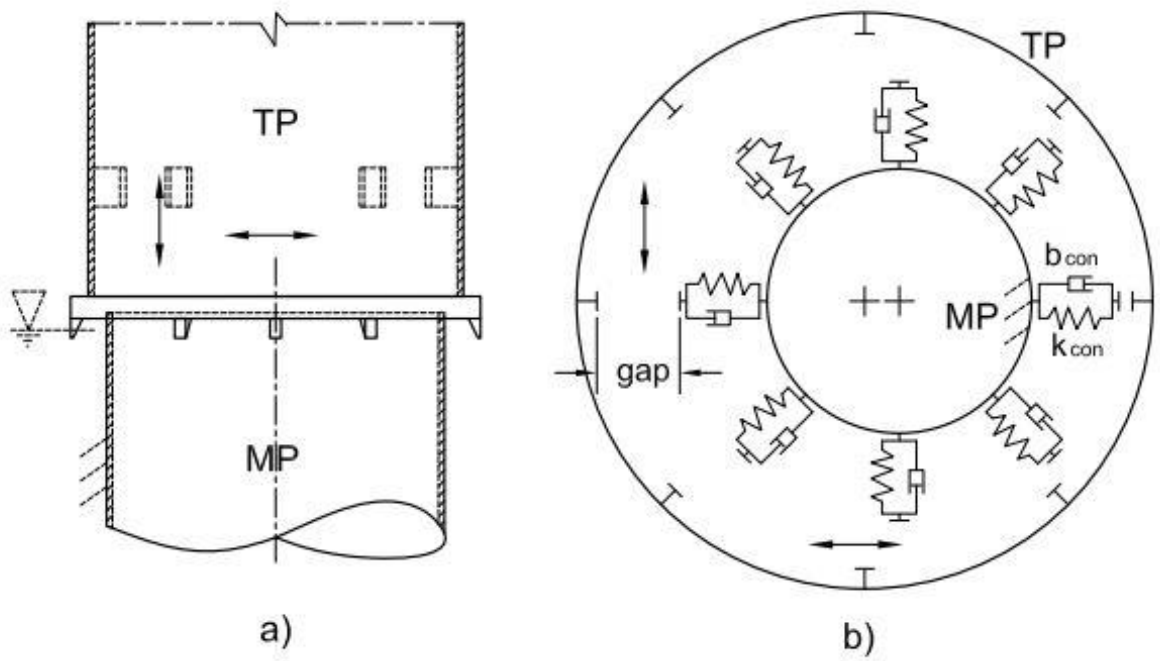


*Figure 14: Radial contact during mating operation including spring-damper representation of impact [24]*

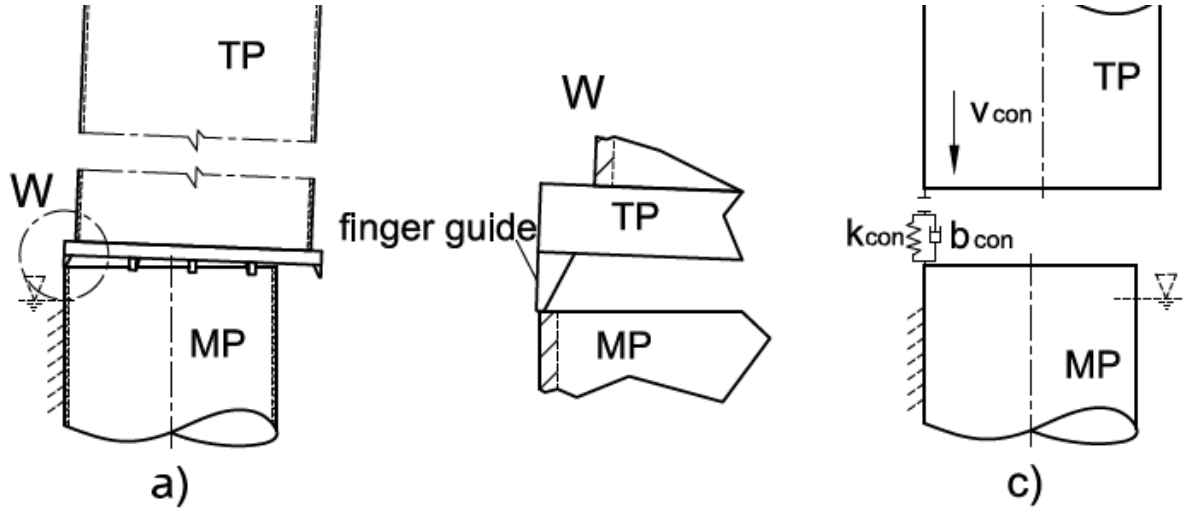


*Figure 15: Axial contact during mating operation including spring-damper representation of impact [24]*

In the literature regarding offshore installation operations, contact-impact is often represented by a linear spring-damper, as in [24] and Figure 14 and Figure 15. Certain values for stiffness and damping are assumed. However, since the use of Slip Joint or Double Slip Joint connections is still rare, specific literature for offshore wind connections is still rare. Therefore, the literature research was broadened.

Research in other fields show that simply assuming constant values for stiffness and damping is not accurate in predicting the response of a collision. Collision responses involve many variables, non-linearities and or irregularities. In order to get a better understanding of collision responses and the processes involved, a research field which comprises research regarding response behavior of contact-impact was studied: namely church bells. An analogy can be made between a church bell clapper impacting the bell, exciting both the clapper and the bell, with repeated impacts over time while both are still vibrating. [25] has made some important findings from experimental research:

1. The first impact that the clapper makes with the bell differs significantly from all consecutive impacts. Figure 16 shows the velocity ratio of a clapper hitting a church bell. For the first impact, the ratio of

the incoming velocity and the outgoing velocity is between 0.25 and 0.5 and the mean velocity ratio is 0.35. For all consecutive impacts, the ratio varies between 0.4 and 1.5, with a mean ratio of 0.8.

2. The difference in velocity ratio for the first impact compared to consecutive impacts can be explained using conservation of energy.

    a. Right before the first impact, no kinetic energy in the form of vibrations is yet present in the bell. All energy present is the kinetic energy of the clapper.
    b. During the first impact, 90% of the kinetic energy of the clapper is transferred into kinetic energy of the bell in the form of vibrations. This is determined through the kinetic energy proportionality with the squared velocities.
    c. Between the first and second impact, the vibrations of the bell decay due to acoustic and material damping. However, the vibrations have decayed only partially before the second impact occurs.
    d. During the second impact, both the bell and the clapper have kinetic energy due to vibrations and motions respectively and experimental results as in Figure 16 show that less kinetic energy of the clapper is transferred into bell vibrations.
    e. For all consecutive impacts, steps c. and d. are repeated.

3. Another observation from the studies of [25] and Figure 16 is that the response of the clapper for an impact with a vibrating bell is chaotic mathematically. The velocity ratio of the clapper as a result of impact becomes unpredictable.

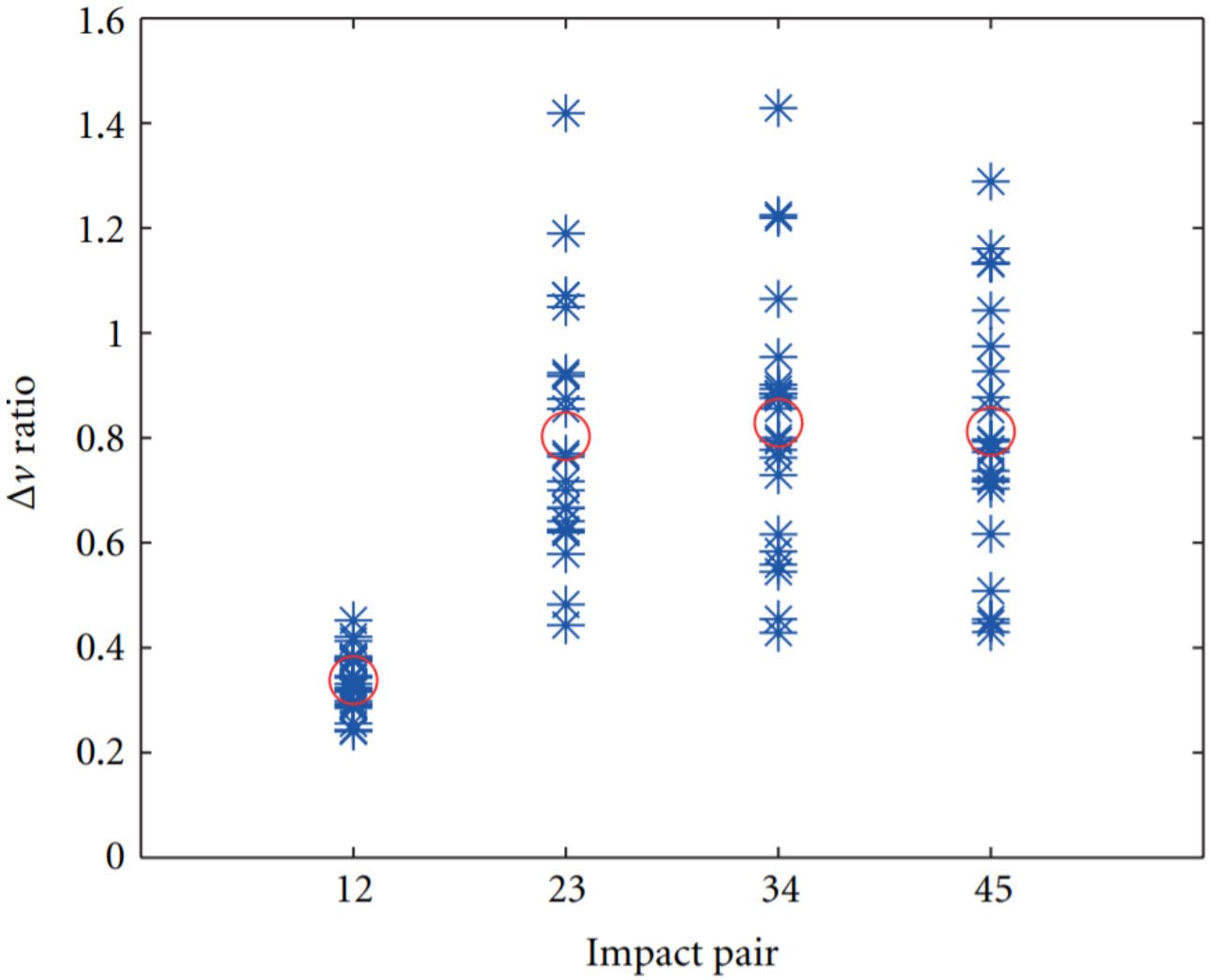


*Figure 16: Experimental results showing the velocity ratio of a clapper against a bell for 4 consecutive impacts. Blue stars representing the velocity ratio of a certain experiment and the red circle being the mean of all experiments.*

Clearly, impact problems are complex and defining stiffness and damping terms describing an impact is not straightforward. In the case of church bells, the collision response appears to be irregular and can only be determined within a certain range of accuracy. For this research, however, it will be assessed whether the analogy is viable using a mathematical model. This can be found in section 3.3.

### 2.1.2 Wind Excitation

During installation of a WTG tower, wind is a source of excitation. In order to define the wind load on the tower during installation, the wind speed should first be quantified. Paragraph 2.1.2.1 provides a description of an offshore wind field including time and spatial variations. The following paragraph explains how the wind velocity translates to a wind load on the WTG tower. Paragraph 2.1.2.3 concludes with a description of how wind velocity, combined with translational and rotational motions of the WTG tower leads to aerodynamic damping. In Appendix A, background information is provided on the WAM model [26], which relates wind and wave parameters.

#### *2.1.2.1 An offshore wind field*

A wind field is turbulent and consequently, the wind speed varies in time and space. This effect has to be considered as it influences the wind load of a WTG tower during installation. First, the time-dependent wind speed variations will be considered. Turbulence is found in a spectrum of frequencies. For an offshore installation campaign, the high frequency turbulence can be neglected as this excitation has negligible impact on the WTG tower due to its high mass and inertia [27]. The low frequency wind variations, or wind gusts, do however influence the motion behavior of the WTG tower during installation [27].

Therefore, the time-dependency of the wind field can be represented in a simple way by a mean wind speed accompanied by occasional wind gusts. [28] Found that a wind gust is a maximum 3-second wind speed increase forecast to occur within a 2-minute interval. Figure 17 shows a time-domain representation of a wind gust, with amplitude *A*. Before and after the wind gust peaks, the wind velocity is below the mean wind speed, and the wind gust can be described by a wavelet function accordingly. This wavelet function as a period of $\tau$ = 10.5 s.

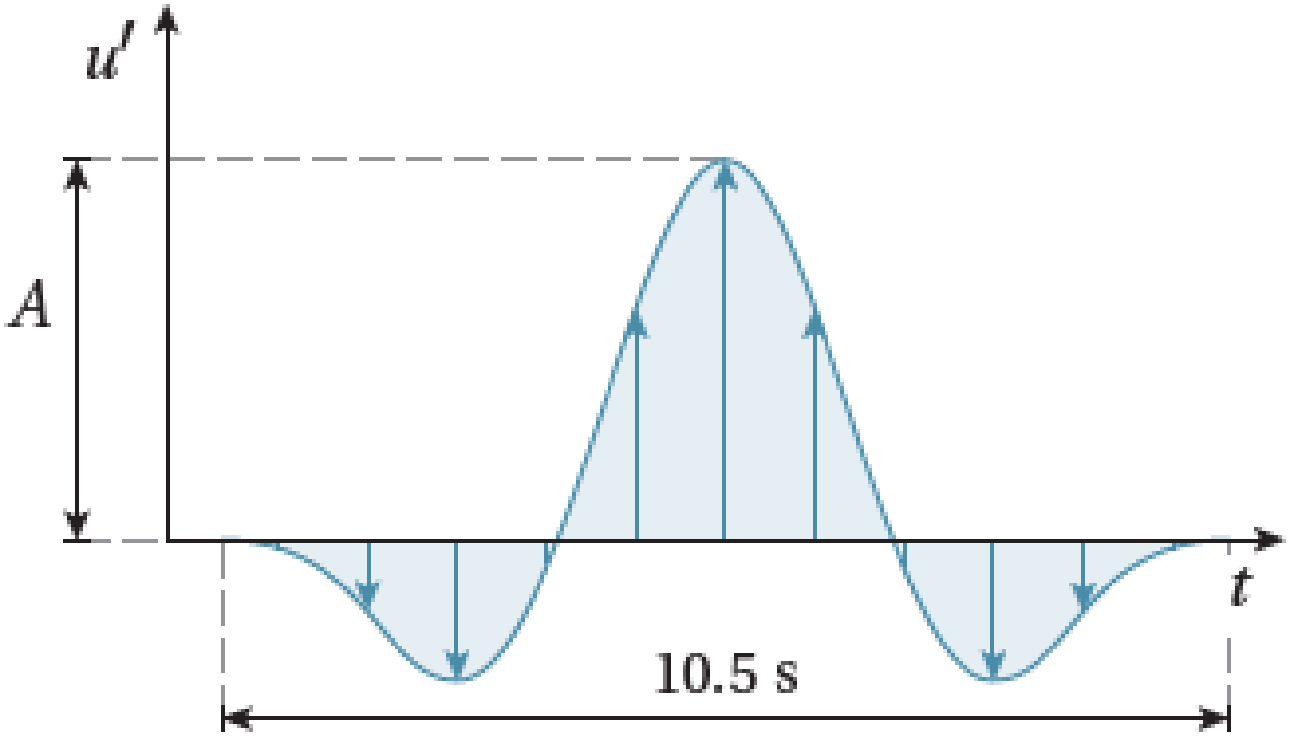


*Figure 17: Wind velocity profile as a function of time during a wind gust according to [28]*

Given that a wind gust is forecast to occur within a 2 minute interval [28], the mathematical description of a 120 second wind cycle including gusts in this research, based on the findings of [28] and [29] is as follows:

$$u(t, H_{10}) = \begin{cases} \bar{u} - 0.37A \sin\left(\frac{3\pi t}{\tau}\right)\left[1 - \cos\left(\frac{2\pi t}{\tau}\right)\right], & for\ 0 \le t \le \tau, \\ \bar{u}, & otherwise, \end{cases} \quad (2.1)$$

Where $u(t,H_{10})$ is the wind speed as a function of time in m/s at a height of 10 m above SWL. $\bar{u}$ is the mean wind speed in m/s, $A$ the wind gust amplitude in m/s, assumed to be 50 % of the mean wind speed according to IEC standards for determining the extreme operating gust. $T$ is the time in s, and $\tau$ the wavelet period in s (10.5 s according to [29]).

A more complex and accurate way of describing the time-dependency of wind velocities is by using a Fourier transformation. KCI The Engineers developed a wind model that determines the time domain or TD wind velocity variations for any site as long as the site-specific surface roughness is known. This parameter for offshore conditions is 0.002 m. The wind field consists of a summation of harmonic functions with different frequencies and amplitudes and random phases. Figure 18 shows an example of such realization for a 20-minute period.

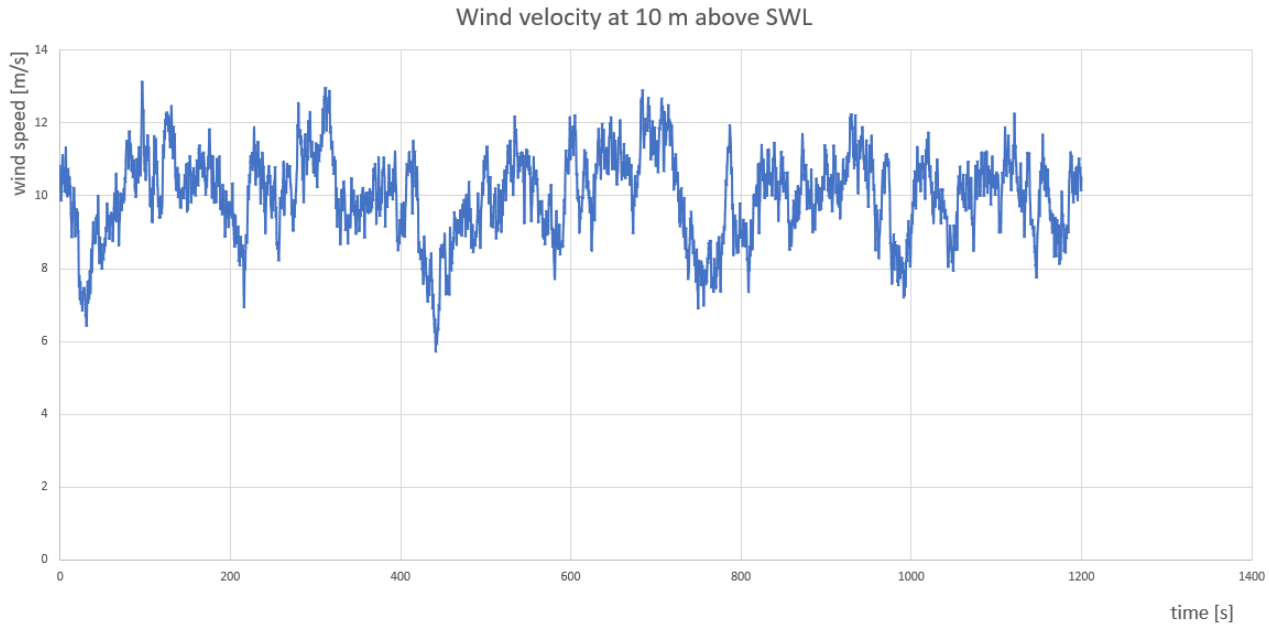


*Figure 18: Time-domain wind velocity realization based on hindcast data*

In space, the wind speed varies both in the horizontal as well as in the vertical direction. However, as described in Appendix A, the assumption is made that the wind direction is constant during installation of a WTG tower. The emphasis of spatial wind speed variations is therefore placed at the vertical direction.

The time-domain wind velocity realization as shown in Figure 18 applies to a height of 10 m above the still water level or SWL. According to [30], the wind velocity profile as a function of the height above SWL can be determined as follows:

$$u(t, z) = u(t, H_{10}) * \left( \frac{ln\left(\frac{z}{z_0}\right)}{ln\left(\frac{H_{10}}{z_0}\right)} \right) \quad (2.2)$$

Where $u(t,z)$ is the wind velocity as a function of time and height above SWL. $Z_0$ is the surface roughness assumed to be 0.002 m for offshore conditions. There is a logarithmic increase in wind speed and thus wind

load above SWL. Assuming that the wind direction is constant in time during installation, the wind velocity profile as a function of height and time is determined.

### *2.1.2.2 Wind velocity to wind load*

From the time and height dependent wind velocity profile determined in paragraph 2.1.2.1, the loads on the WTG tower during installation can be determined. According to [31], it can be assumed for wind load calculations that the WTG tower is cylindrical. The wind loads on the tower can then be determined by:

$$F_w = C_D * q * dA * \sin(\alpha) \tag{2.3}$$

Where

$$q = \frac{1}{2} * \rho * u^2(t,z) \tag{2.4}$$

$$dA = D(z)dz \tag{2.5}$$

Where *dA* in equation 2.3 and 2.5 is the projected area of a tower element to the wind. It is determined by multiplying the diameter at height *z* by the element height *dz*. Integration over the height of the tower yields the total projected area of the tower. *q* in equation 2.3 and 2.4 is the air pressure, which is a function of the air density *ρ* and the wind speed relative to the WTG tower *u(t,z)* as a function of height and time. *α* is the angle between the wind direction and the axis of the exposed element (90°). $C_D$ is the drag coefficient as a function of the Reynolds number, visualized in Figure 19. The Reynolds number *Re* is determined by:

$$Re = \frac{D * u(t, H_{COG})}{\nu} \tag{2.6}$$

Where *D* is the diameter of the tower, $u(t,H_{COG})$ the wind velocity at the center of gravity of the WTG tower in m/s and *v* the kinematic viscosity of air, being 1.48E-5 $m^2/s$ (at 15 °C). The aerodynamic loads on the tower are hereby determined as a function of time and height in accordance with [31].

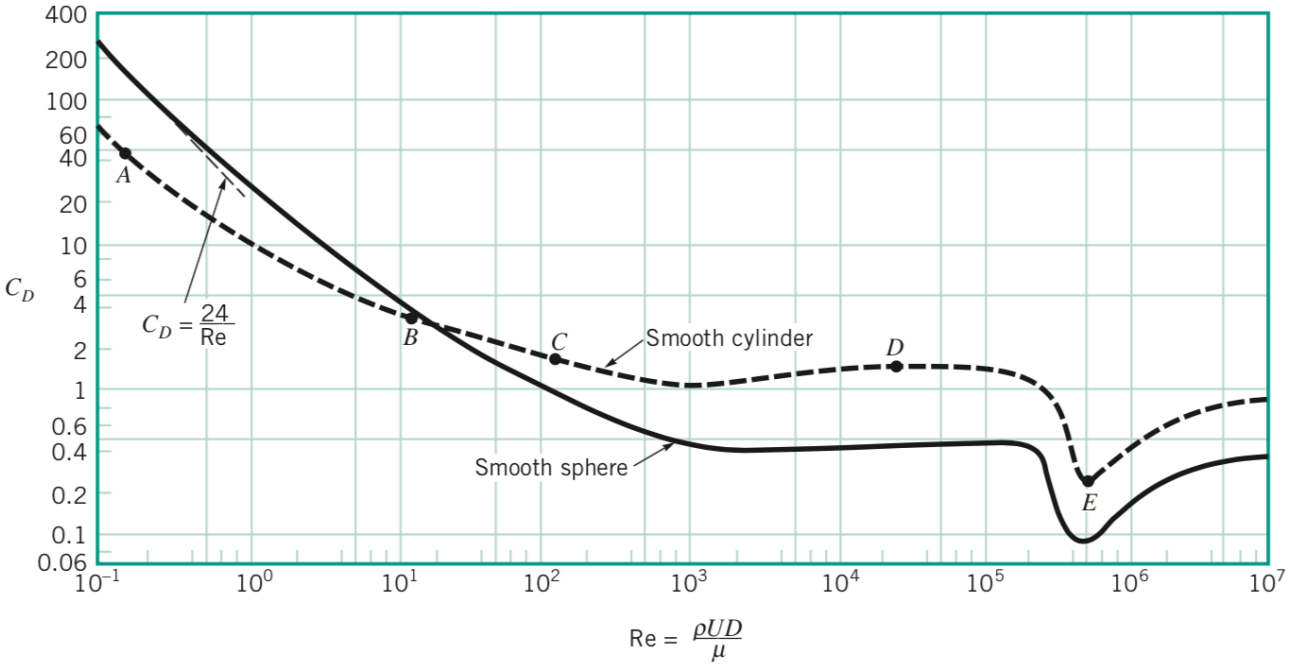


*Figure 19: Drag coefficient $C_d$ as a function of the Reynolds number for an infinitely long cylinder*

### *2.1.2.3 Aerodynamic damping during WTG tower installation*

Aerodynamic damping occurs on an object that has a variable velocity in the direction of the wind field [32]. For a WTG tower suspended by a crane, there are variable velocities in the direction of the wind field. Therefore, there is aerodynamic damping. These motions originate both due to the rotation and horizontal

translation of the wind turbine. The relative velocity of the WTG tower in the wind as stated in paragraph 2.1.2.3 is as follows:

$$u(t,z) = U(t,z) - \dot{x} + z\dot{\alpha} * \cos(\alpha) \tag{2.7}$$

Where, *u(t,z)* is the relative velocity of the WTG tower in the wind, *U(t,z)* the absolute wind velocity, *x'* the horizontal translational velocity of the WTG tower, *α'* the rotational velocity of the WTG tower, *α* the angle of the tower and *z* the distance from the CoG. For small angles *α*, this equation simplifies to:

$$u(t,z) = U(t,z) - \dot{x} + z\dot{\alpha} \tag{2.8}$$

The wind load *q(z,t)* as stated in paragraph 2.1.2.3 becomes:

$$q = \frac{1}{2} * \rho * u^2(t,z) \tag{2.9}$$

$$q = \frac{1}{2} * \rho * (U(t,z) - \dot{x} + z\dot{\alpha})^2 \tag{2.10}$$

$$q = \frac{1}{2} * \rho * (U^2(t,z) + \dot{x}^2 + z^2\dot{\alpha}^2 - 2U(t,z)\dot{x} + 2U(t,z)z\dot{\alpha} - 2z\dot{x}\dot{\alpha}) \tag{2.11}$$

Clearly, *U(t,z)*, *α'* and *x'* are coupled in the wind load equation, proving the relationship between wind velocity and object velocity in the determination of the wind load. For correct modelling of the wind load, this effect has to be incorporated in the model.

## 2.1.3 Crane tip motions

Crane tip motions are a source of excitation during installation of a WTG tower on its support structure. It is described in paragraph 2.1.3.1 how waves induce vessel motions. The following paragraph introduces dynamic positioning or DP and its effects on vessel motions. Paragraph 2.1.3.3 bridges the link between vessel motions and the resulting crane tip motions.

### *2.1.3.1 Wave-induced vessel motions*

Waves induce vessel motions due to pressure variations on the hull of the ship. In reality, waves are irregular and are therefore generally expressed in the frequency domain (FD). The most commonly applied wave spectrum is the JONSWAP spectrum. [33] found that by analyzing North Sea wave data, the North Sea is never fully developed. It is a 'limited fetch' sea and waves can never become fully developed as the lee shore is too close by. For a limited fetch sea, the FD wave spectrum is determined by the JONSWAP spectrum:

$$S_j = \frac{\alpha g^2}{\omega^5} \exp\left(-\frac{5}{4}\left(\frac{\omega_p}{\omega}\right)^4\right)\gamma^r \tag{2.12}$$

The values in this expression are:

- Peak enhancement factor $\gamma^r$, to correct for the fact that no wave spectrum is fully developed. [34] found that the value *γ* is determined by:

$$\gamma = 7.0\left(\frac{gF}{U_{10}^2}\right)^{-\frac{1}{7}} \tag{2.13}$$

- [34] also found that exponent *r* can be determined by

$$r = \exp\left(-\frac{(\omega - \omega_p)^2}{2\sigma^2\omega_p^2}\right) \tag{2.14}$$

- The Philips constant *α*, which can be determined by the following equation, according to [35]:

$$\alpha = 0.076\left(\frac{U_{10}^2}{Fg}\right)^{0.22} \tag{2.15}$$

Where $U_{10}$ is the wind velocity at a height of 10 m above the still water level (SWL), $F$ is the distance from lee side shore (fetch) and $g$ the gravity acceleration.

- Peak frequency $\omega_p$, which is determined by:

$$\omega_p = 22\left(\frac{g^2}{U_{10}F}\right)^{\frac{1}{3}} \tag{2.16}$$

- Spectral width parameter $\sigma$

$$\sigma = \begin{cases} 0.07 & \omega \leq \omega_p \\ 0.09 & \omega > \omega_p \end{cases} \tag{2.17}$$

The JONSWAP wave spectrum is hereby determined. It contains spectral parameters that characterize the surface elevation. The spectral moments $m_n$ are:

$$m_n = \int_0^\infty \omega^n S_j(\omega) d\omega \tag{2.18}$$

The significant wave height $H_{1/3}$ is then calculated as:

$$H_{\frac{1}{3}} = 4 * \sqrt{m_0} \tag{2.19}$$

Given a certain significant wave height $H_{1/3}$ for installation, the corresponding JONSWAP wave spectrum is determined using the zeroth order spectral moment $m_0$. Using mathematical transfer functions, or response amplitude operators (RAO's), the 6 degree of freedom (DOF) motion of the vessel due to the waves is determined. The 6 degrees of freedom are visualized in Figure 20. The translations $x$, $y$ and $z$ are called surge, sway and heave respectively and the rotations $\varphi$, $\vartheta$ and $\psi$ are roll, pitch and yaw.

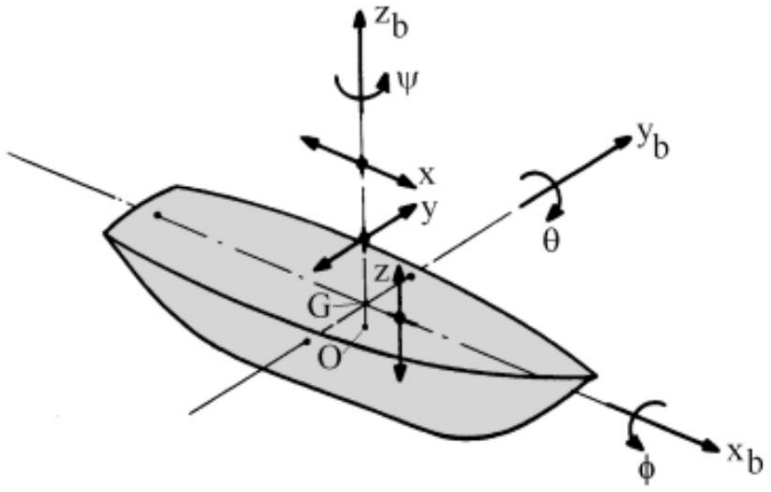


*Figure 20: 6 DOF ship motions (Journée, 2001)*

[36] Found that in the frequency domain, the ship response to the frequency domain wave spectrum is equivalent to a frequency dependent mass-spring-damper system. This finding allows for defining the following equation:

$$(-[\boldsymbol{M} + \boldsymbol{A}(\omega)]\omega^2 + \boldsymbol{B}(\omega)\, i\omega + \boldsymbol{C}) * \vec{x} = \vec{F}(\omega) \tag{2.20}$$

In which:

| | | |
|---|---|---|
| ***M*** | = | Ship inertia matrix (frequency independent) |
| ***A(ω)*** | = | Ship added mass matrix (frequency dependent) |
| ***B(ω)*** | = | Ship hydrodynamic damping matrix (frequency dependent) |
| ***C*** | = | Ship hydrostatic stiffness matrix (frequency independent) |
| *F(ω)* | = | First-order wave excitation force amplitude vector |
| *ω* | = | Frequency |
| *x* | = | Ship motion vector |

Equation 2.20 can be rewritten as:

$$\vec{x}(\omega) = \frac{\vec{F}(\omega)}{(-[\boldsymbol{M} + \boldsymbol{A}(\omega)]\omega^2 + \boldsymbol{B}(\omega)\, i\omega + \boldsymbol{C})} \tag{2.21}$$

Where:

$$\vec{F}(\omega) \propto \zeta_a \exp(i\omega t) \tag{2.22}$$

In which $\zeta$ is the incoming wave amplitude. Assuming that the vessel motions are harmonic, the vessel motions and the corresponding RAO's can be rewritten as in equation 2.23 and 2.24 respectively:

$$\vec{x}(\omega) = \vec{x}_a \exp(i\omega t) \tag{2.23}$$

$$\overrightarrow{RAO}(\omega) = \frac{\vec{x}_a}{\zeta_a} = \frac{\vec{F}_0}{(-[\boldsymbol{M} + \boldsymbol{A}(\omega)]\omega^2 + \boldsymbol{B}(\omega)\, i\omega + \boldsymbol{C})} \tag{2.24}$$

The first-order wave excitation force vector *F(ω)* is determined by integration of the wave pressure acting on the submerged hull of the vessel and is harmonic as shown in equation 2.22. Actually, for the first 3 degrees of freedom, *F(ω)* is a force and for the last 3 degrees of freedom it is a moment. This is because the first three degrees of freedom are translations and the last 3 are rotations. These forces and moments are referred to as Froude-Krilov forces [37] and are a function of the geometry of the vessel. Note that these Froude-Krilov forces have to be corrected by the diffracting waves due to the presence of the hull.

Added mass and damping matrices, Froude-Krilov forces and diffraction forces can be either computed numerically or determined experimentally. For example AQWA or WAMIT are diffraction analysis software packages that define these forces and matrices numerically. Once they are defined, the vessel motion amplitudes as a function of frequency, *x(ω)*, can be calculated. Since linearized theory is used, the motion response spectrum of the vessel due to the wave spectrum can be calculated as defined by [37]:

$$S_\eta(\omega) = \left|\frac{\overrightarrow{x_a}(\omega)}{\zeta(\omega)}\right|^2 S_\zeta(\omega) \tag{2.25}$$

So, given a JONSWAP wave spectrum and vessel RAO's, the vessel motion spectrum is determined according to equation 2.25. Floating offshore installation vessels however have a dynamic positioning or DP system, in order to guarantee station keeping during installation operations. In paragraph 2.1.3.2 the principles of DP system are explained including their effect on the vessel motions.

#### *2.1.3.2 Dynamic Positioning and the effect on vessel motions*

A vessel has 6 degrees of freedom regarding motion in the water, when it is assumed to be a rigid body. 3 of these motions are translations and 3 are rotations as described in paragraph 2.1.3.1. The ship hydrostatic stiffness matrix ***C*** however is diagonal and has a zero value at 3 entries. This means that for three degrees of freedom, there is no restoring force or moment. These are the surge and sway translations and the yaw

rotation. With no restoring force, the vessel is only subjected to environmental loads and will therefore drift away in these degrees of freedom.

Dynamic positioning is an active way of station keeping in these degrees of freedom. Det Norske Veritas and other class societies defined a DP vessel as a vessel that maintains position and heading exclusively by means of active thrusters. Thrust is produced in different directions by propellers, tunnel thrusters and or azimuthing thrusters to obtain this position and heading keeping [38]. In this way a restoring force is created in the three degrees of freedom mentioned above.

A DP system consists of sensors, a reference system, a control system and a power and propulsion system. The sensors measure the vessel movement and compare it to the reference position and heading set. The control system then controls the power and propulsion system such that the difference between the measured and reference values are minimized.

An elegant, accurate and simple way of modeling a DP system is by a spring-damper representation [39]. In this way, the hydrostatic stiffness matrix $\boldsymbol{C}$ is added to the dynamic positioning stiffness matrix $\boldsymbol{C_{DP}}$. The latter matrix includes the restoring forces for the 3 degrees of freedom (surge, sway and yaw) in which it performs active position and heading keeping. A dynamic positioning damping matrix $\boldsymbol{B_{DP}}$ is added to matrix $\boldsymbol{B}$ to prevent overshoot of the position or heading after restoring. The appropriate values inside the dynamic positioning matrices are based on the dynamic positioning capabilities of the installation vessel. The vessel RAO's now become:

$$\overrightarrow{RAO}(\omega) = \frac{\vec{x}_a}{\zeta_a} = \frac{\vec{F}_0}{\left(-[\boldsymbol{M} + \boldsymbol{A}(\omega)]\omega^2 + \left(\boldsymbol{B}(\omega) + \boldsymbol{B_{DP}}(\omega)\right)i\omega + \boldsymbol{C} + \boldsymbol{C_{DP}}\right)} \tag{2.26}$$

#### *2.1.3.3 Crane tip motions due to vessel motions*

With the vessel motions due to the waves as determined in paragraph 2.1.3.1 and corrected for the position and heading keeping due to dynamic positioning as determined in paragraph 2.1.3.2, the vessel motions due to the waves are determined for the DP offshore crane vessel. These vessel motions are around the center of floatation which is the center of the water plane area of the vessel [40].

A vessel coordinate system is introduced and located in the center of floatation and also a coordinate system at the crane tip where the load is suspended, according to [41]. The center of floatation is the crane vessel coordinate system $I^S$ further denoted with superscript s. The crane tip or inertial coordinate system $I^E$ is denoted with superscript E. Figure 21 shows both coordinate systems.

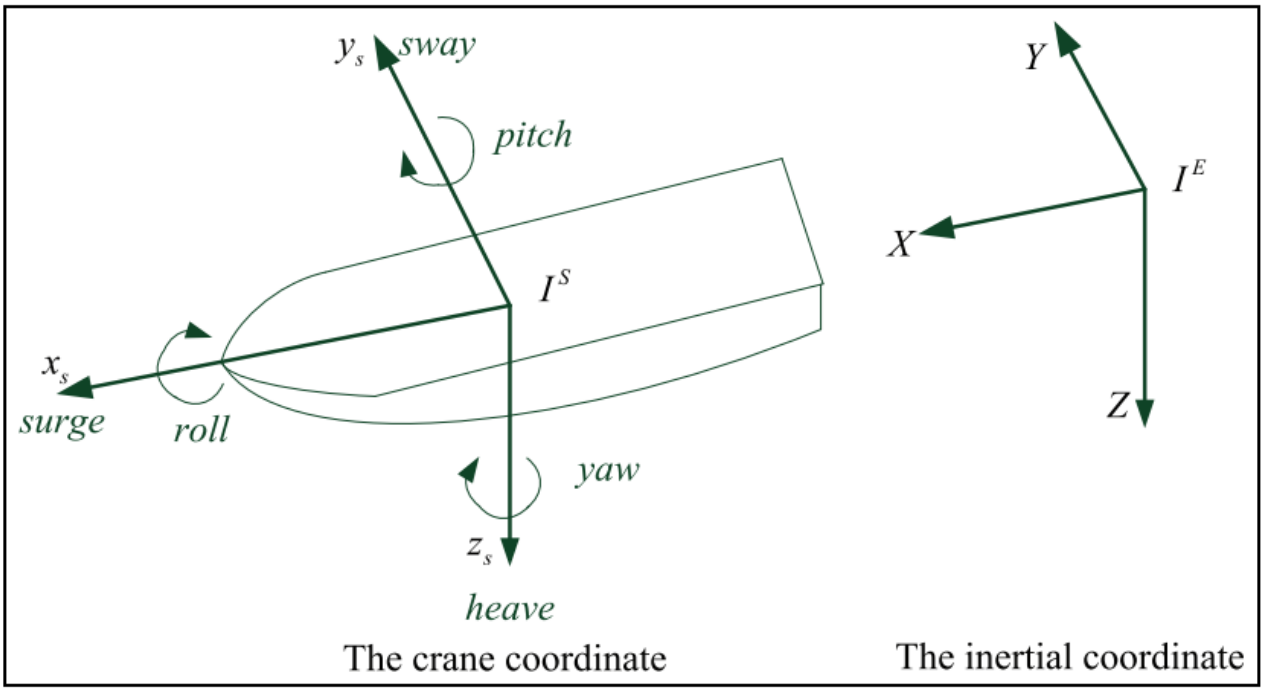


*Figure 21: The vessel and crane tip coordinate systems, according to Xiangguo, L. et al. (2017)*

Assuming that both the vessel and the crane are rigid bodies, there is a fixed distance between the crane tip and the center of floatation of the vessel. Written as a vector, this distance is:

$$\overrightarrow{x_{SE}} = \{x_{SE} \quad y_{SE} \quad z_{SE}\}^T \tag{2.27}$$

In accordance to [40] and Figure 20 the 6 DOF motions of the vessel, relative to an earth fixed coordinate system, are:

$$\overrightarrow{x_a} = \{x_a \quad y_a \quad z_a \quad \phi \quad \theta \quad \psi\}^T \tag{2.28}$$

The crane tip is a point and has therefore only 3 DOF. According to [42], the linearized motions of the crane tip in an earth fixed coordinate system are:

$$\overrightarrow{x_E} = \begin{Bmatrix} x_E \\ y_E \\ z_E \end{Bmatrix} = \begin{Bmatrix} x_a \\ y_a \\ z_a \end{Bmatrix} + \begin{Bmatrix} 0 & -\psi(t) & \theta(t) \\ \psi(t) & 0 & -\phi(t) \\ -\theta(t) & \phi(t) & 0 \end{Bmatrix} \begin{Bmatrix} x_{SE} \\ y_{SE} \\ z_{SE} \end{Bmatrix} \tag{2.29}$$

It should be noted that equation 2.29 is a time domain representation of the crane tip motions. An inverse Fourier transform is necessary in order to realize a time domain representation of the crane tip motions due to the DP vessel in waves.

### 2.1.4 Lifting and tugger ropes

For offshore lifting operations, there are two types of rope that are used. Fiber and wire rope. Fiber ropes consist of either natural or synthetic fibers. Wire rope consists of stranded steel wires. Both types of wires can only be loaded in tension, as for compression, the lines go slack. For offshore applications, fiber rope is mainly used for mooring applications and is not commonly used in offshore lifting operations.

It will therefore be assumed that only steel wire rope is used for the lifting operation of a WTG tower on its support structure. According to [43], steel wire rope can be represented by a linear axial spring-damper, where the stiffness *k* is equal to:

$$k = \frac{EA_{eff}}{L} \tag{2.30}$$

In which:

| | | |
|---|---|---|
| $E$ | = | Youngs Modulus of material |
| $A_{eff}$ | = | Effective area of wire |
| $L$ | = | Initial wire length |

The effective area of steel wire rope is found to be two third of the total cross section area of the rope, as stated by [44]. Dimensionless damping $\zeta$ of steel wire rope is:

$$\zeta = \frac{b}{b_{crit}} = \frac{1}{\sqrt{\left(1 + \left(\frac{2\pi}{\delta}\right)^2\right)}} \tag{2.31}$$

Where $b$ is the damping coefficient, $b_{crit}$ the critical damping coefficient and $\delta$ the logarithmic decrement. The logarithmic decrement follows from measuring two or more successive oscillatory peaks of elongation of the line. The logarithmic decrement is calculated as follows:

$$\delta = \frac{1}{n} \ln\left(\frac{x_i}{x_{i+2}}\right) \tag{2.32}$$

Where $n$ is the number of oscillations and $x_{i+2}$ is the upper peak following peak $x_i$ in the time domain representation of the amplitude of axial oscillations. [45] found that predicting an exact value for the damping of steel wire ropes is hard as it depends on many variables. It is a function of the function of amplitude, frequency and history of vibration. [46] states that the logarithmic decrement lies within a range of 0.02 to 0.20 for six strand and multi-strand wire ropes. It will therefore be assumed that the logarithmic decrement is 0.10, based on the findings of [43] and the dimensionless damping $\zeta$ is then 1.6%.

By representing the steel wire rope lifting and tugger lines as linear spring-damper elements, the physical behavior of the ropes is defined accurately. It should however be noted that this theory only applies for steel wire rope in tension. In compression, the lines go slack. Practice has shown that temporarily slack wires due to pendulum motions of the load in lifting operations lead to very high snapping loads afterwards and unpredictable behavior of the load and lifting arrangement.

## 2.2 Installation requirements

During installation of an offshore WTG tower, there are requirements that limit the WTG tower motions and collisions in installation. It should first be noted that this study focuses on one particular part of the installation and all requirements set therefore only affect this stage of the installation. All requirements affecting other stages of the installation are consequently not considered. As described in subsection 1.2.3 the focus of this research is placed on the lowering and catcher mating of the WTG tower on its support structure. It is assumed that the WTG tower is already aligned in the vertical direction with respect to the support structure. The lowering process as well as the first few collisions that take place between WTG tower catcher and support structure are assessed. The final landing and settling of the DSJ connection are also not incorporated.

Figure 22 shows an animation of an impact between WTG tower and its support structure during the lowering and mating phase of the installation. The white structure is the WTG tower with conical catchers in this example and the yellow structure is the support structure. The grey rings represent the DSJ connection. The tower is still suspended by the crane and lowered, while the first impacts between tower and support structure are made.

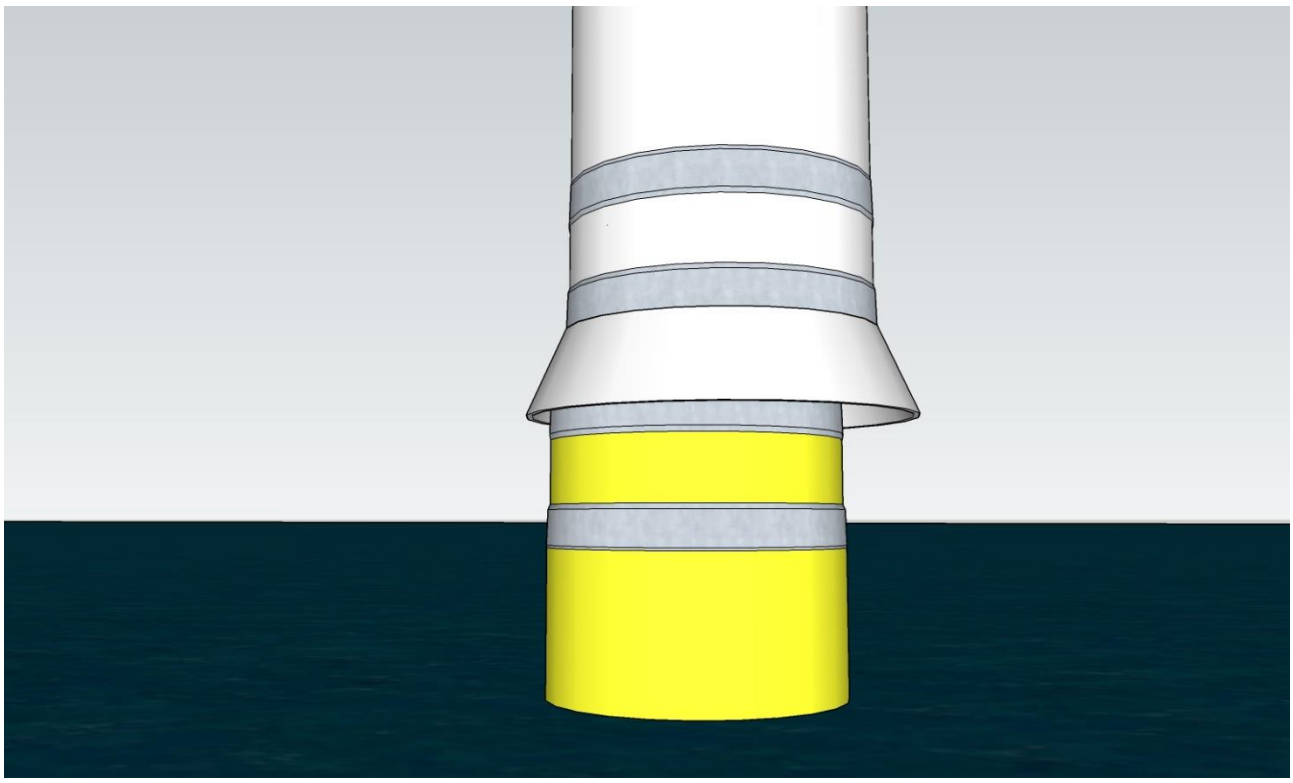

*Figure 22: Animation of an impact between WTG tower and its support structure during the lowering and mating phase of the installation*

The requirements regarding the aforementioned installation phases are based on critical or restrictive events that could occur. For all these events, limiting parameters will be identified in order to determine the allowable limits. These limits define the final installation weather window. Below, the critical and restrictive events are identified, and their limiting parameters and allowable limits are provided.

### 2.2.1 Allowable circular out-crossing rate

The circular out-crossing rate is the number of times per minute that the edges of the upper circumference crosses the edges of the lower circumference of the two mating parts. So, for installation of a WTG tower on its support structure, this is the number of times that the edge of the catcher on the WTG tower as in Figure 22 crosses the edge of the circumference of the top of the support structure per minute.

This criterion is defined by [24] in order to better assess safety during critical offshore installation activities. It states that a WTG tower could be successfully mated with its support structure if circular out-crossing rate is at most 2 times per minute. If this criterion stays within this allowable limit, a failed mating attempt can be prevented. This event is restricting on the installation weather window because higher waves lead to higher WTG motions and consequently a higher circular out-crossing rate. For any installation to be simulated in this research, the installation attempt will be classified as unsuccessful when the circular out-crossing rate exceeds its allowable limit of 2 times per minute. In subsection 5.1.6 it is explained how the circular out-crossing rate is monitored during the installation simulations.

### 2.2.2 Collision-induced structural damage

During the aforementioned stages of the installation operation, collisions occur naturally between the WTG tower and its support structure. Finite element analysis (FEM) is required of the collisions between the connecting parts of both structures to quantify the limiting parameters that define the allowable limits regarding collision-induced structural damage. In the installations analyzed in this research, catchers are used of different shapes and dimensions. For all types of catchers, the equivalent stresses resulting from contact with the support structure will be determined. A maximum contact force will be determined using safety

factors. The finite-element based determination of maximum contact force for this research is explained in the subsections 5.1.3 and 5.1.4.

### 2.2.3 Prevention of slack wires

Lifting and tugger lines can only be loaded in tension as for compression, the lines will go slack. This critical event is caused by excessive motions of the load (WTG tower) or could occur after the WTG tower has landed on its support structure. The criticality of this event is due to the occurrence of snapping loads after the lines tension again. The corresponding loads are very high and resulting motion are unpredictable.

For all WTG tower installation simulations, the tension in all lines will be calculated throughout the entire installation process in order to assess whether slack wires occur. Slack wires may only occur after successful landing, provided that they will not become tensile again due to the vessel motions. Therefore, in this research, an installation is deemed unsuccessful in the occurrence of slack wires. How slack wires are monitored during the simulations and how it is assessed whether this event occurs during installation is explained in subsection 5.1.1.

### 2.2.4 Maximum side-lead angle

The lifting line that hoists the WTG tower during installation hangs vertical in the absence of loading on the WTG tower. However, as a result of crane tip motions due to wind and waves and due to wind loads on the WTG tower, the lifting line angle varies in time. To ensure the structural integrity of the crane, this angle is allowed to be at most between 1 and 3 degrees according to industry representatives. In this research, this installation criterion is incorporated. In subsection 5.1.2, it is explained how in this criterion is incorporated in the installation simulations to ensure the integrity of the crane.

### 2.2.5 Axial impact prevention

During lowering of the WTG tower or due to heave motions of the installation vessel, the WTG tower could make an axial impact with the support structure. This could happen both between the bottom of the catcher and the MP or between the DSJ rings of the top of the MP and the bottom of the WTG tower. This is a critical event that leads to slack wires and potentially damaging concentrated loads on the axially colliding elements. In subsection 5.1.5 it is described how this criterion is monitored during installation simulations.

# 3

# Model development

Model simulations of WTG tower installation on its foundation (monopile or other) are key in assessing the limits in installation as outlined in the research objectives and methodology in subsection 1.2.2 and Figure 13. In chapter 2, the theoretical background is presented including physical phenomena involved in an installation operation. Besides, installation requirements were identified that limit the allowable motions and collisions in installation. This chapter describes the model setup and how physical phenomena are implemented. In the second section, it is described how non-linear contact forces of collisions between the WTG tower catcher and the top DSJ ring of a MP are obtained with finite element analysis. Subsection 2.1.1 showed a literature-based assessment of irregularities in collision responses. Section 3.3 investigates these irregularities using a simple model for collisions with an MP.

## 3.1 Model Description and implementation of physical phenomena

This section describes the model used for simulating the installation of a WTG tower on the MP. First a general model explanation is provided, after which the structural elements and physical properties included in the model are touched upon. This section is concise as the reasoning behind the modeling approach and physical phenomena involved are explained in chapters 1 and 2.

### 3.1.1 The model in general

The model calculates 3 DoF motions of the WTG tower in the time domain in 2D. The three degrees of freedom, visualized in Figure 23, are the horizontal and vertical translation and rotations around the CoG. A 2D approach is valid because the research focuses on lateral motions and collisions of the WTG tower as outlined in section 1.2. The time-domain motions, collisions, forces and other responses are obtained through numerical integration using Backward Euler integration.

The model provides time domain WTG tower motions in 3 DoF, forces in the lifting line as a function of time and contact forces. Also, a simulation is created to visualize the motions and collisions of the tower.

### 3.1.2 Model setup

The model setup is visualized in Figure 23. The WTG tower is the white conical structure that is hoisted at its top by a lifting line suspended at the crane tip. The WTG tower has catchers that collide with the yellow support structure. A close up of such collision is shown on the right in the figure. All structures and physical phenomena are briefly explained below, including how they are modeled.

*Modeling of the WTG tower*

A WTG tower has the shape of a hollow truncated cone. Typically, both the diameter and thickness of a WTG tower decrease over the height of the tower [47]. Therefore, the center of gravity or CoG of the tower is below the middle of the tower. This affects the inertia and motion behavior of the tower and therefore, it must be incorporated in the model. The CoG and moment of inertia around the CoG are

$$Z_{CoG} = \frac{\sum_i m_i z_i}{\sum_i m_i} \tag{3.1}$$

$$I = \sum_i m_i (z_i - z_{CoG})^2 \tag{3.2}$$

Where the tower is divided into *i* segments. $Z_{CoG}$ is the height of the CoG measured from the bottom of the WTG tower and $m_i$ and $z_i$ are the masses and midpoints of the tower segments.

Furthermore, the WTG tower is modeled as a rigid body and catchers are placed on the bottom of the tower to guide the tower over the support structure.

*Modeling of the lifting wire and crane tip excitations*

As shown in subsection 2.1.4, steel lifting wires can be modeled by a spring-damper to account for both stiffness and damping as a result of axial wire elongation. This is incorporated in the model. It is important to note that the lifting line can only be axially loaded in tension as for compression, the line goes slack. In the time-domain simulations of WTG tower motions, the absolute distance between crane tip and WTG tower top is determined in each time step and the corresponding wire force as a result from the wire stiffness is calculated. The time-derivative of this absolute distance is also calculated in each time step to calculate the wire damping force on the WTG tower. In the model, crane tip motions are harmonic and the frequency and amplitude for both horizontal and vertical directions can be varied independently. Subsection 2.1.3 provides a description of the origins of vessel and crane tip motions.

*Wind load and aerodynamic damping modeling*

Subsection 2.1.2 described offshore wind fields and corresponding wind loads on a WTG tower. In the model, the wind load and aerodynamic damping is calculated as a distributed load over the height of the tower. Just as for the calculation of the CoG and the inertia, the tower was segmented into *i* segments and for each segment, the wind force is determined in each time step. The total wind force and wind-induced moment on the tower are determined accordingly in each time step. The wind field is based on a time domain wind spectrum realization as described in subsection 2.1.2.

In subsection 2.1.2 it is also described how the wind velocity relative to the WTG tower motions lead to aerodynamic damping. Aerodynamic damping is caused both due to the horizontal translations and rotations of the WTG tower. Both sources of aerodynamic damping are incorporated in the model.

*Collision modeling*

Collisions are modeled by conditional non-linear spring-dashpots. Conditional in this context means that if any point on the catcher crosses with any point on the monopile, there is contact, and a restoring force is exerted on the WTG tower. The contact force consists of both a damping and a spring term. The damping term accounts for the fact that a part of the kinetic energy before collision will be transferred into decaying vibrations after the collision for both the WTG tower and the support structure. In order to quantify the stiffness and damping coefficient, finite element analysis is necessary. This is described in section 3.2. Section 3.3 describes the irregularities in collision responses to be expected when the WTG tower or monopile vibrates and a collision takes place.

*Concluding remarks on the model setup*

The model allows for the use of different catchers for installation. In this research, conical catchers as well as vertical asymmetric catchers are analyzed. In the subsections 5.1.3 and 5.1.4 both catchers are explained. In

these sections, a finite element analysis-based determination of their maximum contact forces during collisions is provided.

Also, the model allows for using tower guidance in the form of constant forces, springs, or dampers to represent tugger lines to guide the WTG tower during lowering towards its foundation. Besides, the model incorporates horizontal crane tip displacements caused by the crane operator. In the sections 5.2 and 5.3 the effects of these displacements and the use of tower guidance on the WTG tower installation are studied.

The motions of the WTG tower in the model are not linearized. Non-linearities exist in the model with different causes. First of all, collisions between the WTG tower and the foundation are non-linear. Collisions are modeled by a spring-damper in which the spring is non-linear. In section 3.2 the non-linearity of the contact element is determined. Collisions are also a cause of non-linearity in the model because they lead to a sudden change in the system. To be more specific, a collision induces a temporary reaction force on the WTG tower that is not present during the entire installation (i.e. there is no constant contact between the WTG tower and the foundation during installation). Another source of model non-linearity is found in the angles of the WTG tower and lifting line length during installation. This however has a small effect on the WTG motions, since the angles of the WTG tower and the lifting line remain small.

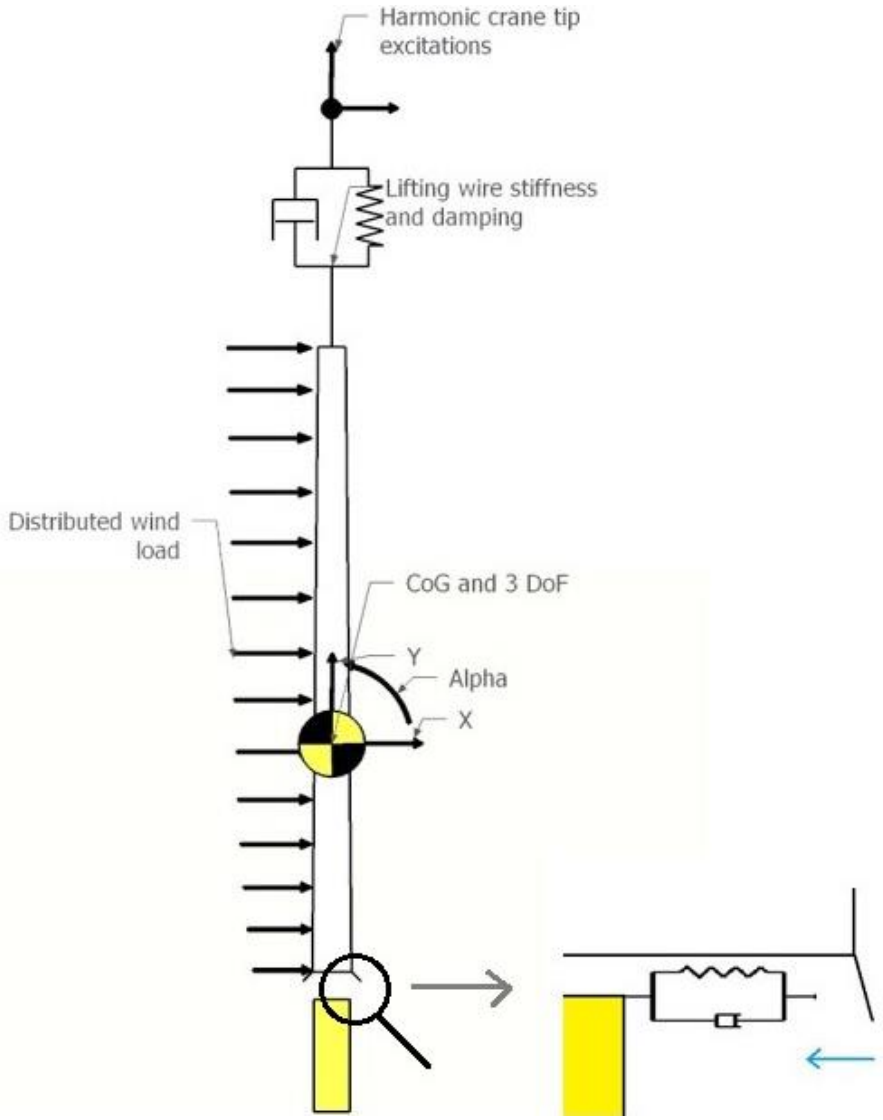


*Figure 23: Overview of the model as used in the simulations, including physical representations for wind load, crane tip, the lifting wire and a close up of how collisions are modeled.*

## 3.2 Finite element analysis-based determination of contact stiffness

Section 2.1.1 provided a literature-based background on collisions. It was found that it is common practice in offshore wind installation research to simply assume values for stiffness and damping in collisions. Research in other fields proved that collision responses are complex and that a simple assumption on response behavior is inaccurate. In order to get an accurate understanding of collision responses, finite element analysis is required. In this research, finite element analysis is performed in ANSYS to describe the values of stiffness and damping. Bending and vibrations of the WTG tower and the MP are the first source of stiffness and damping. The local deformation of the DSJ ring on the top of the MP is the second source of stiffness. The determination of both sources of stiffness and damping are explained below.

A slender EB beam model is used to model the WTG tower and the MP. In this model, the MP is fixed at its bottom (the seabed) and the WTG tower is suspended by the lifting line with a stiffness and damping as described in subsection 2.1.4. An EB beam model with *n* and *m* elements for the WTG tower and the MP is made such that the bottom element of the WTG tower comes into contact with the top element of the MP. Figure 24 visualizes this situation as it would be in reality, where the catcher is omitted for clarification purposes. With an annulus of 25 mm and a horizontal velocity of 0.5 m/s, a collision between the rings occurs after 0,05 s. In Figure 24 this can be best understood by looking at the right picture. The outer ring collides with the inner ring on the right. The WTG tower and the monopile are modeled as Euler-Bernoulli beams or EB beams. This way of modeling incorporates the global vibration behavior of both structural elements as a result of the collision. Both the MP and WTG tower are subdivided into *n* and *m* elements respectively and the masses and stiffnesses of each element comply to the local geometry of the MP or WTG tower at that location. To be more specific, the mass and stiffness of the WTG tower varies with the height due to diameter and thickness variations and as such, the vibration behavior depends on these geometrical properties. This is included in the model.

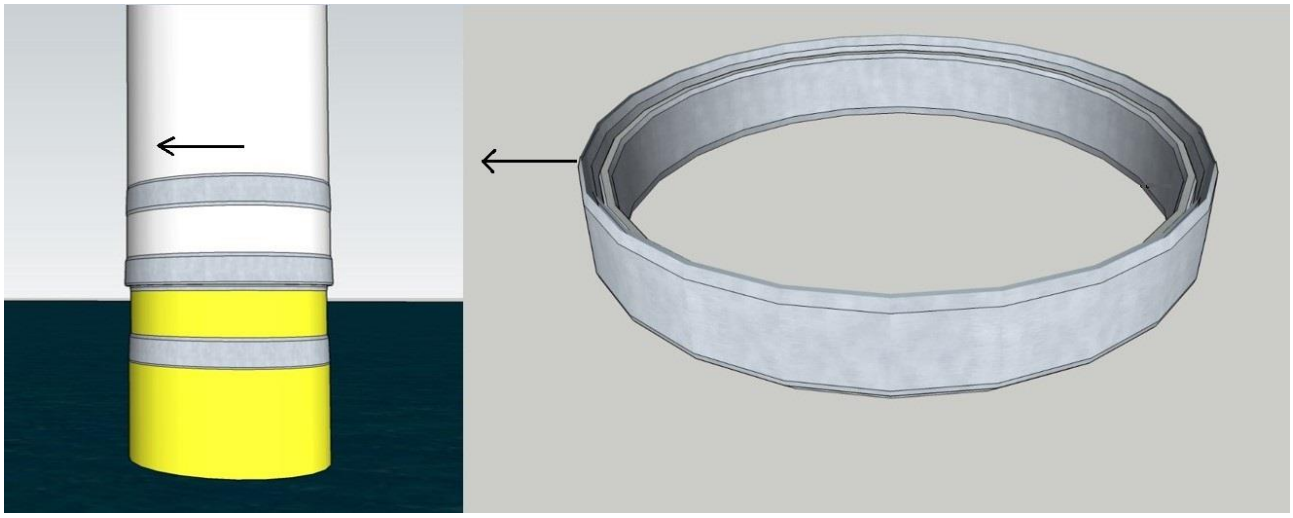

*Figure 24: Visualization of the situation analyzed in ANSYS for obtaining collision responses*

Figure 24 provides a good visualization of how the collision would look like in reality. But it must be noted that the EB-beam model does not include local stiffness (e.g. ovality or out of roundness). The EB-beam model only determines the TD deflections over the height of both structures relative to the longitudinal axis of both structures. The contact stiffness and damping due to bending and vibration of the WTG tower and MP is determined with the contact forces between the bottom WTG tower and the top of the MP and the horizontal deflection at that location relative to the undeformed situation. Section 4.1 shows the results of this analysis, describes the corresponding stiffness and damping and how this model is used to validate the simulation model.

An EB-beam model does not include local stiffness (e.g. ovality or out of roundness). The local stiffness is characterized by the deflection of the DSJ ring on top of the MP as it is in contact with the catcher on the bottom of the WTG tower. Figure 25 visualizes this contact.

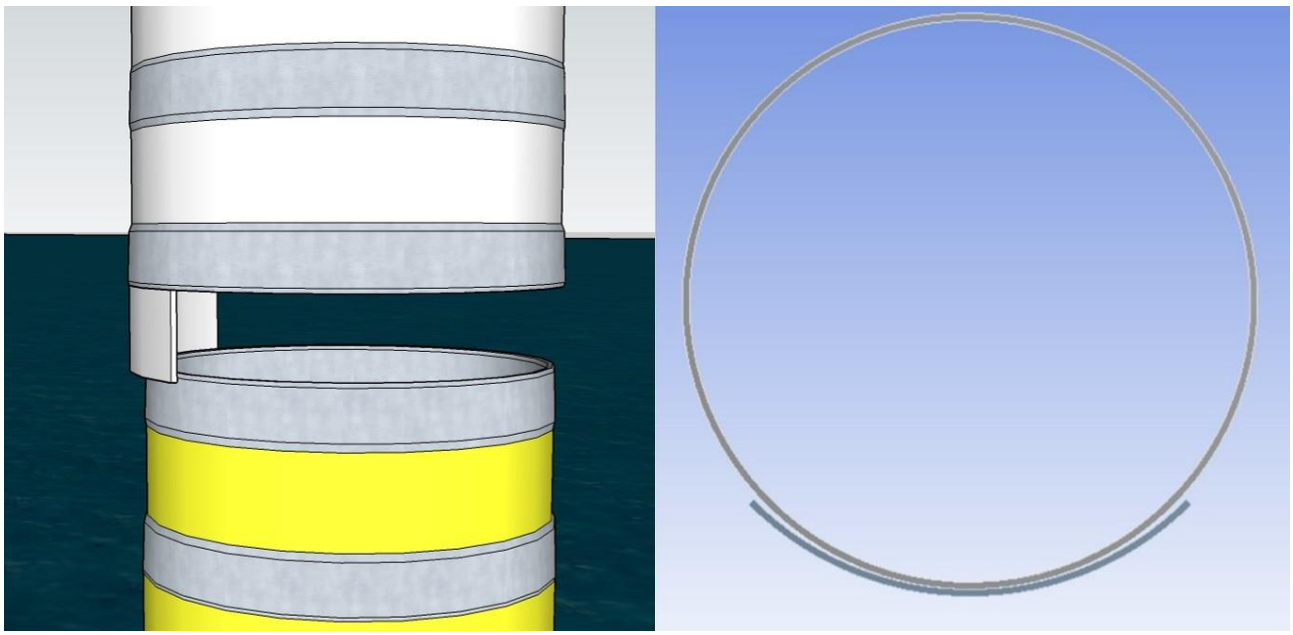

*Figure 25: Visualization of contact between the catcher on the bottom of the WTG tower (white) against the top DSJ ring of the MP (yellow)*

It is important to note that the catcher has a radius that is slightly larger than the radius of the DSJ ring. Figure 25 shows that for an undeformed DSJ ring, contact with the catcher is concentrated at a point. However, as the contact force increases between the catcher and the DSJ ring, the contact area increases as the DSJ ring deforms. The consequence of this increasing contact area is that the local contact stiffness is non-linear. Finite element analysis is used to determine the non-linear local contact stiffness. Different scenarios have been analyzed in ANSYS in which the DSJ ring had a constant outer and inner radius of 4 and 3.9 m, respectively. The inner radius of the catcher changes in the three scenarios between 4.05, 4.15 and 4.25 m. The resulting non-linear contact forces found in these three different scenarios are plotted in Figure 26.

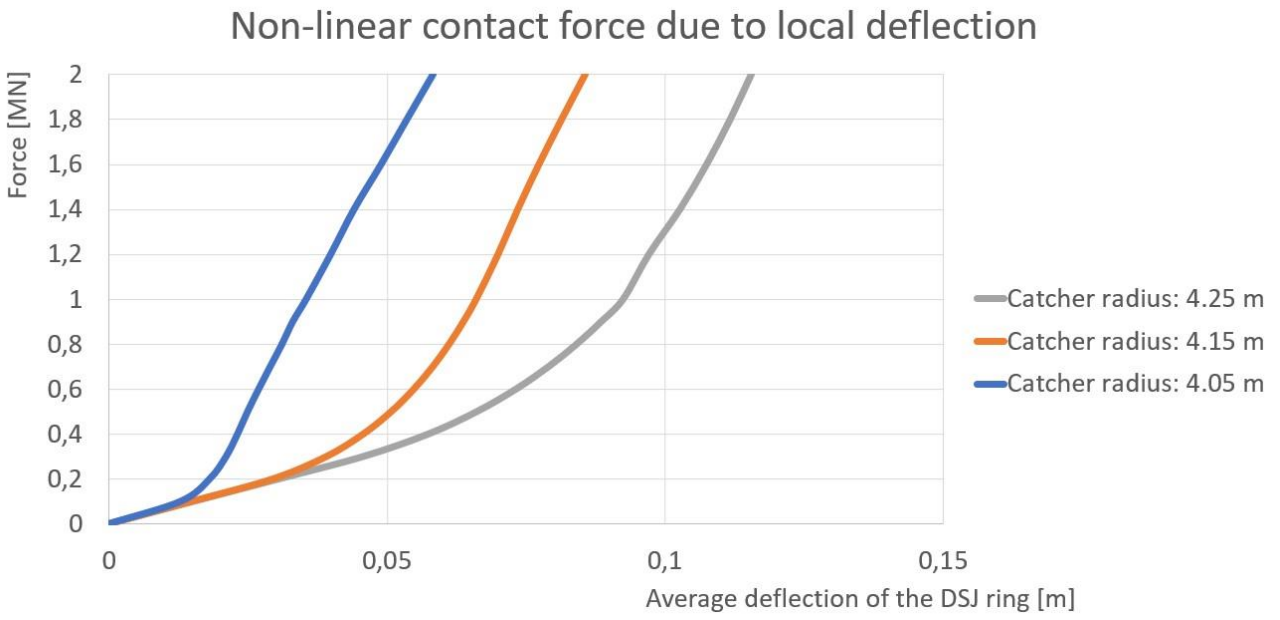


*Figure 26: Non-linear local contact force against the average deflection of the DSJ ring for various catcher radii.*

With both the non-linear local stiffness and the linear bending stiffness determined, the equivalent stiffness can be determined. The equivalent stiffness results from the both the bending stiffness and the local stiffness being connected in series (i.e. the force in both springs is equal, whereas the deflection is not). Figure 27 shows this equivalent stiffnesses for the different catcher radii analyzed.

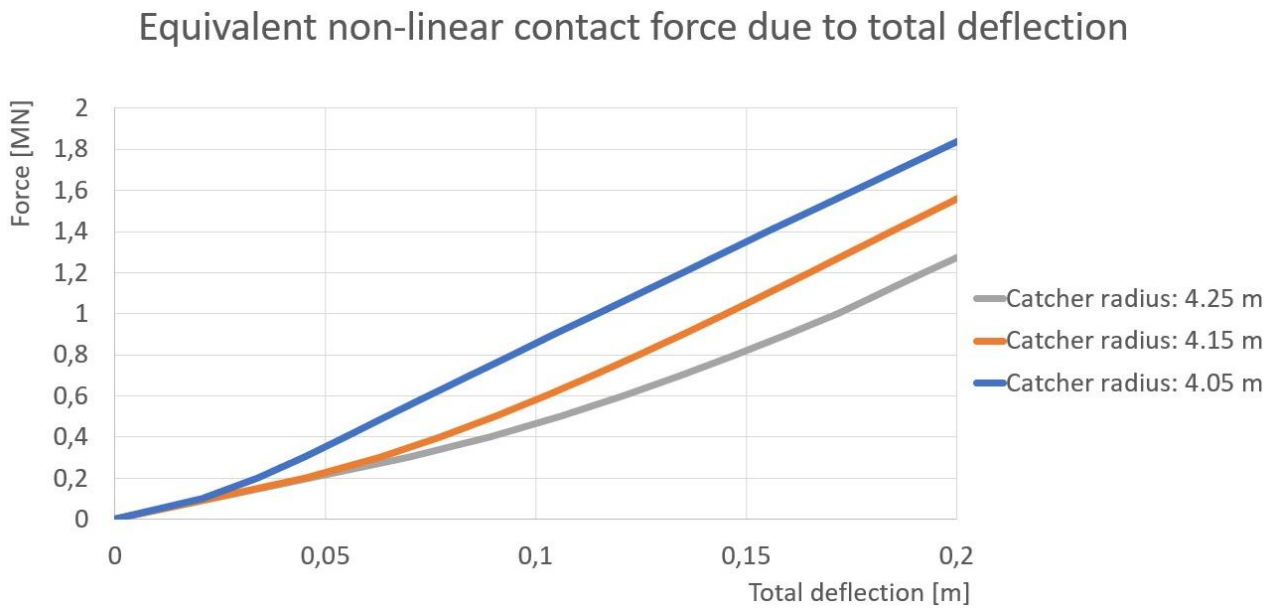


*Figure 27: Equivalent contact stiffness for different catcher radii consisting of non-linear local stiffness and linear bending stiffness*

In order to implement the non-linear contact stiffness in the model used to simulate the installation of a WTG tower onto its foundation, an equation has been defined to describe the non-linear stiffnesses as in Figure 27.

$$F_{eq}(x) = Ax + B(\tanh(Cx + D) + \tanh(D)) \tag{3.3}$$

In which $F_{eq}(x)$ is the equivalent contact stiffness as a function of the deflection $x$. The constants $A$, $B$, $C$ and $D$ depend on the catcher radius:

| CONSTANT | R = 4.05 M | R = 4.15 M | R = 4.25 M |
|---|---|---|---|
| ***A*** | 4.8 | 4.37 | 4.32 |
| ***B*** | 0.55 | 0.65 | 0.5 |
| ***C*** | 12 | 10 | 10 |
| ***D*** | 1.4 | 1.9 | 2.2 |

*Table 1: Constants associated with equation 3.3 that describes the non-linear equivalent contact stiffness as a function of the deformation*

The description of this catcher radius specific non-linear stiffness is implemented in the model to simulate the installation of a WTG tower onto its foundation. In subsection 2.1.1, it is described that it is common practice in offshore literature to simply assume constant values for contact stiffness and damping. This section describes a way to describe these values more realistically by subdividing the equivalent stiffness into global bending stiffness and local deflection stiffness, which are considered as springs connected in series.

In the aforementioned subsection, it also appeared from a study to church bells, that collisions in a vibrating system do not necessarily have to be described by a single contact event. Also, a certain irregularity appears in the collision responses (i.e. there is some variability in velocities after relative to before collisions). Subsection 3.3 describes how a simple model is developed to study these effects on collisions between a rigid body and a MP.

## 3.3 Irregularities in collision responses: A simple model

In subsection 2.1.1 collisions between a WTG tower and its support structure were discussed from a theoretical point of view. It was shown that in the literature regarding offshore installations, it is common practice to assume values for stiffness and damping, often without much substantiation. Research in the field of church bells however showed that collision responses are often irregular. The irregularity was much higher when the bell vibrated before a collision. Of course, a church bell and its clapper are not equivalent to a monopile and the WTG tower in installation. Therefore, a simple collision model is set up to analyze collision responses and corresponding irregularities in collisions between the WTG tower and the monopile during installation. This section is subdivided into two subsections. Subsection 3.3.1 introduces the simple model and explains the collision responses for an undamped non-vibrating monopile. The following subsection introduces damping against vibration in the monopile and studies the collision responses as well as the effects of monopile vibrations on subsequent collision responses. The final subsection 3.3.3 discusses the applicability of the results of this simple model to collisions between a WTG tower and a MP.

### 3.3.1 Collision responses for an undamped non-vibrating monopile

For this simple model, the assumption is made that the monopile is a fixed-free Euler-Bernoulli beam that is excited in its first mode of vibration when a rigid body impacts the pile at its free end. It is also assumed that collisions are perfectly elastic and that the vibrations of the monopile are undamped. Using these assumptions, the modal stiffness, first natural frequency, and corresponding modal mass of the monopile are:

$$k_{MP} = \frac{3EI}{L^3} \tag{3.4}$$

$$\omega_{MP} = \left(\frac{1.8751}{L}\right)^2 * \sqrt{\frac{EI}{\rho}} \tag{3.5}$$

$$M_{MP} = \frac{k_{MP}}{\omega_{MP}^2} = 0.295441\rho L \tag{3.6}$$

Under the assumption that the monopile is only excited in its first mode of vibration due to impact, the undamped monopile can be described by a mass-spring system as depicted in Figure 28. In this figure, *M* is the mass and *V* is the velocity of the rigid body. The monopile is at rest initially. The damping coefficient $c_{MP}$ is 0 Ns/m for this undamped monopile.

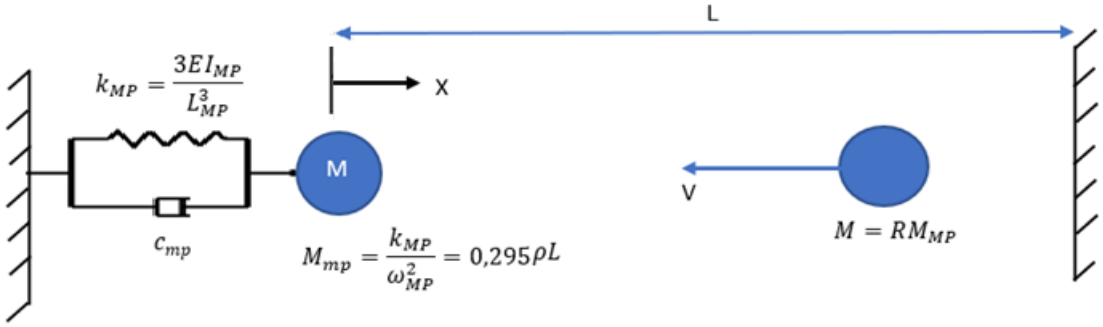


*Figure 28: Monopile representation as a mass-spring system. A rigid body with mass M and velocity V will impact with the top of the monopile*

Using conservation of momentum and conservation of energy, the velocities of both bodies following a perfectly elastic collision, and consequently using a restitution coefficient of 1, can be determined. For conservation of momentum:

$$M_{MP}V_{MP,i} + MV_i = M_{MP}V_{MP,f} + MV_f \tag{3.7}$$

$$V_{MP,i} + RV_i = V_{MP,f} + RV_f$$

$$\boldsymbol{R(V_f - V_i) = V_{MP,i} - V_{MP,f}}$$

For conservation of energy:

$$\frac{1}{2}M_{MP}V_{MP,i}^2 + \frac{1}{2}MV_i^2 = \frac{1}{2}M_{MP}V_{MP,f}^2 + \frac{1}{2}MV_f^2$$

$$V_{MP,i}^2 + RV_i^2 = V_{MP,f}^2 + RV_f^2$$

$$RV_f^2 - RV_i^2 = V_{MP,i}^2 - V_{MP,f}^2$$

$$\boldsymbol{R(V_f - V_i)(V_f + V_i) = (V_{MP,i} - V_{MP,f})(V_{MP,i} + V_{MP,f})} \quad (3.8)$$

Combining equations 3.7 and 3.8 yields:

$$V_{MP,f} = \frac{2RV_i + V_{MP,i}(1-R)}{R+1}$$

$$V_f = V_{MP,i} - V_i + \frac{2RV_i + V_{MP,i}(1-R)}{R+1} \quad (3.9)$$

Where $R$ is the ratio of masses $M$ and $M_{MP}$, $V$ and $V_{MP}$ the corresponding velocities and subscripts $f$ and $i$ represent the final and initial velocities, respectively. Except for the collisions, there is no restoring force on the rigid body. The monopile however has a stiffness which is represented by a spring as seen in Figure 28.

Using the assumption of a perfectly elastic collision in this problem, the collisions are consequently an instantaneous event. They are solved for the final velocities of both bodies using the equations above. The time dependent motions are solved using a Backward Euler time integration to assess the problem given in Figure 28 and described above, the results confirm the findings of [25]. When varying the mass of the incoming rigid body, the results show that the velocity ratio of the rigid body before and after the impact vary with the mass ratio. The mass and velocity ratio in this simple model are respectively defined as:

$$R = \frac{M}{M_{MP}} \quad (3.10)$$

$$\Delta V = \frac{V_i}{V_f} \quad (3.11)$$

Figure 29 and Figure 30 show the velocities of the tip of the monopile and the rigid body as a function of time. The orange line represents the tip speed of the monopile, and the blue line represents the rigid body velocity. Energy is conserved as can be seen the grey line in both figures. This represents the energy balance, or the mass normalized kinetic energy added to the mass normalized potential energy. The variations that do occur are an error resulting from the Backward Euler numerical time integration. However, this error appears to cancel out in the harmonic motions and consequently, the error does not build up in time and the energy in the system remains constant on average. Figure 29 shows the velocity profiles of both bodies for

mass ratio $R$ = 0.6. Figure 30 shows the velocity ratios of both bodies for mass ratio $R$ = 2.6. All discontinuities in both charts represent an impact between the bodies.

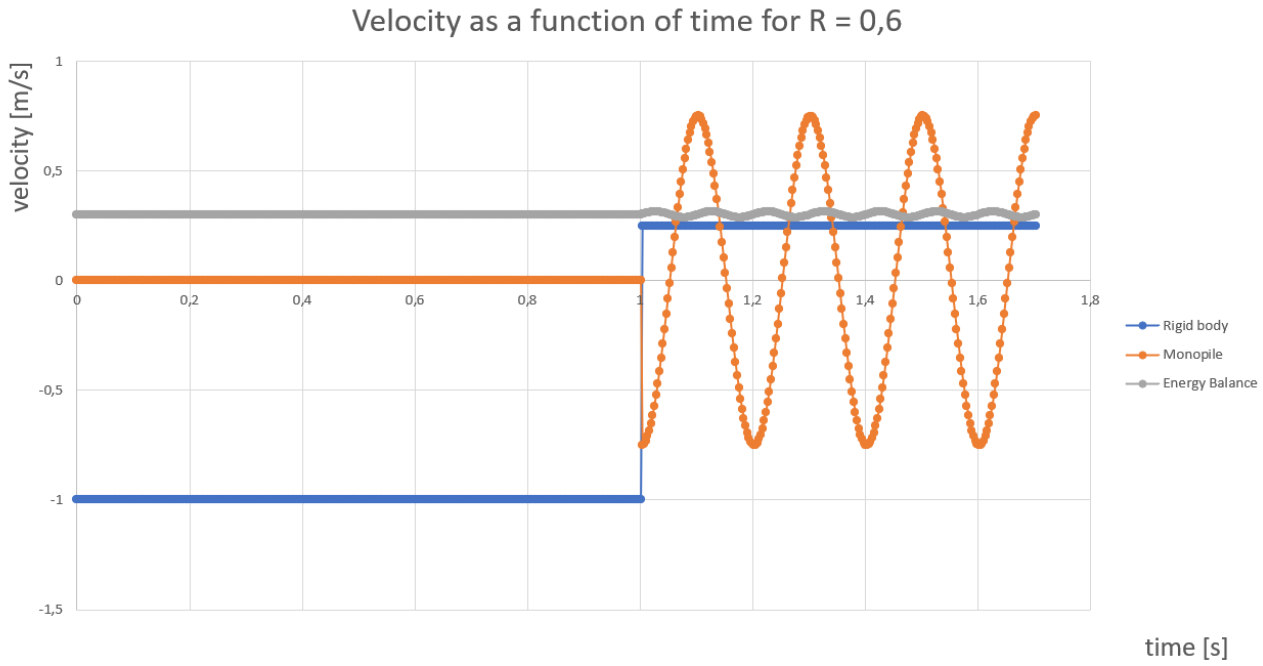


*Figure 29: Velocity profile as a function of time for the rigid body and the undamped monopile using a mass ratio of 0.6*

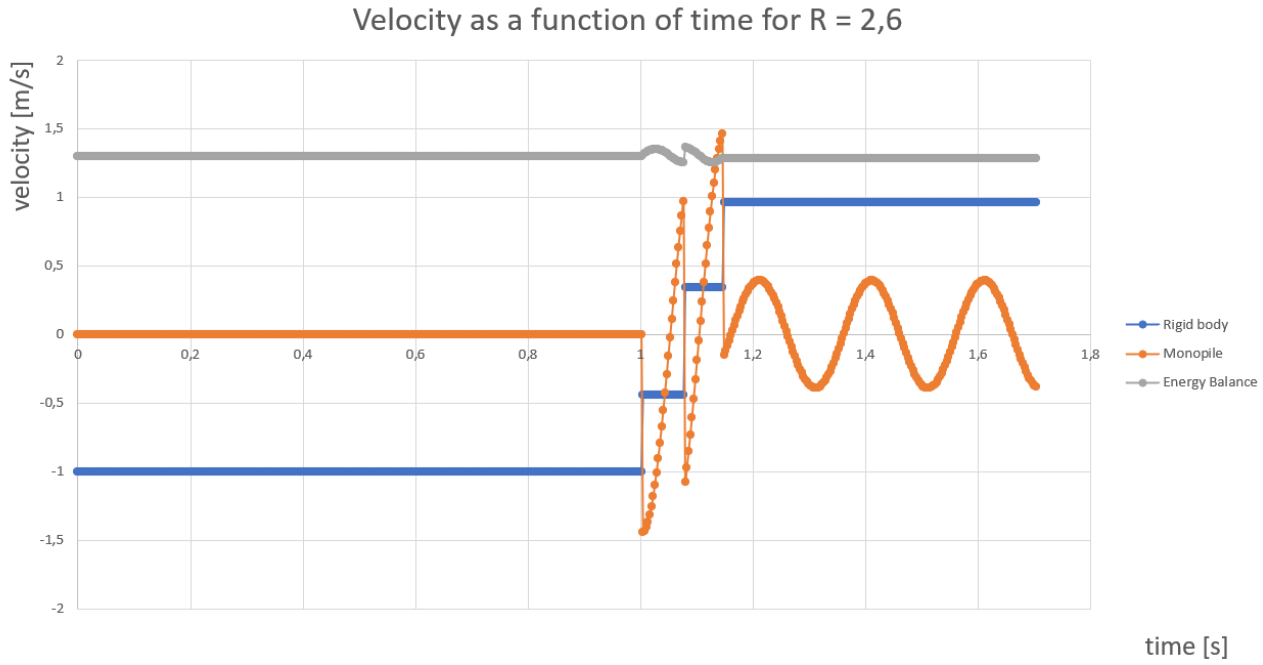


*Figure 30: Velocity profile as a function of time for the rigid body and the undamped monopile using a mass ratio of 2.6*

From Figure 29 and Figure 30 a few conclusions can be drawn:

- In both cases, the initial velocities are the same. The rigid body has an incoming velocity of 1 m/s and the tip velocity of the monopile is 0 m/s. However, their final velocities differ significantly. For $R$ = 0.6, only 25% of the initial velocity is left in the rigid body. This means that around 90 % of its initial kinetic energy is finally transferred into vibrations of the monopile. If $R$ = 2.6, the final velocity of the rigid body is 96% of the initial velocity and as such, it has transferred just 8 % of its initial kinetic energy to the vibrations of the monopile. Clearly, energy transfer between the two bodies in this simple collision model is all but constant.

- The impact between rigid body and monopile, under the assumptions made, is not necessarily represented by 1 bounce. It can be seen that for $R$ = 0.6, the impact consists of 1 instantaneous bounce. For $R$ = 2.6, the impact consists of 3 instantaneous bounces, all occurring after each other in a time domain of little more than 0.1 s.

To create insight in the final kinetic energy transfer from the rigid body to the monopile and the velocity ratio of the final velocity divided by the initial velocity of the rigid body, Figure 31 is created. In this figure, the black line is the velocity ratio as a function of mass ratio of the rigid body and the orange line represents the total kinetic energy transfer from rigid body to monopile as a function of the mass ratio. The red lines correspond to the mass ratios used in Figure 29 and Figure 30. Every discontinuity represents an added collision in the system before the rigid body returns towards infinity. Corresponding values are presented on the left and right vertical axes respectively.

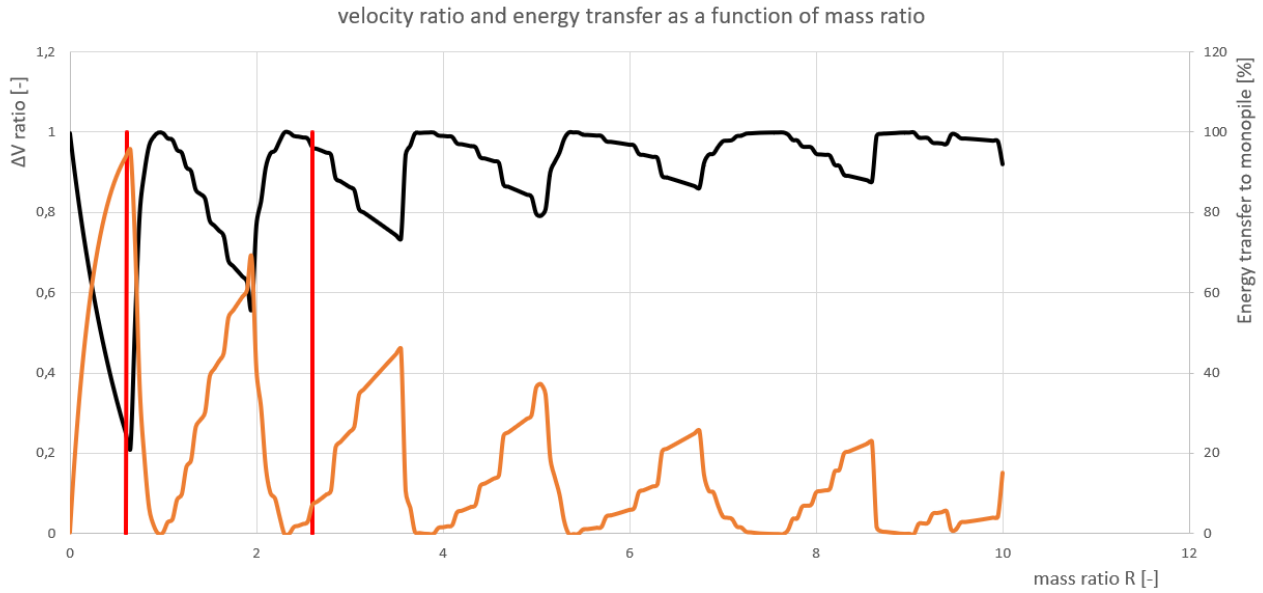


*Figure 31: Velocity ratio (black) and energy transfer (orange) as a function of mass ratio*

In reality, the response of a monopile to an impact cannot be represented by the first mode of vibration only. Nor can the assumption be made that the collisions are perfectly elastic. However, even with a simple model, a great level of complexity is found in physically describing the responses of a collision. The following subsection continues with the simple model as in Figure 28. The collision responses are determined for vibrating systems and damping against vibration is also introduced. After that subsection, a conclusion will be made with regards to the applicability of these simplified model results to this research.

### 3.3.2 Irregularities in collision responses for a damped vibrating monopile

The simple model introduced in the previous subsection is extended and generalized in order to study the effects of vibrations on collision responses. Figure 32 shows this model. There are two masses $M_1$ and $M_2$ and a mass ratio of $R = M_2/M_1$. Body $M_1$ has a spring and damper attached to it with a stiffness and damping coefficient $k$ and $c$, respectively. The free body $M_2$ has an initial incoming velocity $V$. A wall is placed at distance $L$.

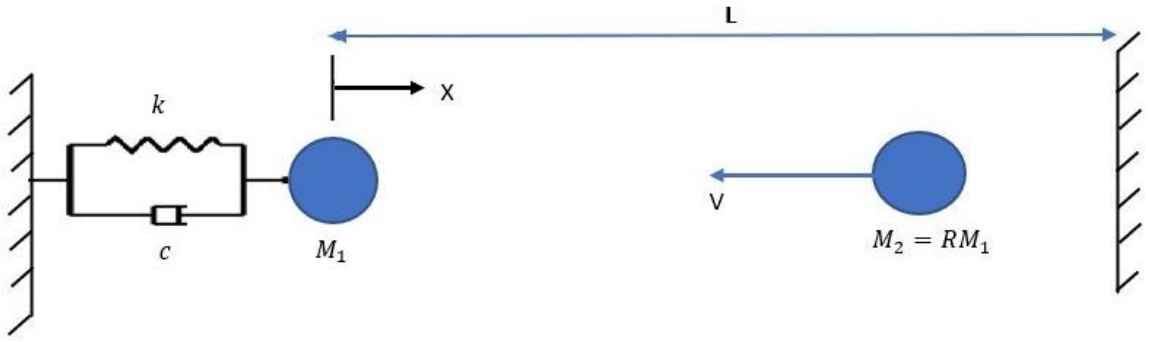


*Figure 32: Generalized simple collision model*

As in the previous section, the stiffness *k* and mass $M_1$ correspond to the first modal stiffness and mass of the monopile given in equations 3.4 and 3.6. All collisions of $M_2$ with $M_1$ or the wall are perfectly elastic, so the coefficient of restitution is 1. Three variables are introduced in the system:

- Damping *c* [Ns/m]. The damping coefficient is a variable in the analysis. In order to make the analysis accurate for WTG tower installation collisions, it is assumed that the monopile is underdamped. Values for the damping coefficient used are 0, 50000, 100000 and 150000 Ns/m. For these values, monopile vibrations decay in amplitude by between 0% and 60% in one second.
- Mass ratio *R* [-]. The mass ratio is a variable in the analysis as well. As shown in the previous subsection a small change in mass ratio can have large variations in velocity responses due to the occurrence of multiple bounces for higher mass ratios. Therefore, the mass ratio *R* used for the analysis ranges between 0.01 and 10 with steps of 0.01. 1000 different mass ratios are analyzed.
- In order to study the effect of the phase of harmonic motion of $M_1$ after the first collision, the wall length *L* is varied as well. The wall length is varied between 1.085 and 1.115 m, with steps of 0.002 m. In this range, it is determined that at least 3 periods of $M_1$ motions are spanned. Therefore, the effect of wall distance or $M_1$ phase shift is fully incorporated to study the effects on outgoing velocities $V_2$ and $V_3$.

There are four velocities that are of importance. The first velocity *V* is the initial incoming velocity before any collision took place. Velocity $V_1$ is the velocity after the first collision of both masses. Note that a collision can consist of multiple bounces and that $V_1$ is measured when the free body returns to the wall after the full first interaction with the mass-spring-damper. Velocity $V_2$ and $V_3$ are the velocities of the free body after the second and third interaction with the mass-spring-damper, respectively. Below, for the aforementioned three velocities, the dependence on the mass ratio and damping coefficient are explained. For clarification purposes, graphs are in Appendices B and C.

*Velocity $V_1$*

For the wall distance averaged mean velocity $V_1$ as a function of mass ratio, presented in Figure B. 1 of Appendix B, the situation without damping is familiar. This blue line is the situation as presented in subsection 3.3.1. The orange, grey and yellow line represent the velocities with a damped MP with a damping coefficient of 50,000, 100,000, and 150,000 Ns/m respectively. For the wall distance averaged mean velocity $V_1$, a few conclusions can be drawn.

- Before the first discontinuity at $R \sim 0.65$, damping has no effect on the response. This can be explained due to the fact that below this value, a collision consists of a single bounce. As a result of the assumption of perfectly elastic collisions, this bounce is an instantaneous event. Damping plays therefore no role. For higher mass ratios, damping does play a role for $V_1$. This is because multiple bounces represent the collision. Between these instantaneous bounces, damping affects the velocity of mass $M_1$ and therefore, it affects bounces except the first one in a single collision.

- On average, $V_1$ decreases for increasing values for damping when the mass ratio $R > 0.65$. This can be explained due to the fact that kinetic energy drains from $M_1$ before the last bounce occurs. It can be seen therefore, that $V_1$ for a damped system is less than 100% of the initial velocity $V_0$.
- It is interesting to observe that for increasing damping and mass ratios of $R > 5$, multiple collisions tend to happen for lower $R$. This can be seen as a horizontal shift in Figure B. 1 in Appendix B in the discontinuities that represent an added bounce.

*Velocity $V_2$*

First, it should be noted that Figure B. 2 in Appendix B represents the mean velocity $V_2$ as a function of mass ratio $R$. The mean is taken over all outcomes $V_2$ for different wall distances. The graph contains these results for 4 different values for damping as mentioned before. So, before looking at the wall distance induced irregularities, a few conclusions on the mean velocity $V_2$ can be drawn.

- Clearly, not only the wall distance induces irregularities in velocity $V_2$. For the undamped situation (blue line), great variations are seen for incremental changes in the mass ratio. This effect is especially strong for mass ratios of $R < 2$. For increasing damping coefficients, there appear to be less irregularities in $V_2$ resulting from variations in the mass ratio.
- Without damping, the mean $V_2$ does not drop to close to 0, like with $V_1$ for mass ratio $R \sim 0.65$. With increasing damping however, this effect occurs again with $V_2$. An explanation for this effect is that for increasing damping, the mass-spring-damper is almost at rest before the second collision and the response converges to the response for $V_1$ albeit at a lower final velocity.
- On average, the wall distance averaged mean $V_2$ decreases for increasing damping values.

*Velocity $V_3$*

First, it should be duly noted that Figure B. 3 in Appendix B represents the mean velocity $V_3$ as a function of mass ratio $R$. The mean is taken over all outcomes $V_3$ for different wall distances. The graph contains these results for 4 different values for damping as mentioned before. Before looking at the wall distance induced irregularities in the next section, a few conclusions can be drawn on the mean velocity $V_3$.

- It should be noted first that some data is missing in Figure B. 3 of Appendix B. This concerns the damped (orange, grey and yellow) situations with a mass ratio $R \sim 0.65$. Due to the very low velocities $V_1$, $V_2$ and $V_3$ at these mass ratios, the collision resulting in $V_3$ occurred after a longer time than calculated in the model.
- For the undamped situation (blue line), great variations in the mean $V_3$ are seen for small changes in the mass ratio. Clearly, mass ratio variations also induce irregularities for the mean velocity $V_3$. The variations reduce for increasing damping against vibration.
- The mean $V_3$ declines on average for increasing damping coefficients.

*Wall distance induced variations in the velocities*

The previous section focused on the wall distance averaged mean values for $V_2$ and $V_3$. This section focuses on the variations of the velocities $V_2$ and $V_3$ as induced by the wall distance variations. Graphs related to this subject can be found in Appendix B. For these analyses, the velocities $V_2$ and $V_3$ are used. In Appendix C, the first 4 graphs relate to velocity $V_2$ for different damping conditions and the final 4 graphs relate to velocity $V_3$ for different damping ratios.

It should be noted here that in the graphs, the wall distance averaged mean velocities are presented. The variations induced by the wall distance are presented by the minimum and maximum velocities in the set of different wall distances, indicated by the black line. A few conclusions on the standard deviation or wall distance induced velocity variations can be drawn.

- Wall distance induced velocity variations decrease for increasing mass ratios. This effect is stronger for the undamped cases than the damped cases. This applies to both $V_2$ and $V_3$.

- The minimum and maximum velocities $V_2$ and $V_3$ in the set of wall distances for a certain damping coefficient as a function of mass ratio is not smooth. Apparently, wall distance induced velocity variations differ significantly for different mass ratios. These irregularities seem to coincide with mass-ratio induced irregularities in the velocities.
- The wall distance induced variations for the velocity $V_3$ are greater than for $V_2$ for all damping cases and mass ratios.

### 3.3.3 Concluding remarks and applicability of simple collision model

Based on the results presented and discussed above, it is clear that both the mass ratio and the time between consecutive collisions result in irregular response velocities for collisions in vibrating systems. Put simply, accurate prediction of responses is difficult. It can be concluded that collision responses in vibrating systems are only statistically predictable within a certain range of accuracy.

However, the simple model used here contains some assumptions that cannot be straightforward applied to collisions between WTG towers and monopiles. First of all, collisions are assumed to be perfectly elastic (i.e. a coefficient of restitution of 1). Secondly, it is assumed that the monopile is excited in its first mode only. Finally, the WTG tower is simplified to a rigid body. Due to these assumptions, it was possible to shed a first light on vibration-induced collision response irregularities. However, as these assumptions do not necessarily apply in reality, no solid conclusions can be drawn based on this analysis to real collisions between a WTG tower and a MP. It is however recommended for future research to study vibration induced collision response irregularities in collisions between the WTG tower and its foundation during installation and mating operations. Based on this analysis and the literature findings described in subsection 2.1.1, vibrations in either the WTG tower or the foundation may affect collision responses during installation and mating operations.

# 4

# Validation and Model Updating

This chapter presents the validation of the model used to simulate the installation of a WTG tower on its support structure. In the first section, it is described how using finite element analysis results are used to validate the simulation model. The second section describes how the simulation model is updated based on finite element analysis results to incorporate bending effects of the tower and monopile through a contact element.

## 4.1 Simulation model validation

Chapter 3 introduces the model made and used to simulate the installation of a WTG tower on its support structure. Figure 23 provided an overview of the model as used in the simulations, including physical representations for wind load, crane tip, the lifting wire and a close up of how collisions are modeled. It also shows the contact element used to determine impact loads and collision responses. Collisions between the WTG tower and its support structure are modeled by a conditional spring-damper element.

Conditional in this context means that as soon as the catcher geometry intersects with one of the tips of the support structure, the spring and damper restore the motion, by exerting a contact load on the WTG tower.

In order to validate the simulation model, it is important that the finite element model from ANSYS is physically identical to the simulation model. Since the simulation model is based on rigid body dynamics of the WTG tower and MP, the FEM model should also be based on rigid body dynamics. Therefore, the WTG tower and MP are set rigid in ANSYS.

Due to the rigid MP and WTG tower, there is no bending nor vibrations in either structures. The absence of these actions means that they do not contribute to the impact loads. The impact loads determined in the control model in ANSYS are solely based on the stiffness of the contact element describing the local deflections. This contact element is present in both the control model in ANSYS and the simulation model in Excel.

In order to create a physical twin between the models, the initial conditions and variables are in both models set identical. The crane tip is motionless, the WTG tower has an initial velocity of 0.5 m/s to the left, the radial annulus between the WTG tower and support structure is 25 mm, the lifting line length is fixed and there are no environmental loadings.

In terms of impact loads, a strong match is found between the control model in ANSYS and the simulation model. Figure 33 shows the impact loads of the collisions between the WTG tower and the MP for the control

model in ANSYS on the top and the impact loads found in the Excel model on the bottom. If a negative peak occurs, it means that the WTG tower bottom collides with the right end of the top of the MP. Positive peaks indicate a collision at the left top of the MP. A strong match is found both in terms of timing and size of the impact loads.

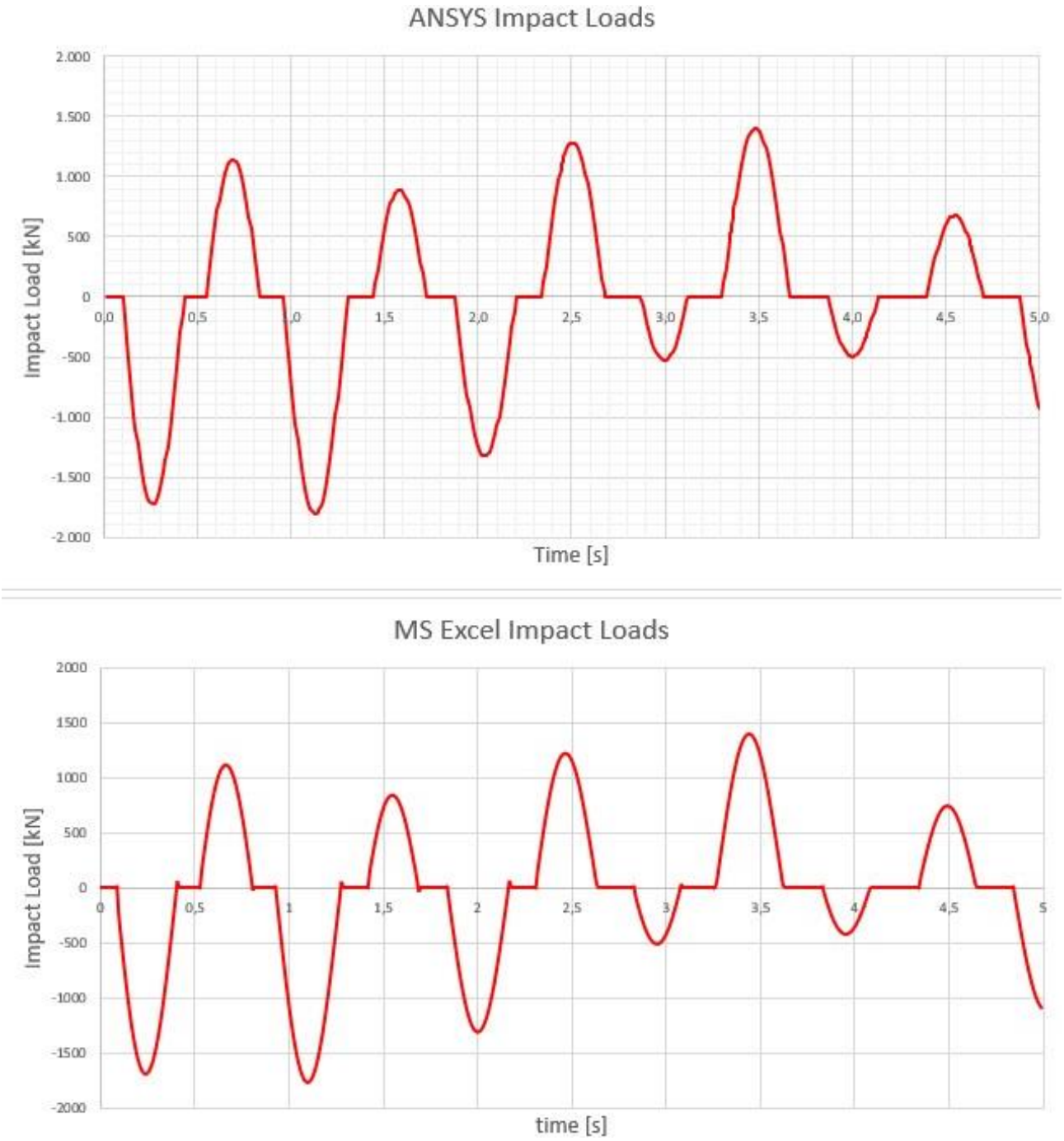


*Figure 33: Impact loads based on rigid body dynamics in the control model (top) and simulation model (bottom).*

The motions of the WTG tower found by both models are also compared for validation. In Appendix D, the motions of the WTG tower are shown for both models as a time-lapse. The top line represents the lifting line, the middle line the center line of the WTG tower and the bottom line the center line of the MP. The displacement is given over a simulation period of 4.8 s at intervals of 0.3 s. The results from the control model in ANSYS are given in black and the results from the simulation model are given in colors. Note that the tower has a length of around 120 m and the horizontal displacements are amplified and in reality, around 60 cm at maximum. A close match is found both in terms of motions and impact loads.

It should be mentioned again here that this validation concerns rigid body dynamics. In reality, the WTG tower and monopile are flexible and this affects the impact load behavior and to a lesser extent the motions of the WTG tower. The next section discusses the finite element analysis of collisions between a flexible WTG tower and a flexible MP. It also presents how the simulation model is updated in order to incorporate these effects.

## 4.2 Model updating

The finite element model in ANSYS used for model updating is based on a slender Euler-Bernoulli or slender EB beam model. With a hollow truncated conically shaped WTG tower, the variable bending stiffness and mass distribution is determined over the height. Also, the local stiffness based on local deflections of the mating elements is incorporated as it was used in the model validation. So, there are two sources of stiffness in the flexible structures control model in ANSYS, namely bending stiffness and local stiffness.

In the Excel simulation model, which is based on rigid body dynamics, the bending stiffness effects cannot be incorporated. The aim is therefore to update the local stiffness to a value that makes the resulting contact load pattern match as closely as possible to the results found in the control model in ANSYS.

Figure 34 displays the contact loads found in the control model on the top and the contact loads from the updated simulation model on the bottom. The high frequency components found in the ANSYS model originate at the bending vibrations from the WTG tower and MP. These are not found in the Excel simulation model, because it is based on rigid body dynamics. However, with the updated values for stiffness and damping, the overall impact load pattern shows a match between the simulation model and the control model. The crests and throughs in both graphs indicate impacts on the left and right side of the monopile respectively. They are numbered 1 to 7 and there is a strong correspondence is size and timing of these events.

Motions are also compared in order to validate whether the updated model complies to the control model in ANSYS. In Appendix E, the motions of the WTG tower are shown for both models as a time-lapse. The top line represents the lifting line, the middle line the center line of the WTG tower and the bottom line the center line of the MP. The displacement is given over a simulation period of 4.8 s at intervals of 0.3 s. The results from the control model in ANSYS are given in black and the results from the simulation model are given in colors. Note that the tower has a length of around 120 m and the horizontal displacements are amplified and in reality, around 60 cm at maximum. A close match is found both in terms of motions.

Both the contact loads and the motions of the WTG tower seen in Figure 34 and Appendix E respectively show a match between the control model in ANSYS and the simulation model in MS Excel. Therefore, the effects of flexibility of the WTG tower and MP are appropriately incorporated in the simulation model.

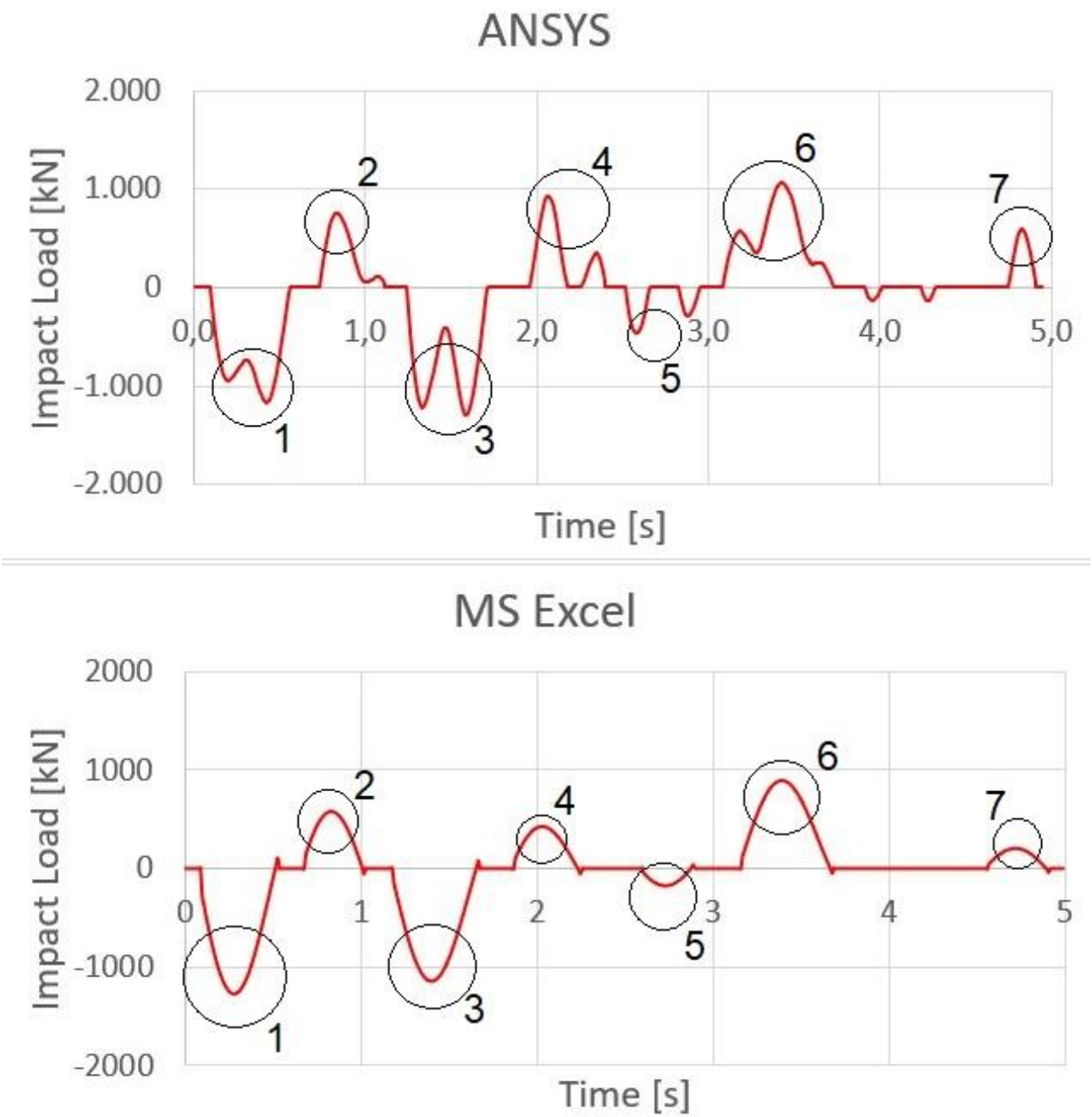


*Figure 34: Impact loads based on flexible body dynamics in the control model (top) and the updated rigid body dynamics in the simulation model (bottom).*

# 5

# Installation Limits

Section 3.1 outlines how a model is made in order to analyze and simulate the installation of a WTG tower on a monopile. This chapter explains how it can be assessed, using that model, what the motion and collision limits are for installation of a WTG tower on a monopile. In the first section, it is explained what the installation requirements are that determine the installation limits. In the second and third sections, the installation limits are assessed for two different crane tip excitations. One, whose frequency corresponds to a jack-up vessel and the other, whose frequency corresponds to a floating vessel. These sections also assess the effect of tower guidance on the installation limits. The fourth section compares the results and explains how the installation limits found, serve as a first exploration of workability of installation.

The final section in this chapter discusses the method and results obtained in this research. It also provides for a first look to installation in 3D and identifies potential associated motion and collision effects.

## 5.1 Installation requirements

Installation limits are determined by the requirements that an installation should comply to, in order for the installation to be deemed successful. WTG tower motions and collisions are limited due to the occurrence of critical or restrictive events. Two types of catchers are considered in this research. A vertical asymmetric catcher and a conical catcher. Figure 35 displays both types of catchers on the left and right respectively. Most of the installation requirements apply to both types of catchers, whereas some requirements specifically apply to a certain type of catcher. Below, all installation requirements are explained in the subsections 5.1.1 to 5.1.7.

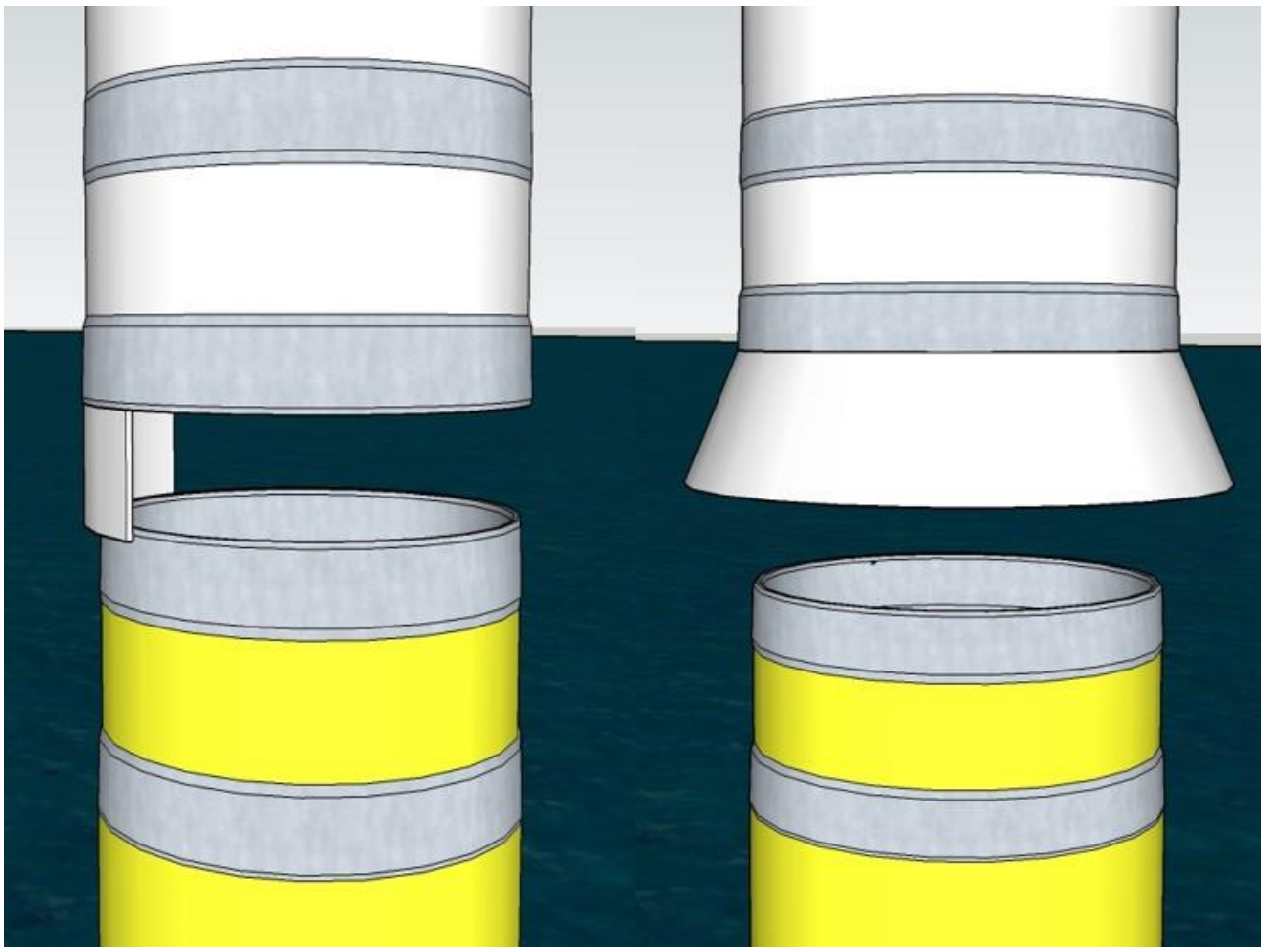

*Figure 35: Visualization of a conical (left) and vertical asymmetric catcher (right) on the WTG tower (white)*

### 5.1.1 Prevention of slack wires

Slack wires are a critical event as they could lead to large and unpredictable snapping loads with potentially damaging consequences for the installation vessel or WTG tower. Independent of the catcher type chosen, this critical event must always be avoided. Therefore, during the simulations, the wire force is monitored in order to ensure continuous tensile load in the wire. If the tensile wire force at some point during the installation becomes zero, slack wires occur, and the installation is deemed unsuccessful. An example of allowable tensile wire forces during installation is shown in Figure 36.

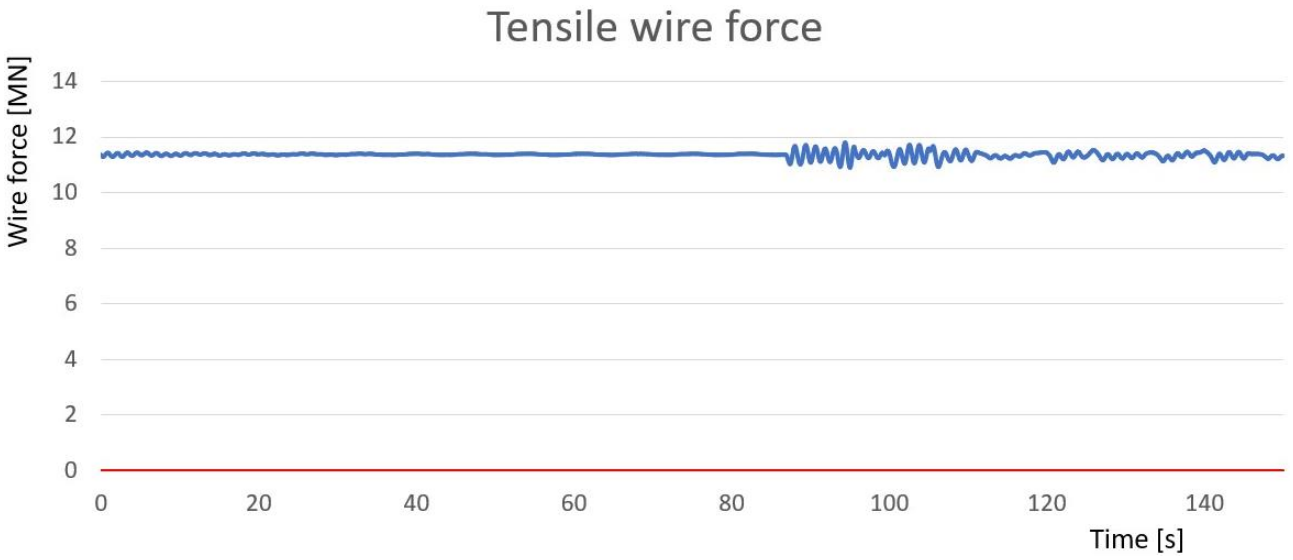


*Figure 36: Axial tensile wire force of the lifting line as a function of time.*

### 5.1.2 Allowable side-lead angle

Independent of the catcher type used for installation, the lifting line hoisting the WTG tower has a limited allowable side-lead angle. In general, the side-lead angle is allowed to be at most between 1 and 3 degrees. In this research, the maximum allowable side-lead angle is set at 3 degrees. During installation simulations, the side-lead angle is monitored in order to ensure that it stays within the limit of 3 degrees. Figure 37 shows an example of the side-lead angle during installation of a WTG tower. Clearly, in this example, the installation limit is reached as the side-lead angle exceeds 3 degrees.

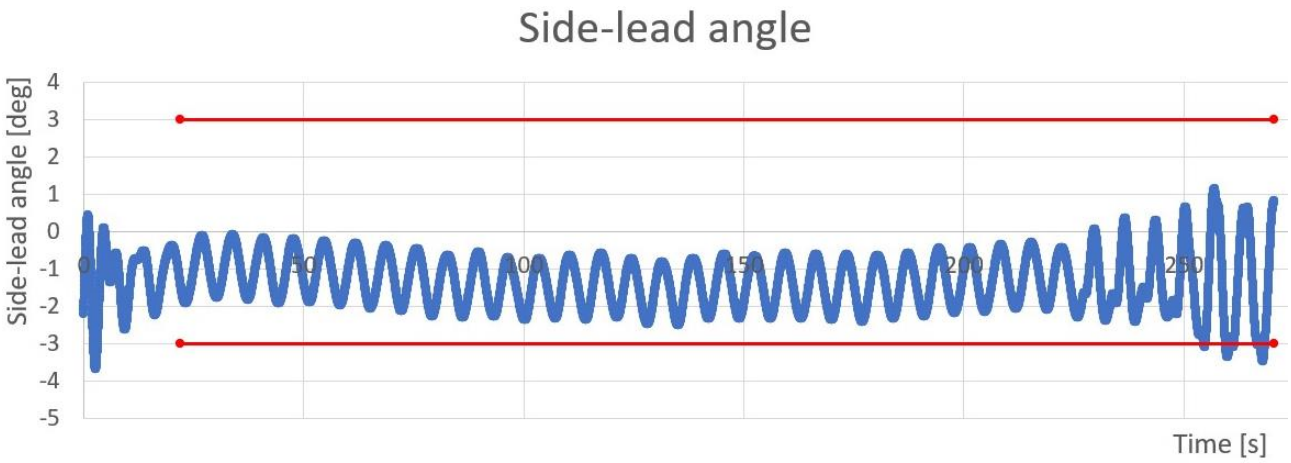


*Figure 37: Side-lead angle of the lifting line as a function of time.*

### 5.1.3 Allowable contact force between the vertical asymmetric catcher and the monopile

In order to prevent structural damage, the force during contact between the vertical asymmetric catcher and the monopile has a limit. Before the maximum allowable contact force can be determined, it should first be assessed what the contact force is. As explained in chapter 3, the contact force consists of both damping and non-linear stiffness. This non-linear stiffness resulted from the combined WTG tower and MP bending and local deflection of the DSJ rings.

With the description of the contact force, the maximum allowable contact force can be determined. Figure 38 shows the equivalent von Mises stress in the catcher and the WTG tower resulting from an outwardly directed distributed load applied at the bottom of the catcher. Although the edges between the catcher and the WTG tower bottom are rounded, it can be seen that the equivalent stress peaks at the edge. With the use of S355 steel, the yield stress of the material is 355 MPa. In accordance with industry practice and safety standards a high safety factor of 1.5 is applied. Therefore, the highest allowable equivalent stress is set at 237 MPa. This corresponds to a contact force of at most 700 kN.

This maximum allowable contact force applies to the vertical asymmetric catcher as in Figure 38. During the determination allowable limits in sections 5.2 and 5.3, the catcher design is subjected to improvements if necessary, aimed to increase the motion and collision limits in installation. This means, if it appears that the allowable contact force is limiting the installation, the catcher will need to be strengthened.

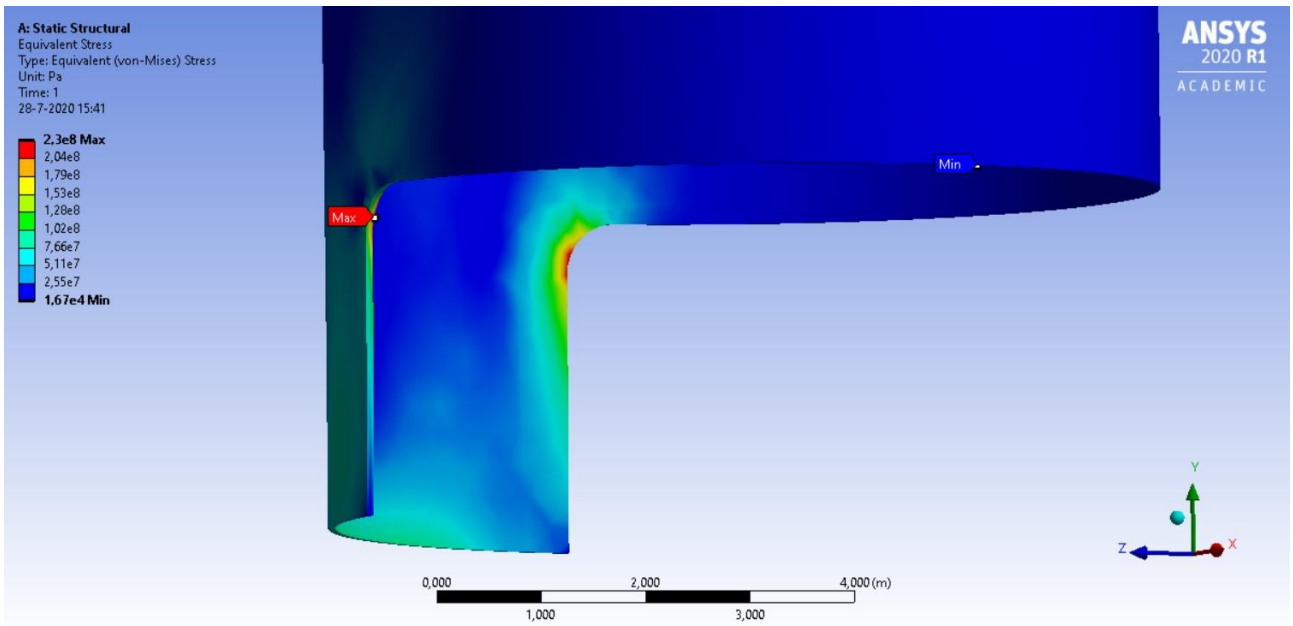


*Figure 38: Finite element analysis based determination of Equivalent (von Mises) stress in the vertical asymmetric catcher and bottom of the WTG tower as a result from a contact force on the bottom of the catcher*

The contact force between the catcher and monopile during any installation simulation will be monitored in order to ensure that it stays within the limit. Figure 39 provides the contact force of an example simulation in which it appears that the contact force exceeds the limit of 700 kN once, making the installation unsuccessful.

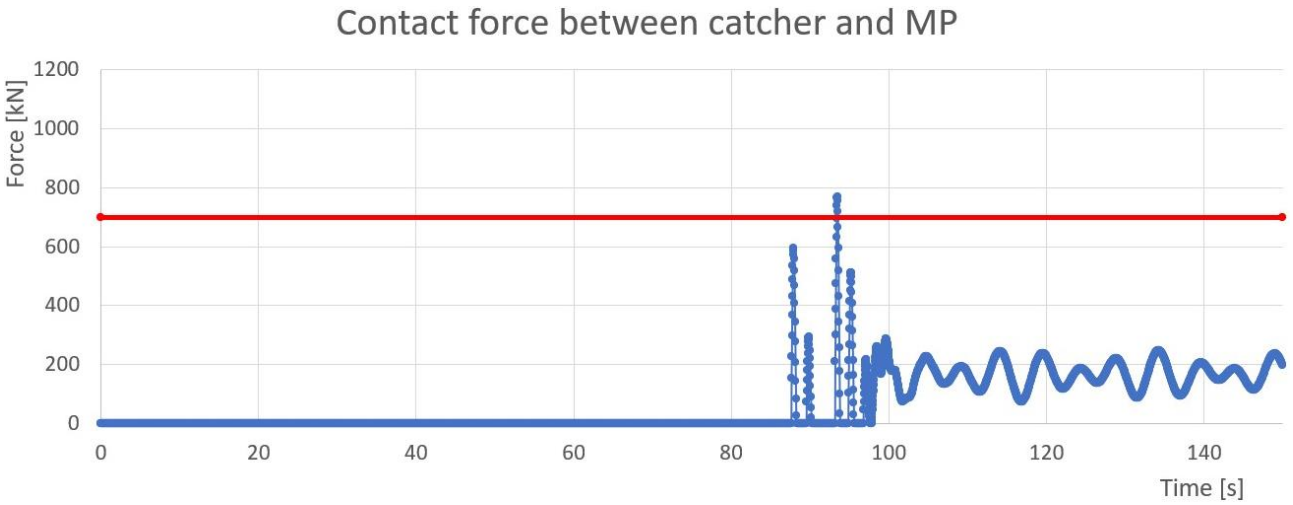


*Figure 39: Example of contact force (blue) between catcher and monopile during installation attempt, where the red line indicates the force limit*

### 5.1.4 Allowable contact force between the conical catcher and the monopile

In order to prevent structural damage, the force during contact between the conical catcher and the monopile has a limit. Before the maximum allowable contact force can be determined, it should first be assessed what the contact force is. As explained in chapter 3, the contact force consists of both damping and non-linear stiffness. This non-linear stiffness resulted from the combined WTG tower and MP bending and local deflection of the DSJ rings.

Also, for the conical catcher, with the description of the contact force, the maximum allowable contact force can be determined. Figure 40 shows the equivalent von Mises stress in the catcher and the WTG tower resulting from a force applied at the bottom of the catcher. It can be seen that the highest von Mises stress is found at the location of the impact. The area of interest however is the connection between the WTG

tower and the catcher. With the use of S355 steel, the yield stress of the material is 355 MPa. In accordance with industry practice and safety standards a high safety factor of 1.5 is applied. Therefore, the highest allowable equivalent stress is set at 237 MPa. This corresponds to a contact force of at most 3 MN for the conical catcher. This is significantly higher than the 700 kN found for the vertical asymmetric catcher.

This maximum allowable contact force applies to the vertical asymmetric catcher as in Figure 38. During the determination allowable limits in sections 5.2 and 5.3, the catcher design is subjected to improvements if necessary, aimed to increase the motion and collision limits in installation. This means, if it appears that the allowable contact force is limiting the installation, the catcher will need to be strengthened.

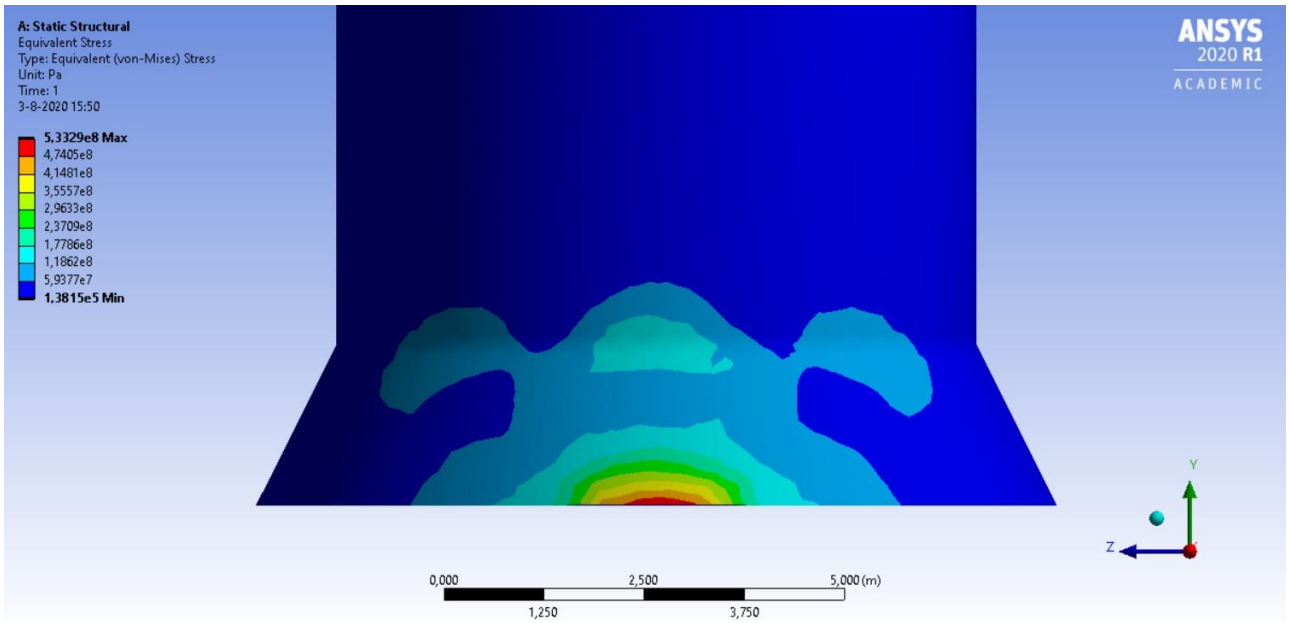


*Figure 40: Finite element analysis based determination of Equivalent (von Mises) stress in the conical catcher and bottom of the WTG tower as a result from a contact force on the bottom of the catcher*

The contact force between the catcher and monopile during any installation simulation will be monitored in order to ensure that it stays within the limit. Figure 41 provides the contact force of an example simulation in which it appears that the contact force exceeds the limit of 3 MN once, making the installation unsuccessful.

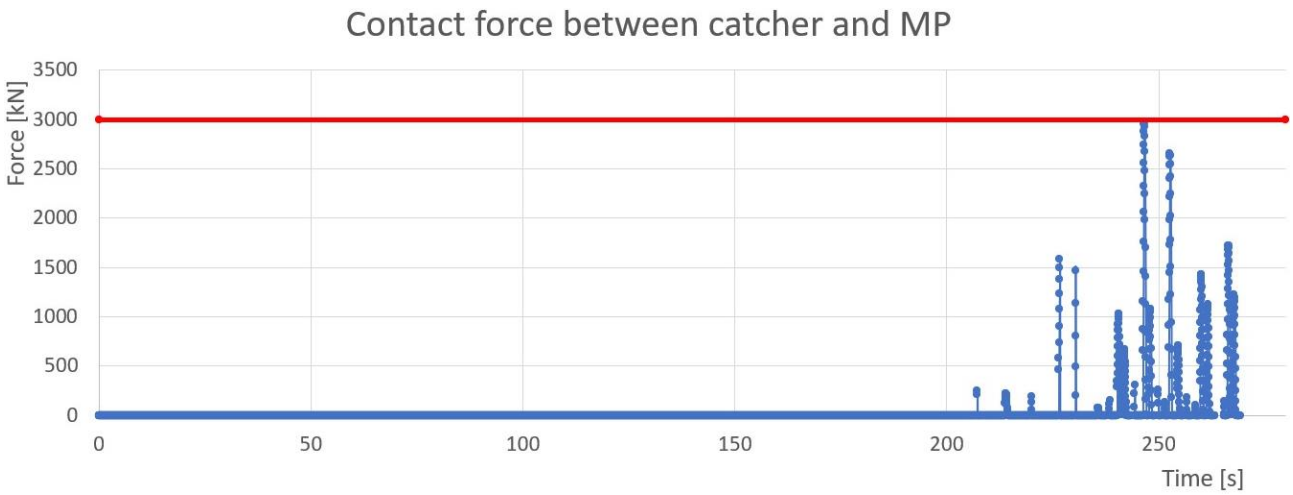


*Figure 41: Example of contact force (blue) between catcher and monopile during installation attempt, where the red line indicates the force limit*

### 5.1.5 Axial impact prevention

For the vertical asymmetric catcher (Figure 35, left), axial impact could occur between the catcher and the monopile or between the DSJ rings. Both are critical events that lead to unsuccessful installation. As the WTG tower is lowered towards the MP, there is a possibility of axial impact between the catcher and monopile. Figure 42 shows the horizontal displacement of the catcher. On the left of the black line, axial contact could occur between the catcher and MP if the red line is crossed on the upside. On the right of the black line, axial impact could occur between the DSJ rings if the red line is crossed on the downside. This requirement only applies to the vertical asymmetric catcher. Subsection 5.1.6 explains a requirement for the conical catcher.

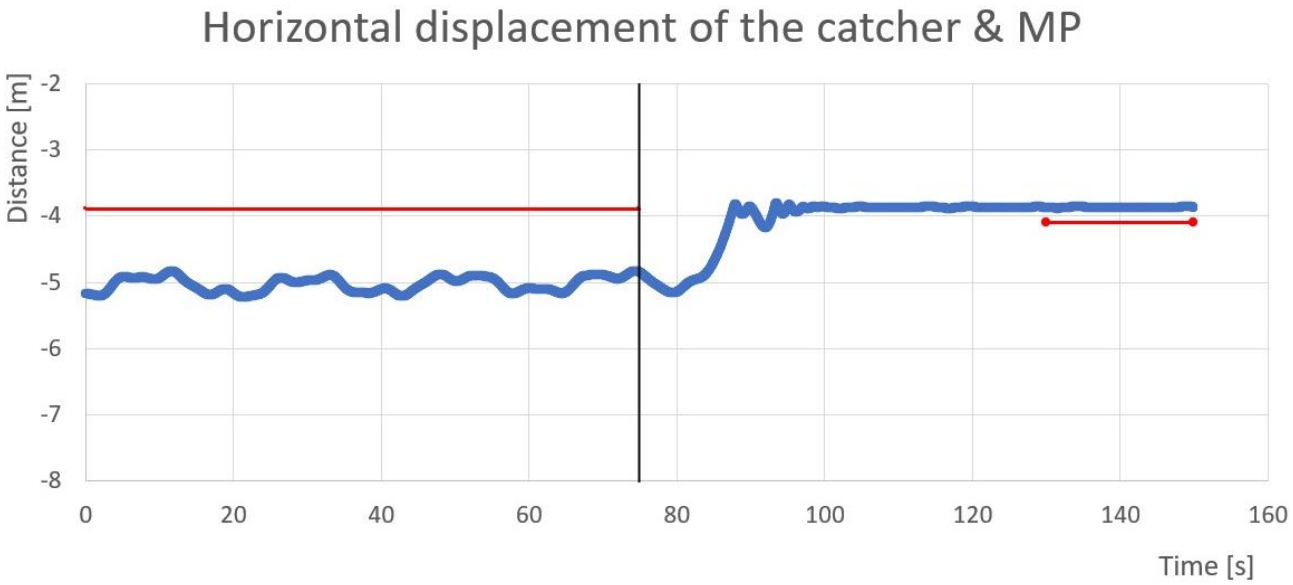


*Figure 42: Horizontal coordinate of the catcher (blue). Vertical black line indicates point in time where the catcher bottom has surpassed the MP top. Red lines indicate limits of catcher displacement to prevent axial impact.*

### 5.1.6 Circular out-crossing rate

Subsection 2.2.1 described the circular out-crossing rate. This installation requirement applies to offshore installations with mating elements that are circumferential. The DSJ rings are circumferential as is the bottom of the conical catcher. This criterion therefore applies to the conical catcher and not to the vertical asymmetric catcher. To the latter, the axial impact prevention criterion applies, described in subsection 5.1.5.

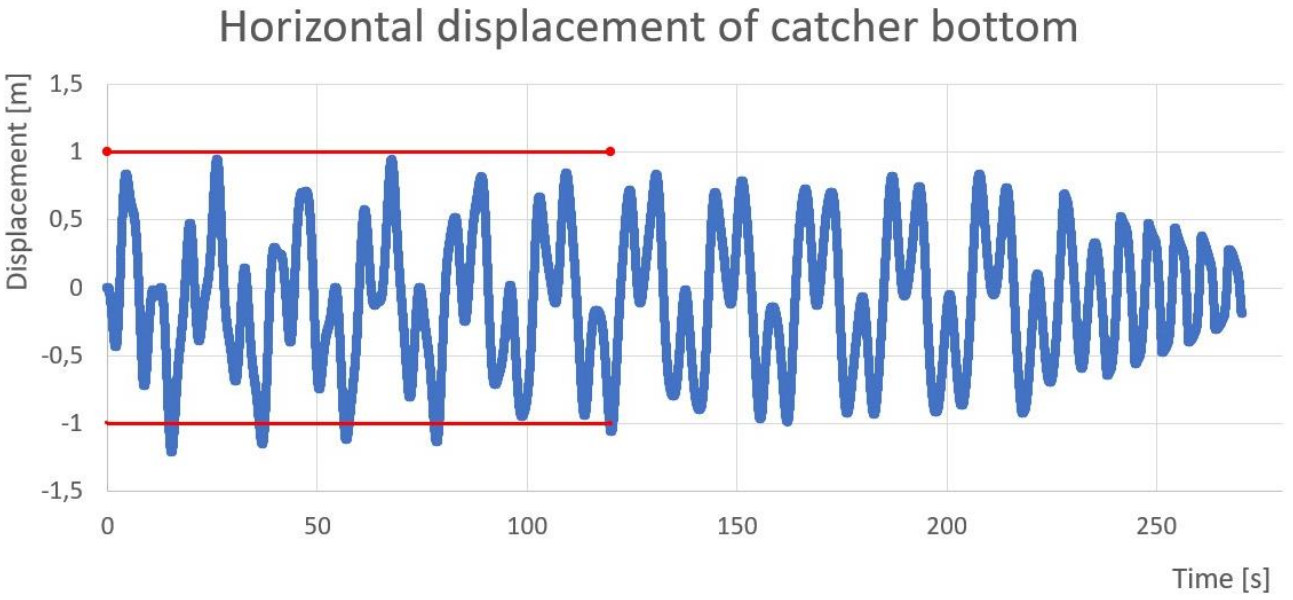


*Figure 43: Example of the circular out-crossing rate. The blue line indicates the horizontal displacement of the center of the catcher, whereas the red lines indicate the displacement at which an out-crossing occurs.*

The circular out-crossing rate states that installation can occur if the circumferences of the DSJ ring on the top of the MP crosses the circumference of the bottom of the conical catcher at most 2 times per minute. Constant monitoring of the bottom displacements of the conical catcher are therefore required to ensure that the installation complies to this requirement. In all simulations, the horizontal displacements of the bottom of the catcher are monitored over a period of 120 s in order to obtain a reliable estimate of the circular out-crossing rate. Figure 43 shows an example, where in the first two minutes, the WTG tower is suspended above the MP and the horizontal displacements are assessed. It can be seen that the circumferences of the bottom of the catcher and the top of the MP cross each other frequently.

### 5.1.7 Concluding remarks on requirements for assessment of allowable limits

The subsections 5.1.1 to 5.1.6 explained the requirements that determine the limits on offshore WTG tower installations. Table 2 displays which criteria apply for the combination of installation vessel types and catcher types. For the installation of the WTG tower on the MP, all criteria have to be satisfied.

| | **Jack-up vessels** | **Floating installation vessels** |
|---|---|---|
| **Conical catcher** | • Circular out-crossing rate<br>➔ Allowed to be ≤ 2 $min^{-1}$<br>• Prevention of slack wires<br>➔ Continuous tensile loading of lifting line<br>• Maximum allowable contact force<br>➔ Allowed up to 3 MN<br>• Allowable side-lead angle<br>➔ Allowed up to 3 degrees | • Circular out-crossing rate<br>➔ Allowed to be ≤ 2 $min^{-1}$<br>• Prevention of slack wires<br>➔ Continuous tensile loading of lifting line<br>• Maximum allowable contact force<br>➔ Allowed up to 3 MN<br>• Allowable side-lead angle<br>➔ Allowed up to 3 degrees |
| **Vertical asymmetric catcher** | • Prevention of slack wires<br>➔ Continuous tensile loading of lifting line<br>• Axial impact prevention<br>➔ Not allowed between catcher & MP, nor between DSJ rings.<br>• Maximum allowable contact force<br>➔ Allowed to be up to 700 kN.<br>• Allowable side-lead angle<br>➔ Allowed up to 3 degrees | • Prevention of slack wires<br>➔ Continuous tensile loading of lifting line<br>• Axial impact prevention<br>➔ Not allowed between catcher & MP, nor between DSJ rings.<br>• Maximum allowable contact force<br>➔ Allowed to be up to 700 kN.<br>• Allowable side-lead angle<br>➔ Allowed up to 3 degrees |

*Table 2: Applicability of installation criteria for catchers and installation vessels*

There are many variables affecting the motion and collision behavior and as such, the installation limits of the WTG tower in installation. Sections 5.2 and 5.3 describe how the installation limits are assessed for two different crane tip excitations that, in terms of frequency, correspond to a jack-up vessel and floating installation vessel, respectively.

## 5.2 Installation limits and catcher selection with jack-up vessel crane tip excitation

In this section, the limits are determined for installation with a vertical asymmetric catcher and for installation with a conical catcher. The crane tip excitation corresponds to a jack-up vessel. To assess the installation limits, a base case is defined and described in subsection 5.2.1. Subsection 5.2.2 describes how through an iterative process, the limits for installation with jack-up vessel characteristics using a vertical asymmetric catcher is determined. Subsection 5.2.3 repeats this exercise for a conical catcher.

### 5.2.1 Base case definition

The aim of defining a base case is to focus on the procedure of determining and optimizing the installation limits. Optimization is focused at improving the mean wind velocity for installation. As such, a first exploration is performed to workability of installation. In the base case, variables are selected for which the limits are determined and optimized. First of all, WTG tower dimensions are selected and shown in Table 3. The dimensions, except for the inertia, are based on the GE Haliade-X 12 MW wind turbine, as stated by General Electric. The inertia is determined based on the dimensions in Table 3.

| ***WTG tower property*** | **Quantity** | **Unity** |
|---|---|---|
| *Length* | 129.1 | m |
| *Bottom width* | 8 | m |
| *Top width* | 5.5 | m |
| *Bottom thickness* | 70 | mm |
| *Top thickness* | 35 | mm |
| *Mass* | 1159 | tons |
| *Inertia* | 1.5e9 | kgm2 |

*Table 3: WTG tower specifications as used for the determination of allowable limits*

Subsection 2.1.2 and 2.1.3 respectively provided a literature-based description of wind and waves respectively. For the base case definition, the key takeaway is that wind loads on a structure are equal to a constant, times the wind velocity squared. Under most circumstances, wave heights are also proportional to the wind velocity squared. Since wave heights are proportional to wave-induced vessel motions, a base case for this exercise is defined that incorporates jack-up vessel crane tip motions that are proportional to the mean wind velocity at 10 m above SWL squared. This approach comes associated with uncertainty, since crane tip motions are different for each installation vessel and the wind and wave relationship is stochastic. Therefore, in section 5.4, the sensitivity of the installation limits will be assessed for vessel or crane tip specific variables.

| ***Jack-up vessel property*** | **Quantity** | **Unity** |
|---|---|---|
| *Horizontal crane tip frequency* | 0.9 | rad/s |
| *Horizontal crane tip amplitude* | $0.01*U^2_{\text{meanwind@10SWL}}$ | m |
| *Vertical crane tip frequency* | 0.9 | rad/s |
| *Vertical crane tip amplitude* | $0.001*U^2_{\text{meanwind@10SWL}}$ | m |

*Table 4: Jack-up vessel specifications as used for the determination of installation limits*

Both the vertical asymmetric catcher and the conical catcher have specific installation behavior and requirements and their dimensions are variable. The catcher that allows for the highest mean wind velocity

in installation is deemed preferable for installation. The maximum allowable contact force for both types of catchers are described in subsections 5.1.3 and 5.1.4. If it appears that the maximum allowable contact force is limiting in installation, the catcher will be strengthened, and the updated maximum allowable contact force will be determined using finite element analysis.

In the following subsections, the installation limits will be assessed for a vertical asymmetric catcher and a conical catcher. This limit, expressed in mean wind velocity at 10 m above SWL, will be optimized iteratively for the different variables in installation and the use of WTG tower guidance.

### 5.2.2 Determination and optimization of installation limits using a vertical asymmetric catcher

The installation requirements described in section 5.1 provide the basis for assessing installation limits. The installation limits are expressed in the mean wind velocity at 10 m above SWL on which both the wind spectrum and the crane tip motions are based as described in subsection 5.2.1. For the initial assessment of the allowable limits, apart from crane operator induced crane tip displacements, no WTG tower guidance is used. The vertical asymmetric catcher is a cylinder segment with a height of 3 m, a radius of 4.15 m and an inscribed angle of 90 degrees. Figure 38 provides a visualization of this catcher type including a finite element-based determination of equivalent stresses resulting from a collision. The installation limits are determined iteratively. Below, the iterations are given. The specifications of an iteration are given before the results. After the results, the conclusions of the iterations are given which provide the basis for the following iteration.

*Iteration 1*

The specifications for the first iteration of installation with jack-up vessel characteristics using a vertical asymmetric catcher are as follows.

- A catcher without stiffeners is used. This catcher and corresponding equivalent stresses resulting from contact with the MP are shown in Figure 38. The maximum allowable contact force is 700 kN for this catcher as described in subsection 5.1.3.
- Apart from crane operator induced crane tip displacements, no WTG tower guidance is used.
- The initial horizontal location of the crane tip is -1 m. This can be seen as an equilibrium position around which the wind induced horizontal crane tip motions oscillate. The reason for this initial horizontal position is to prevent the bottom of the catcher from making axial impact with the MP during lowering of the WTG tower as described in subsection 5.1.5.
- The final horizontal crane tip location, also in the form of an equilibrium position, is a variable. In Figure 44 this variable is seen on the vertical axis. The aim of this final horizontal location is to 'hang' the tower with the catcher against the MP and as such, to prevent bouncing behavior between the catcher and the MP with the probability of axial impact between the DSJ rings.
- The lifting line length is a variable seen on the horizontal axis in Figure 44.
- Numbers in Figure 44 indicate the maximum allowable mean wind velocity at 10 m above SWL at which installation could occur. Colors in Figure 44 indicate which requirement (see legend) limits the installation.


*Figure 44: Allowable wind velocities (numbers in table) including the limiting criterion (colors in table) for lifting line lengths (horizontal) and operator crane tip displacements (vertical)*

The following can be concluded from the first iteration:

- The highest allowable mean wind velocity is 4.1 m/s found at a lifting line length of 15 m and a final horizontal crane tip location of 2.6 or 3 m. This mean wind velocity corresponds to the lower end of the value 3 (gentle breeze) on the Beaufort wind force scale.
- Installation is in all cases limited by the maximum impact force of 700 kN (blue color).
- Therefore, a stronger catcher is needed in the second iteration.

*Iteration 2*

The specifications for the second iteration of installation with jack-up vessel characteristics using a vertical asymmetric catcher are as follows.

- It was concluded after the first iteration that the catcher was not strong enough and that the maximum allowable contact force limited the installation. Therefore, a stronger catcher is determined using ANSYS finite element analysis. Figure 45 shows the design and equivalent stresses resulting from contact between the catcher and the MP. In this updated catcher design, stiffeners are placed on its back which are not present in the initial catcher design (Figure 38). The procedure for determining the maximum allowable impact load are given in subsection 5.1.3. Repeating this procedure for the updated catcher yields a maximum allowable impact force of 1170 kN instead of 700 kN.
- Except for the updated catcher design, all other variables are the same as in the first iteration.
- Numbers in Figure 46 indicate the maximum allowable mean wind velocity at 10 m above SWL at which installation could occur. Colors in Figure 46 indicate which requirement (see legend) limits the installation.

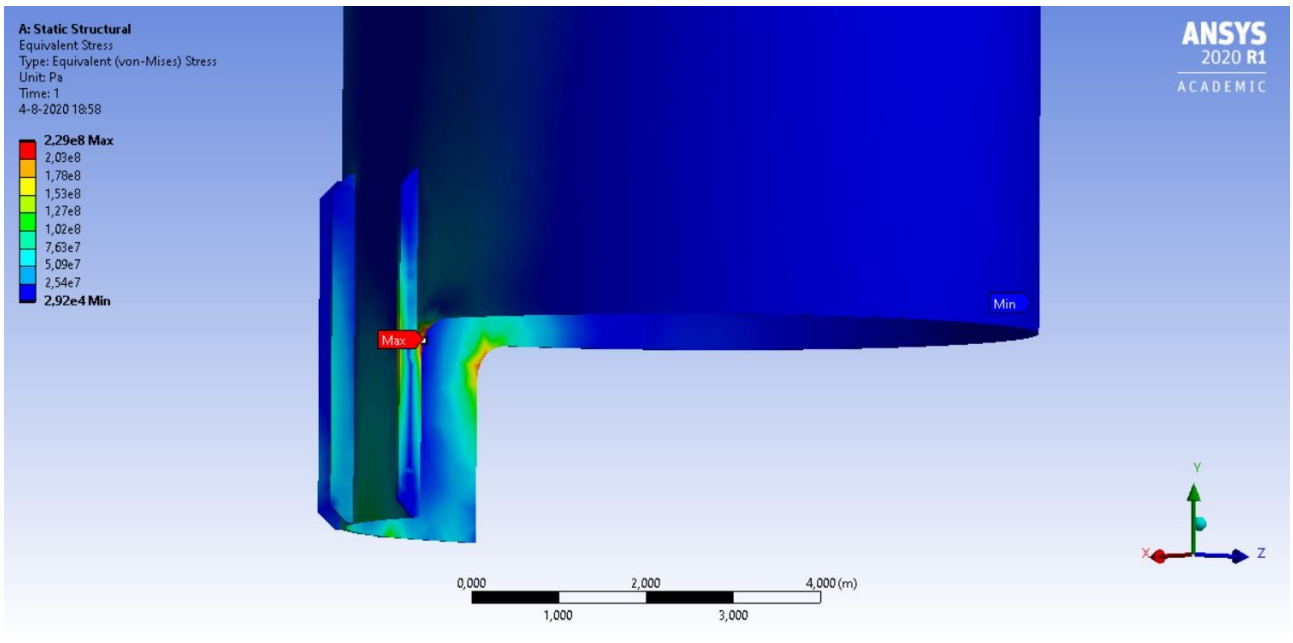


*Figure 45: Stronger catcher design with stiffeners on the back. Based on the equivalent von Mises stress, the maximum impact force increases from 700 kN to 1170 kN.*

**Lifting line length [m]**

| Crane tip displacement [m] | 15 | 18 | 21 | 24 | 27 | 30 |
|---|---|---|---|---|---|---|
| 2,6 | 6 | 5,9 | 5,3 | 5,2 | 4,8 | 4,3 |
| 3 | 6 | 6 | 5,3 | 5,4 | 4,8 | 4,5 |
| 3,4 | 6 | 6 | 5,3 | 5,5 | 4,8 | 4,6 |
| 3,8 | 6 | 6 | 5,4 | 5,2 | 4,9 | 4,8 |
| 4,2 | 6 | 6 | 5,4 | 5,2 | 5 | 4,9 |
| 4,6 | 6 | 6 | 5,4 | 5,3 | 5,1 | 5,1 |
| 5 | 6 | 6 | 5,4 | 5,3 | 5,2 | 5,1 |

**LEGEND**

| Axial catcher and MP impact | Axial DSJ rings impact | Side-lead angle > 3 degrees | Slack wires occurence | Impact force > 1170 kN |
|---|---|---|---|---|

*Figure 46: Allowable wind velocities (numbers in table) including the limiting criterion (colors in table) for lifting line lengths (horizontal) and operator crane tip displacements (vertical)*

The following can be concluded from the second iteration:

- Highest allowable mean wind velocity is 6 m/s found at a lifting line length of 15 m and 18 m and a final horizontal crane tip location of 3 m to 5 m. This mean wind velocity corresponds to the lower end of the value 4 (moderate breeze) on the Beaufort wind force scale.
- The installation is limited by the maximum allowable contact force requirement (blue), the probability of axial impact between the catcher and the MP (yellow) or between the DSJ rings (orange).
- In the simulations, it appears that the crane operator induced horizontal displacements of the crane tip of have one positive and one negative effect:

- Positive: It reduces the probability of bouncing behavior occurring between the catcher and monopile, meaning there is reduced risk of axial impact between the DSJ rings (orange color is not found in the results for higher crane tip displacements).
- Negative: Due to the relatively large crane tip displacement, there is an increased probability of contact forces exceeding their allowable limit (>1170 kN).

- For the third iteration, the crane operator induced horizontal crane tip displacements are reduced in magnitude. A constant horizontal force will be applied at the bottom of the tower to pull the tower with the vertical asymmetric catcher against the MP. The magnitude of this force will be varied in order to study its effects on installation limits.
- With regards to the stiffened vertical asymmetric catcher, this design will in all future iterations with the vertical asymmetric catcher be applied. An iteration with the catcher without stiffeners will therefore not be performed in later iterations.

*Iteration 3*

The specifications for the third iteration of installation with jack-up vessel characteristics using a vertical asymmetric catcher are as follows.

- As concluded from the results in the second iteration, the crane operator induced horizontal crane tip displacements have to be reduced to increase the allowable wind velocity for installation. They will be set constant at the following values.
- Initial position crane tip (by operator): -1.1 m. As in all other iterations, this value is an equilibrium position around which the wind velocity induced harmonic crane tip displacements oscillate.
- Final position crane tip (by operator): 0.6 m. As in all other iterations, this value is an equilibrium position around which the wind velocity induced harmonic crane tip displacements oscillate.
- A constant force is applied at the bottom of the tower which starts to pull as soon as the bottom of the catcher has surpassed the top of the MP. In order to study its effects on installation limits, this force is iteratively varied. The forces analyzed are seen on the vertical axis in Figure 47.
- The different lifting line lengths are seen on the horizontal axis in Figure 47.
- Except for the reduction in operator induced crane tip displacements and the addition of a constant force on the bottom of the WTG tower, all other variables are the same as in the second iteration.
- Numbers in Figure 47 indicate the maximum allowable mean wind velocity at 10 m above SWL at which installation could occur. Colors in the Figure 47 indicate which requirement (see legend) limits the installation.

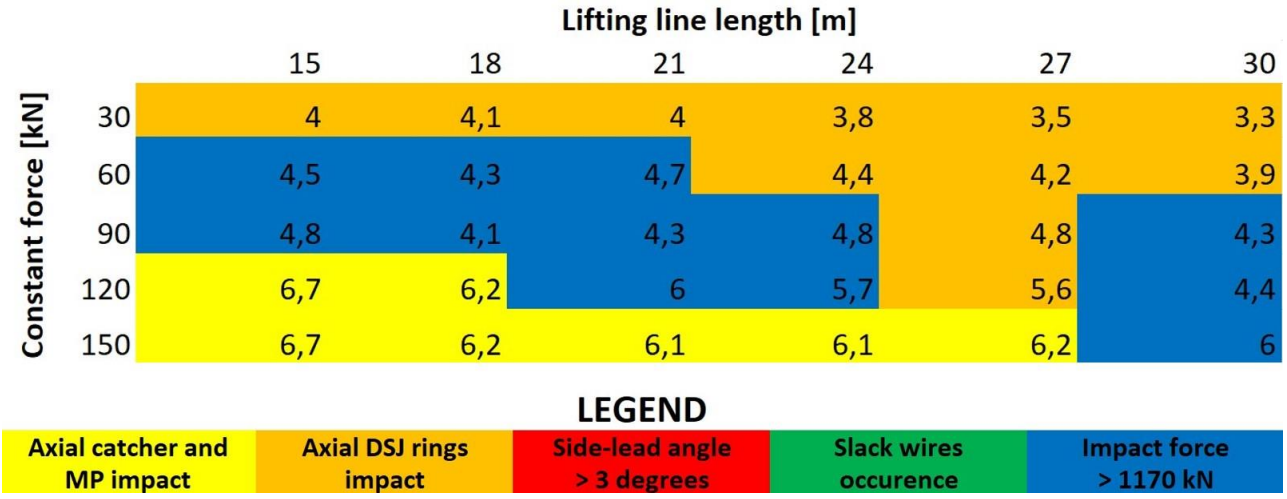


*Figure 47: Allowable wind velocities (numbers in table) including the limiting criterion (colors in table) for lifting line lengths (horizontal) and constant tension winch force (vertical).*

The following can be concluded from the third iteration:

- Highest allowable mean wind velocity is 6.7 m/s found at a lifting line length of 15 m and a constant force of 120 kN or 150 kN. This mean wind velocity corresponds to the value 4 (moderate breeze) on the Beaufort wind force scale.
- The installation is alternately limited by probability of axial impact between the catcher and the monopile (yellow) and in the other cases by bouncing behavior between the catcher and MP (orange) or by the maximum contact force criterion (blue).
- It appears that a short lifting line length yields higher allowable mean wind velocities in installation than a long lifting line length. Therefore, in the fourth iteration, lifting line lengths will be analyzed from 10 to 25 m instead of 15 to 30 m.
- In order to decrease the probability of axial impact between the catcher and the MP (yellow) or between the DSJ rings (orange), the crane operator induced displacements of the crane tip will be increased slightly for the fourth iteration.

*Iteration 4*

The specifications for the fourth iteration of installation with jack-up vessel characteristics using a vertical asymmetric catcher are as follows.

- Crane operator induced displacements of the crane tip are increased:
- Initial position of the crane tip: -1.4 m instead of -1.1 m. As in all other iterations, this value is an equilibrium position around which the wind velocity induced harmonic crane tip displacements oscillate.
- Final position of the crane tip 0.9 m instead of 0.6 m. As in all other iterations, this value is an equilibrium position around which the wind velocity induced harmonic crane tip displacements oscillate.
- The lifting line lengths analyzed are between 10 m to 25 m instead of 15 m to 30 m as used in previous iterations. The different lifting line lengths are seen on the horizontal axis in Figure 48.
- A constant force is applied at the bottom of the tower which starts to pull as soon as the bottom of the catcher has surpassed the top of the MP. In order to study its effects on installation limits, this force is iteratively varied. The forces analyzed are seen on the vertical axis in Figure 48.
- Except for the increase in operator induced crane tip displacements, all other variables are the same as in the third iteration.
- Numbers in Figure 48 indicate the maximum allowable mean wind velocity at 10 m above SWL at which installation could occur. Colors in the Figure 48 indicate which requirement (see legend) limits the installation.

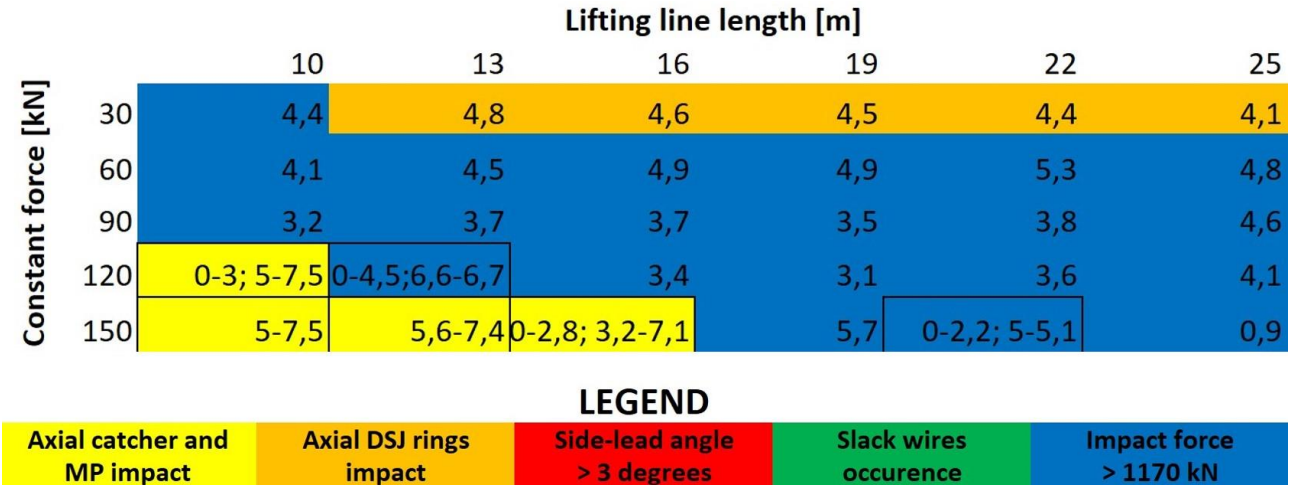


*Figure 48: Allowable wind velocities (numbers in table) including the limiting criterion (colors in table) for lifting line lengths (horizontal) and constant tension winch forces (vertical).*

The following can be concluded from the fourth iteration:

- Highest allowable mean wind velocity is 7.5 m/s found at a lifting line length of 10 m and a constant force of 120 kN or 150 kN applied horizontally at the bottom of the WTG tower to pull it towards the MP. This mean wind velocity corresponds to the upper end of the value 4 (moderate breeze) on the Beaufort wind force scale.
- In Figure 48, some values are framed. This indicates that that there is a range of wind velocities for which installation can occur as seen in the figure. These ranges of allowable wind velocities can be contributed to different criteria limiting the installation at different wind velocities (eg. Axial impact between the DSJ rings may be limiting below 4 m/s wind, whereas the maximum contact force limits the installation above this velocity).
- It appears after four iterations that the allowable wind velocities are still limited to moderate breeze conditions (Beaufort 4). Figure 48 also indicates that the installation is predominantly limited due the maximum contact force criterion (blue), and the risk of axial impact (orange and yellow). The violation of these requirements is caused by motions of the bottom of the WTG tower. Therefore, in the next iteration, the motions of the bottom of the bottom of the WTG tower will be linearly damped in order to try to increase the allowable wind velocity for installation.

*Iteration 5*

The specifications for the fifth iteration of installation with jack-up vessel characteristics using a vertical asymmetric catcher are as follows.

- Crane operator induced displacements of the crane tip are increased slightly:
- Initial position of the crane tip: -2 m instead of -1.4 m. As in all other iterations, this value is an equilibrium position around which the wind velocity induced harmonic crane tip displacements oscillate.
- Final position of the crane tip 1.5 m instead of 0.9 m. As in all other iterations, this value is an equilibrium position around which the wind velocity induced harmonic crane tip displacements oscillate.
- The lifting line lengths analyzed are between 15 m and 30 m again as used in iterations 1 to 3. The different lifting line lengths are seen on the horizontal axis in Figure 49.
- The constant horizontal force aimed to pull the WTG tower with its catcher against the MP is not applied any more. Linear damping is now applied to the horizontal motions of the bottom of the WTG tower. The vertical axis in Figure 49 shows the damping coefficient analyzed.
- Except for the increase in operator induced crane tip displacements, the application of linear damping to the horizontal motions of the bottom of the WTG tower and the removal of constant forcing on the WTG tower bottom, all other variables are equal as in the previous iteration.
- Numbers in Figure 49 indicate the maximum allowable mean wind velocity at 10 m above SWL at which installation could occur. Colors in the Figure 49 indicate which requirement (see legend) limits the installation.

| WTG tower bottom damping [kNs/m] \ Lifting line length [m] | 15 | 18 | 21 | 24 | 27 | 30 |
|---|---|---|---|---|---|---|
| 0 | 5 | 4,5 | 4,5 | 3,7 | 3,6 | 3,5 |
| 200 | 5,6 | 5,4 | 5,2 | 4,9 | 4,6 | 4,3 |
| 400 | 6,4 | 6,1 | 5,9 | 5,5 | 5,2 | 4,8 |
| 600 | 7 | 6,8 | 6,4 | 6,1 | 5,7 | 5,3 |
| 800 | 7,6 | 7,3 | 7 | 6,6 | 6,1 | 5,7 |
| 1000 | 8,2 | 7,9 | 7,5 | 7,1 | 6,6 | 6,1 |
| 1200 | 8,7 | 8,4 | 8 | 7,6 | 7 | 6,5 |
| 1400 | 9,2 | 8,8 | 8,4 | 8 | 7,4 | 6,9 |
| 2000 | 10,6 | 10,2 | 9,7 | 9,2 | 8,5 | 7,9 |
| 2500 | 10,7 | 10,7 | 10,7 | 10,1 | 9,4 | 8,8 |
| 3000 | 10,8 | 10,8 | 10,7 | 10,2 | 10,3 | 9,5 |

**LEGEND**

| Axial catcher and MP impact | Axial DSJ rings impact | Side-lead angle > 3 degrees | Slack wires occurence | Impact force > 1170 kN |
|---|---|---|---|---|

*Figure 49: Allowable wind velocities (numbers in table) including the limiting criterion (colors in table) for lifting line lengths (horizontal) and damping coefficients (vertical).*

The following can be concluded from the fifth iteration:

- Highest allowable mean wind velocity is 10.8 m/s found at a lifting line length of 15 m and a damping coefficient of 3000 kNs/m. This mean wind velocity corresponds to the lower end of the value 6 (strong breeze) on the Beaufort wind force scale.
- The installation for damping coefficients below 2000 kNs/m is limited by the probability of axial impact between the rings of the DSJ. Above 2000 kNs/m, the installation is limited by the probability of axial impact between the catcher and the MP.
- After five iterations, the installation with jack-up vessel characteristics using a vertical asymmetric catcher is allowed to occur with mean wind velocities at 10 m above SWL of up to 10.8 m/s. As mentioned before, it is out of the scope of this research to incorporate specific crane vessels in the installation simulations. Therefore, uncertainty comes associated with the jack-up vessel characteristics. A sensitivity analysis will therefore be performed in section 5.4 to study the effects of the vessel associated variables on the installation limits.

*Concluding remarks of installation with jack-up vessel characteristics using a vertical asymmetric catcher*

The installation limits, expressed in allowable mean wind velocities, are determined for installation using a vertical asymmetric catcher with crane excitation corresponding to jack-up vessel characteristics. Apparently, for the conditions applied, if the horizontal motions of the bottom of the WTG tower are damped, the allowable mean wind velocity at 10 m above SWL is limited to 10.8 m/s.

It is one of the aims of this research to compare the vertical asymmetric catcher with the conical catcher in terms of allowable mean wind velocity for installation. Therefore, in the following subsection, the allowable mean wind velocities for installation will be determined for the conical catcher. The same typical jack-up vessel crane tip excitations will be applied. It should be noted that some iterations performed in this subsection will not be repeated in the following subsection. Applying constant horizontal forcing on the bottom of the WTG tower will not be further investigated as the simulations indicated that the improvement in the allowable mean wind velocity is negligible compared to the improvement observed for applying linear damping to the WTG tower bottom motions.

Ultimately, when the results are obtained for both catchers and the crane tip excitations that correspond to a jack-up and a floating vessel, a sensitivity study will be performed that is described in section 5.4.

### 5.2.3 Determination and optimization of allowable limits using a conical catcher

The installation requirements described in section 5.1 provide the basis for assessing installation limits. The installation limits are expressed in the mean wind velocity at 10 m above SWL on which both the wind spectrum and the crane tip motions are based as described in subsection 5.2.1. For the initial assessment of the installation limits, no WTG tower guidance is used. The conical catcher is a hollow truncated cone with a thickness equal to the thickness of the DSJ ring at the bottom of the WTG tower. The height of this cone is 2 m and the width a variable which will be analyzed in the iterative procedure of determining and optimizing the allowable wind velocity. Figure 40 provides a visualization of this catcher type including a finite element-based determination of equivalent stresses resulting from a collision. The allowable limits are determined iteratively. Below, the iterations are given. The specifications of an iteration are given before the results. After the results, the conclusions of the iterations are given which provide the basis for the following iteration.

*Iteration 1*

The specifications for the first iteration of installation with jack-up vessel characteristics using a conical catcher are as follows.

- For consistency purposes, the wind field applied is based on the same wind spectrum realization and the crane tip motions as a function of the wind velocity is equal to the one used for the asymmetric vertical catcher.
- For the conical catcher, there is no active crane operator action performed during lowering of the WTG tower. There is only a fixed displacement of the crane tip which is a function of the mean wind velocity. This displacement aims to counteract the mean wind such that the motion equilibrium position of the center of the catcher is above the center of the MP.
- For the first iteration, no guidance of the WTG tower in the form of constant forcing or damping is applied.
- For the conical catcher, some installation requirements are the same as for the vertical asymmetric catcher:
    - Slack wires are not allowed. For background information on this requirement, see subsection 5.1.1.
    - The side-lead angle of the lifting line is allowed to be at most 3 degrees. For background information on this requirement, see subsection 5.1.2.
- Other installation requirements for the conical catcher are different from the requirements for a vertical asymmetric catcher:
    - The circular out-crossing rate is allowed to be at most 2 times per minute. For background on the circular out-crossing rate, see subsection 5.1.6.
    - The maximum allowable contact force between the catcher and the MP is 3 MN for the conical catcher instead of 700 or 1170 kN for the vertical asymmetric catcher. For background on this requirement, see the subsections 5.1.3 and 5.1.4.
- For the first iteration, the lifting line length is used as a variable. The different lifting line lengths analyzed are seen on the horizontal axis in Figure 50.
- For the first iteration, the catcher width is also used as a variable. The different catcher widths analyzed are seen on the vertical axis in Figure 50.
- Numbers in Figure 50 indicate the maximum allowable mean wind velocity at 10 m above SWL at which installation could occur. Colors in the Figure 50 indicate which requirement (see legend) limits the installation.

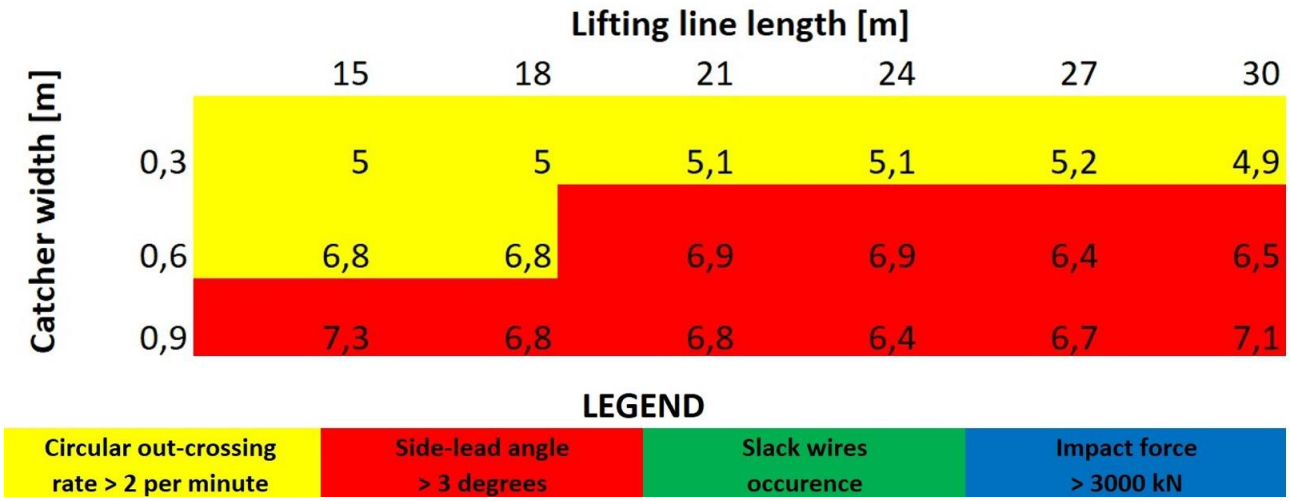


*Figure 50: Allowable wind velocities (numbers in table) including the limiting criterion (colors in table) for lifting line lengths (horizontal) and catcher widths (vertical)*

The following can be concluded from the first iteration:

- The highest allowable mean wind velocity is 7.3 m/s found at a lifting line length of 15 m and a catcher width of 0.9 m. This mean wind velocity corresponds to the upper end of the value 4 (moderate breeze) on the Beaufort wind force scale. Without actions from the crane operator during lowering or other forms of WTG tower guidance, this is a significantly higher wind velocity than found in the first iteration for the vertical asymmetric catcher.
- For low catcher widths, the installation is limited by the circular out-crossing rate. For higher catcher widths, the installation is limited by the maximum side-lead angle.
- In the second iteration, the catcher width will be fixed at 0.9 m. The maximum allowable wind velocity will be determined for different contact damping coefficients.

*Iteration 2*

The specifications for the second iteration of installation with jack-up vessel characteristics using a conical catcher are as follows.

- In the second iteration, the catcher width is fixed at 0.9 m as that yielded the highest allowable wind velocity for installation in the previous iteration.
- In the second iteration, the linear contact damping coefficient will be varied in order to study its effects on allowable wind velocities. Figure 51 shows the allowable wind velocities with the contact damping coefficient on the vertical axis.
- The lifting line length remains the second variable and is given on the horizontal axis in Figure 51.
- Except for the variable contact damping and the fixed catcher width, all other variables are the same as in the first iteration.
- Numbers in Figure 51 indicate the maximum allowable mean wind velocity at 10 m above SWL at which installation could occur. Colors in Figure 51 indicate which requirement (see legend) limits the installation.

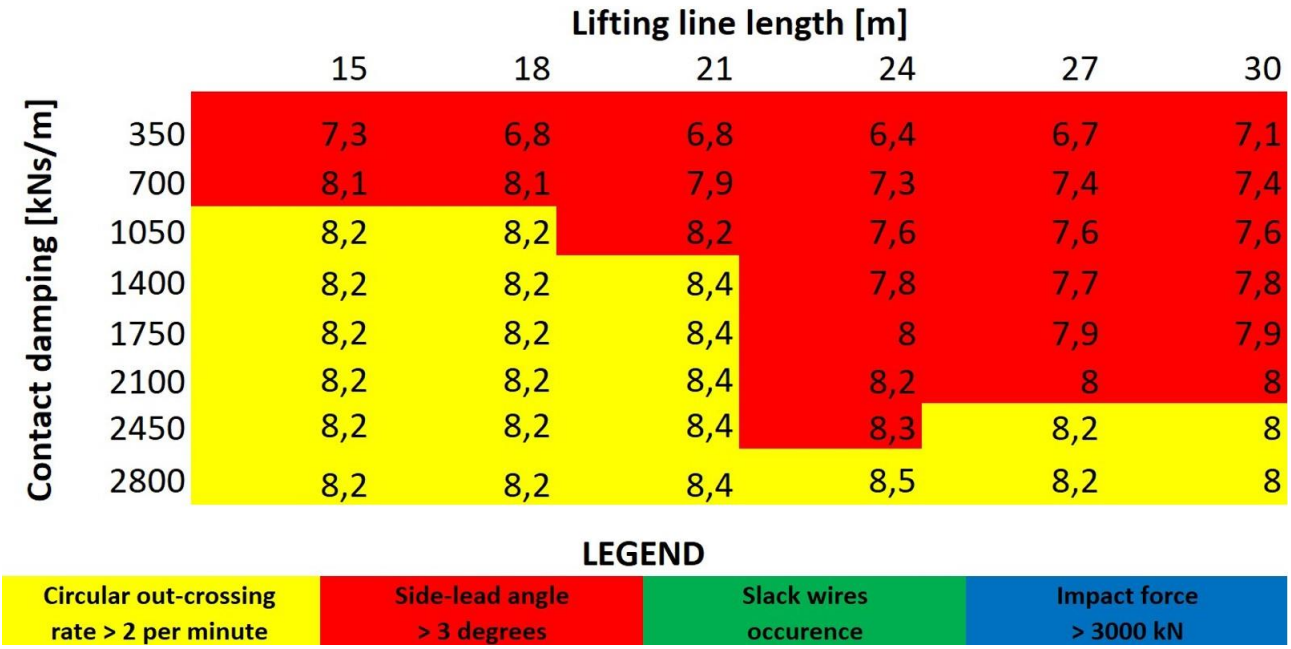


*Figure 51: Allowable wind velocities (numbers in table) including the limiting criterion (colors in table) for lifting line lengths (horizontal) and contact damping coefficients (vertical)*

The following can be concluded from the second iteration:

- Highest allowable mean wind velocity is 8.5 m/s found at a lifting line length of 24 m and a contact damping coefficient of 2800 kNs/m. This mean wind velocity corresponds to the lower end of the value 5 (fresh breeze) on the Beaufort wind force scale.
- For low contact damping coefficients, the installation is limited by the side-lead angle (red in Figure 51), whereas for increasing damping, the installation becomes limited by the circular out-crossing rate (yellow in Figure 51).
- The contact damping coefficient has no influence on the circular out-crossing rate, since the circular out-crossing rate is determined before contact takes place. By increasing the contact damping, the highest allowable mean wind velocity stays 8.5 m/s.
- Therefore, damping should be applied to the WTG tower motions in a way that affects both the side-lead angle and the circular out-crossing rate. For this reason, just as for the vertical asymmetric catcher, horizontal linear damping will be applied to the horizontal motions of the bottom of the WTG tower in the third iteration.
- In the third iteration, the contact damping will be reset at its initial value of 350 kNs/m.

*Iteration 3*

The specifications for the third iteration of installation with jack-up vessel characteristics using a conical catcher are as follows.

- As concluded from the results in the second iteration, damping the motions of the bottom of the WTG tower yields higher allowable wind velocities for installation. For installation using a vertical asymmetric catcher, it was shown that a maximum allowable wind velocity of 10.8 m/s is to be obtained with the application of linear damping to the WTG tower bottom motions. In this iteration, this damping will be applied to the installation with the conical catcher. The damping coefficient is a variable, visualized on the vertical axis in Figure 52.
- The lifting line length will be varied as well. This is visible on the horizontal axis in Figure 52.
- Except for linearly damping the horizontal motions of the bottom of the WTG tower, all other variables are the same as in the previous iteration.

- Numbers in Figure 52 indicate the maximum allowable mean wind velocity at 10 m above SWL at which installation could occur. Colors in Figure 52 indicate which requirement (see legend) limits the installation.

| WTG tower bottom damping [kNs/m] \ Lifting line length [m] | 15 | 18 | 21 | 24 | 27 | 30 |
|---|---|---|---|---|---|---|
| 0 | 7,3 | 6,6 | 6,7 | 6,4 | 6,7 | 7,1 |
| 200 | 9,2 | 9 | 8,1 | 7,8 | 7,6 | 7,5 |
| 400 | 10,1 | 9,7 | 9 | 8,5 | 8,2 | 8 |
| 600 | 10,6 | 10,1 | 9,6 | 9,1 | 8,8 | 8,5 |
| 800 | 10,7 | 10,2 | 9,8 | 9,5 | 9,2 | 9 |
| 1000 | 10,8 | 10,5 | 10,2 | 9,9 | 9,6 | 9,3 |
| 1200 | 11 | 10,8 | 10,5 | 10,2 | 9,9 | 9,6 |
| 1400 | 11,3 | 11 | 10,8 | 10,5 | 10,1 | 9,8 |
| 2000 | 11,8 | 11,4 | 11,1 | 10,8 | 10,5 | 10,1 |
| 2500 | 11,9 | 11,6 | 11,2 | 10,8 | 10,5 | 10,1 |
| 3000 | 11,9 | 11,6 | 11,2 | 10,8 | 10,5 | 10,1 |

**LEGEND**

| Circular out-crossing rate > 2 per minute | Side-lead angle > 3 degrees | Slack wires occurence | Impact force > 3000 kN |
|---|---|---|---|

*Figure 52: Allowable wind velocities (numbers in table) including the limiting criterion (colors in table) for lifting line lengths (horizontal) and damping coefficients (vertical).*

The following can be concluded from the third iteration:

- Highest allowable mean wind velocity is 11.9 m/s found at a lifting line length of 15 m and a damping coefficient of a linear damper that dampens the horizontal motions of the bottom of the WTG tower bottom of 2500 kNs/m or 3000 kNs/m. This mean wind velocity corresponds to the value 6 (strong breeze) on the Beaufort wind force scale.
- The installation is in all cases limited by the maximum side-lead angle of 3 degrees (red).
- After three iterations, the installation with jack-up vessel characteristics using a conical catcher is allowed to occur with wind velocities of up to 11.9 m/s.

*Concluding remarks of installation with jack-up vessel characteristics using a conical catcher*

After iteratively determining and optimizing the allowable wind velocities for installation, it appeared that it is limited at 11.9 m/s for the conical catcher, which is higher than the 10.8 m/s found for the vertical asymmetric catcher. To put these wind velocities in perspective, they correspond to the mid and low end of the value of 6 on the Beaufort wind force scale, respectively.

The values found are associated with uncertainty. Especially with regards to the crane tip motions, since it is out of the scope of this research to incorporate a specific crane vessel. Therefore, in section 5.4, the results will be subjected to a sensitivity study related to crane tip specific variables. As such, a first exploration of workability of installation is provided.

## 5.3 Installation limits and catcher selection with floating vessel crane tip excitation

In this section, the limits are determined for installation with a vertical asymmetric catcher and for installation with a conical catcher. The crane tip excitation corresponds to a floating installation vessel. To assess the installation limits, a base case is defined and described in subsection 5.3.1. Subsection 5.3.2

describes how through an iterative process, the limits for installation with floating installation vessel characteristics using a vertical asymmetric catcher is determined. Subsection 5.2.3 repeats this exercise for a conical catcher.

For the assessment of limits in installation with floating installation vessel characteristics, not the same amount of iterations is performed as for the installation with jack-up vessel characteristics. The reason for this is twofold:

1. The results from a certain iteration with jack-up vessel characteristics appeared to do not significantly improve workability or to be practically impossible to be executed from a crane operator perspective.
2. In the case of the vertical asymmetric catcher in the jack-up vessel, a stronger catcher design was determined. The stiffened catcher design is applied to the floating vessel installations using a vertical asymmetric catcher as well. The catcher without stiffeners as in Figure 38 will not be applied anymore.

For both aforementioned reasons, there are just two iterations for installation with a floating vessel. Both are described for the vertical asymmetric catcher and the conical catcher in the subsections 5.3.2 and 5.3.3 respectively. Ultimately, in section 5.4, the results for both the jack-up vessel and floating vessel are compared and a sensitivity analysis is performed.

### 5.3.1 Base case definition

The aim of defining a base case is to focus on the procedure of determining and optimizing the installation limits. Optimization is focused at improving the mean wind velocity for installation. As such, a first exploration is performed to workability of installation. In the base case, variables are selected for which the limits are determined and optimized. First of all, WTG tower dimensions are selected and shown in Table 3 (subsection 5.2.1). The dimensions are based on the GE Haliade-X 12 MW wind turbine, as stated by General Electric.

For the assessment of installation limits based on floating vessel characteristics, the crane tip excitation is quite different from the jack-up vessel. The crane tip motion amplitudes are increased. The vertical amplitude is a factor 10 higher than for the jack-up vessel and the horizontal amplitude is 5 times higher. The amplitudes are modelled with the same dependency on the wind velocity as for the jack-up vessel. The frequency is with 0.5 rad/s lower than the 0.9 rad/s applied for the jack-up vessel. The crane tip excitations with floating vessel characteristics are given in Table 5.

| ***Floating vessel property*** | **Quantity** | **Unity** |
|---|---|---|
| *Horizontal crane tip frequency* | 0.5 | rad/s |
| *Horizontal crane tip amplitude* | $0.05*U^2_{\text{meanwind@10SWL}}$ | m |
| *Vertical crane tip frequency* | 0.5 | rad/s |
| *Vertical crane tip amplitude* | $0.01*U^2_{\text{meanwind@10SWL}}$ | m |

*Table 5: Floating vessel specifications as used for the determination of allowable limits*

Both the vertical asymmetric catcher and the conical catcher have specific installation behavior and requirements and their dimensions are variable. The catcher that allows for the highest mean wind velocity in installation is deemed preferable for installation. The maximum allowable contact force for both types of catchers are described in subsections 5.1.3 and 5.1.4. If it appears that the maximum allowable contact force is limiting in installation, the catcher will be strengthened, and the updated maximum allowable contact force will be determined using finite element analysis.

In the following subsections, the installation limits will be assessed for a vertical asymmetric catcher and a conical catcher. This limit, expressed in mean wind velocity at 10 m above SWL, will be optimized iteratively for the different variables in installation and the use of WTG tower guidance.

### 5.3.2 Determination and optimization of installation limits using a vertical asymmetric catcher

The installation requirements described in section 5.1 provide the basis for assessing installation limits. The allowable limits are expressed in the mean wind velocity at 10 m above SWL on which both the wind spectrum and the crane tip motions are based as described in subsection 5.3.1. For the initial assessment of the installation limits, apart from crane operator induced crane tip motions, no WTG tower guidance is applied. The vertical asymmetric catcher is a cylinder segment with a height of 3 m, a radius of 4.15 m and an inscribed angle of 90 degrees. Figure 38 provides a visualization of this catcher type including a finite element-based determination of equivalent stresses resulting from a collision. The installation limits are determined iteratively. Below, the iterations are given. The specifications of an iteration are given before the results. After the results, the conclusions of the iterations are given which provide the basis for the following iteration.

*Iteration 1*

The specifications for the first iteration of installation with floating vessel characteristics using a vertical asymmetric catcher are as follows.

- The stiffened vertical asymmetric catcher is applied. This catcher and corresponding equivalent stresses resulting from contact with the MP are shown in Figure 45. The maximum allowable contact force is 1170 kN for this catcher.
- The initial location of the crane tip is -2 m. This is to be considered as an equilibrium position around which the wind induced horizontal crane tip motions oscillate. The reason for this initial horizontal position is to prevent the bottom of the catcher from making axial impact with the MP during lowering of the WTG tower as described in subsection 5.1.5.
- The final horizontal crane tip location, also in the form of an equilibrium position, is a variable. In Figure 53, this variable is seen on the vertical axis. The aim of this final horizontal location is to 'hang' the tower with the catcher against the MP and as such, to prevent bouncing behavior between the catcher and MP with the probability of axial impact between the DSJ rings.
- The lifting line is variable, seen on the horizontal axis in Figure 53.
- Numbers in Figure 53 indicate the maximum allowable mean wind velocity at 10 m above SWL at which installation could occur. Colors in Figure 53 indicate which requirement (see legend) limits the installation.

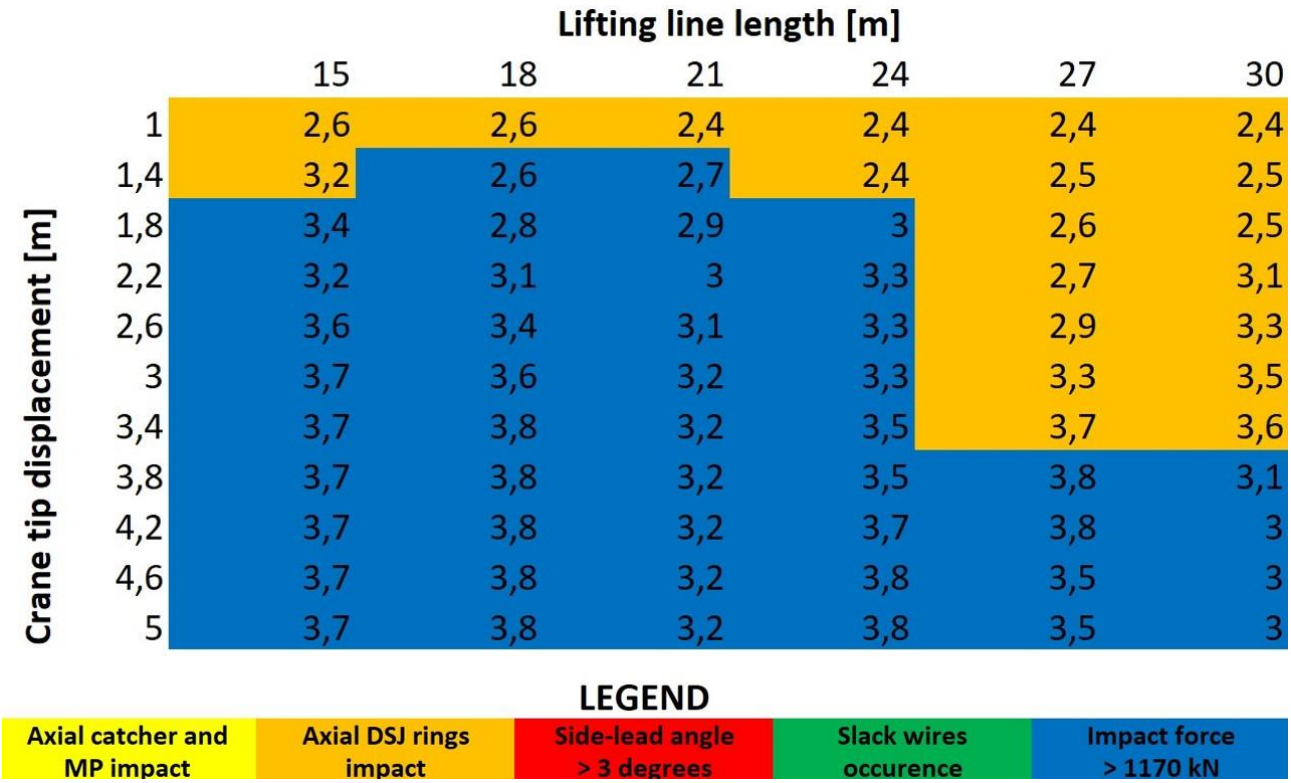


*Figure 53: Allowable wind velocities (numbers in table) including the limiting criterion (colors in table) for lifting line lengths (horizontal) and operator crane tip displacements (vertical)*

The following can be concluded from the first iteration:

- Highest allowable mean wind velocity is 3.8 m/s found at a lifting line length of 18 and 24 m and a final horizontal crane tip location of 5 m. This mean wind velocity corresponds to the lower end of the value 3 (gentle breeze) on the Beaufort wind force scale.
- The installation is limited by the maximum allowable contact force requirement (blue) and the probability of axial impact between the DSJ rings (orange).
- Both aforementioned installation requirements are based on horizontal motions of the bottom of the WTG tower in installation. In the second iteration, linear damping will be applied at the horizontal motions of the bottom of the WTG tower, with the aim to decrease the dependency of the installation limits on the aforementioned variables and to increase the allowable mean wind velocity in installation.

*Iteration 2*

The specifications for the second iteration of installation with a floating vessel using a vertical asymmetric catcher are as follows.

- The crane operator induced horizontal displacements of the crane tip are set constant. The initial location of the crane tip remains -2 m. The final location, after contact between the catcher and MP is 2.6 m. Again, the aforementioned values represent equilibrium positions around which the wind velocity induced harmonic crane tip displacements oscillate.
- The initial lifting line length is again a variable, seen on the horizontal axis in Figure 54.
- The damping coefficient of the linear damper that dampens the horizontal motions of the bottom of the WTG tower are variable and given on the vertical axis in Figure 54.
- Numbers in Figure 54 indicate the maximum allowable mean wind velocity at 10 m above SWL at which installation could occur. Colors in Figure 54 indicate which requirement (see legend) limits the installation.


*Figure 54: Allowable wind velocities (numbers in table) including the limiting criterion (colors in table) for lifting line lengths (horizontal) and damping coefficients (vertical).*

The following can be concluded from the second iteration:

- Highest allowable mean wind velocity is 9.7 m/s found at a lifting line length of 30 m and a damping coefficient of 3000 kNs/m. This mean wind velocity corresponds to the upper end of the value 5 (fresh breeze) on the Beaufort wind force scale.
- The installation for low (< 400 kNs/m) damping coefficients is limited by the maximum allowable contact force requirement (blue). For damping coefficients below 400 kNs/m and 2000 kNs/m, the installation is limited by the risk of axial impact between the rings of the DSJ. For damping coefficients above 2000 kNs/m, the installation is limited by the risk of axial impact between the catcher and MP (yellow) and by the maximum allowable side-lead angle (red).
- Installation with floating vessel characteristics and the use of a vertical asymmetric catcher, is allowed to occur with mean wind velocities at 10 m above SWL of up to 9.7 m/s. In the following subsection, the same analysis, with the same floating vessel excitation characteristics, is repeated for a conical catcher. As uncertainty comes associated with the vessel specific variables, a sensitivity analysis will be performed in section 5.4 to study the effects of vessel associated variables on the installation limits and provide a first exploration of workability.

*Concluding remarks of installation with floating vessel characteristics using a vertical asymmetric catcher*

The installation limits, expressed in allowable mean wind velocities, are determined for installation using a vertical asymmetric catcher with crane excitation corresponding to jack-up vessel characteristics. Apparently, for the conditions applied, if the horizontal motions of the bottom of the WTG tower are damped, the allowable mean wind velocity at 10 m above SWL is limited to 9.7 m/s.

It is one of the aims of this research to compare the vertical asymmetric catcher with the conical catcher in terms of allowable mean wind velocity for installation. Therefore, in the following subsection, the allowable mean wind velocities for installation will be determined for the conical catcher. The same typical floating installation vessel crane tip excitations will be applied.

Ultimately, when the results are obtained for both catchers and the crane tip excitations that correspond to a jack-up and a floating vessel, a sensitivity study will be performed that is described in section 5.4.

### 5.3.3 Determination and optimization of installation limits using a conical catcher

The installation requirements described in section 5.1 provide the basis for assessing installation limits. The installation limits are expressed in the mean wind velocity at 10 m above SWL on which both the wind spectrum and the crane tip motions are based as described in subsection 5.3.1. For the initial assessment of the installation limits, no WTG tower guidance is used. The conical catcher is a hollow truncated cone with a thickness equal to the thickness of the DSJ ring at the bottom of the WTG tower. The height of this cone is 2 m and the width a variable which will be analyzed in the iterative procedure of determining and optimizing the allowable wind velocity. Figure 40 provides a visualization of this catcher type including a finite element-based determination of equivalent stresses resulting from a collision. The installation limits are determined iteratively. Below, the iterations are given. The specifications of an iteration are given before the results. After the results, the conclusions of the iterations are given which provide the basis for the following iteration.

*Iteration 1*

The specifications for the first iteration of installation with floating vessel characteristics using a conical catcher are as follows.

- For consistency purposes, the wind field applied is based on the same wind spectrum realization and the crane tip motions as a function of the wind velocity is equal to the one used for the vertical asymmetric catcher.
- For the conical catcher, there is no active crane operator action performed during lowering of the WTG tower. There is only a fixed displacement of the crane tip which is the function of the mean wind velocity. This displacement aims to counteract the mean wind such that the motion equilibrium position of the center of the catcher is right above the center of the MP.
- For the first iteration, no guidance of the WTG tower in the form of constant forcing or damping is applied.
- For the conical catcher, some installation requirements are the same as for the vertical asymmetric catcher:
    - Slack wires are not allowed. For background information on this requirement, see subsection 5.1.1.
    - The side-lead angle of the lifting line is allowed to be at most 3 degrees. For background information on this requirement, see subsection 5.1.2.
- Other installation requirements for the conical catcher are different from the requirements for a vertical asymmetric catcher:
    - The circular out-crossing rate is allowed to be at most 2 times per minute. For background information on the circular out-crossing rate, see subsection 5.1.6.
    - The maximum allowable contact force between the catcher and the MP is 3 MN for the conical catcher instead of 700 kN or 1170 kN for the vertical asymmetric catcher. For background information on this requirement, see subsections 5.1.3 and 5.1.4.
- The lifting line length is used as a variable, seen on the horizontal axis in Figure 55.
- For the first iteration, the catcher width is also a variable. The different catcher widths analyzed are seen on the vertical axis in Figure 55.
- Numbers in Figure 55 indicate the maximum allowable mean wind velocity at 10 m above SWL at which installation could occur. Colors in Figure 55 indicate which requirement (see legend) limits the installation.

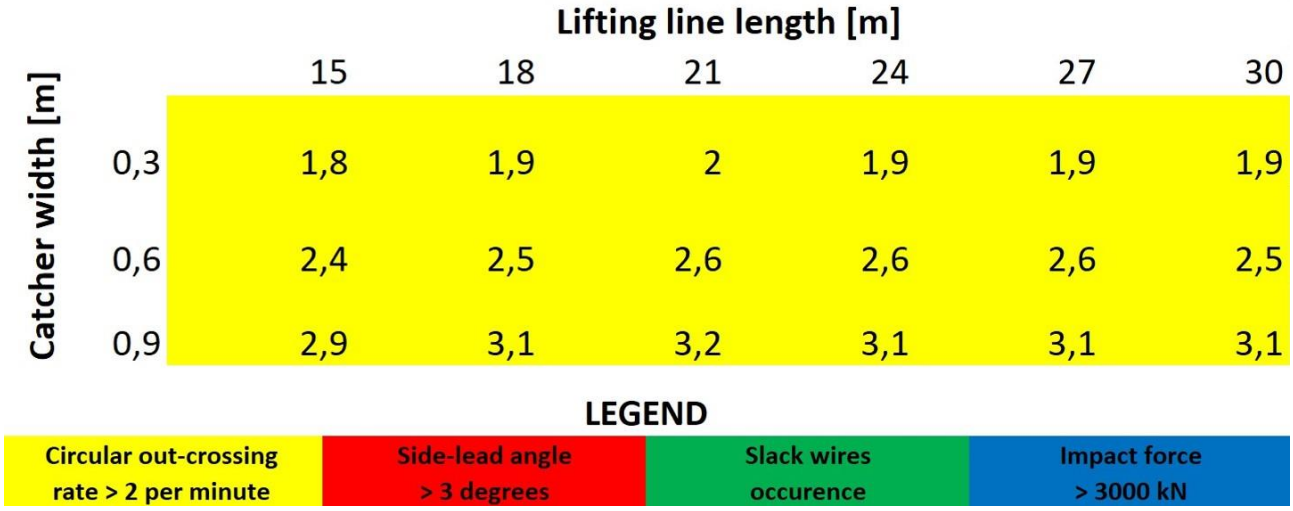


*Figure 55: Allowable wind velocities (numbers in table) including the limiting criterion (colors in table) for lifting line lengths (horizontal) and conical catcher widths (vertical).*

The following can be concluded from the first iteration:

- The highest allowable mean wind velocity is 3.2 m/s found at a lifting line length of 21 m and a catcher width of 0.9 m. This mean wind velocity corresponds to the upper end of the value 2 (light breeze) on the Beaufort wind force scale. This wind velocity is considerably lower than the 7.3 m/s found for the conical catcher in installation with jack-up vessel characteristics. The crane tip frequency and higher amplitude create different WTG tower motion behavior with considerably larger horizontal motions of the WTG tower bottom. Therefore, without any tower guidance, the allowable mean wind velocity is limited to 3.2 m/s due to the circular out-crossing rate requirement (yellow).
- In the second iteration, the catcher width is fixed at 0.9 m. Constant damping will be applied to the horizontal motions of the WTG tower bottom. The maximum allowable mean wind velocity in installation will be determined for different damping coefficients and lifting line lengths.

*Iteration 2*

The specifications for the second iteration of installation with a floating vessel using a vertical asymmetric catcher are as follows.

- In the previous subsection it was shown that for installation with floating vessel characteristics, using a vertical asymmetric catcher, the maximum allowable mean wind velocity with WTG tower bottom damping is 9.7 m/s. The same exercise is repeated for the conical catcher in this iteration. The bottom motions of the WTG tower are linearly damped. The damping coefficient is variable and seen on the vertical axis in Figure 56.
- The lifting line is variable too and seen on the horizontal axis in Figure 56.
- Except for the application of linear damping to the horizontal motions of the bottom of the WTG tower, all other variables are the same as in the previous iteration.
- Numbers in Figure 56 indicate the maximum allowable mean wind velocity at 10 m above SWL at which installation could occur. Colors in Figure 56 indicate which requirement (see legend) limits the installation.

| WTG tower bottom damping [kNs/m] \ Lifting line length [m] | 15 | 18 | 21 | 24 | 27 | 30 |
|---|---|---|---|---|---|---|
| 0 | 2,9 | 3,1 | 3,2 | 3,1 | 3,1 | 3,1 |
| 200 | 4,8 | 4,8 | 4,8 | 4,9 | 4,9 | 4,9 |
| 400 | 6,1 | 6,1 | 6,1 | 6,2 | 6,2 | 6,2 |
| 600 | 7,1 | 7,2 | 7,3 | 7,3 | 7,2 | 7,2 |
| 800 | 8,2 | 8,2 | 8,2 | 8,2 | 8,2 | 8,1 |
| 1000 | 8,8 | 8,9 | 8,9 | 9 | 9 | 9 |
| 1200 | 9,6 | 9,7 | 9,8 | 9,8 | 9,8 | 9,8 |
| 1400 | 10,3 | 10,4 | 10,5 | 10,5 | 10,5 | 10,5 |
| 2000 | 11,7 | 11,8 | 12,1 | 12,1 | 12,4 | 12,5 |
| 2500 | 13,1 | 13,1 | 12,9 | 13,1 | 12,8 | 12,8 |
| 3000 | 13 | 12,6 | 12,3 | 12,6 | 12,1 | 12,2 |

**LEGEND**

| Circular out-crossing rate > 2 per minute | Side-lead angle > 3 degrees | Slack wires occurence | Impact force > 3000 kN |
|---|---|---|---|

*Figure 56: Allowable wind velocities (numbers in table) including the limiting criterion (colors in table) for lifting line lengths (horizontal) and damping coefficients (vertical).*

The following can be concluded from the second iteration:

- The highest allowable mean wind velocity is 13 m/s found at a lifting line length of 15 m and a damping coefficient of 3000 kNs/m. This mean wind velocity corresponds to the upper end of the value 6 (strong breeze) on the Beaufort wind force scale.
- For damping coefficients up to 2000 kNs/m limited by the circular out-crossing rate requirement (yellow). For damping coefficients above 2000 kNs/m, the installation is limited by the side-lead angle requirement.

*Concluding remarks of installation with floating installation vessel characteristics using a conical catcher*
After iteratively determining and optimizing the allowable wind velocities for installation, it appeared that the wind velocity is limited at 13 m/s for the conical catcher, which is higher than the 9.7 m/s found for the vertical asymmetric catcher. To put these wind velocities in perspective, they correspond to the values of 6 and 5 on the Beaufort wind force scale, respectively.

The values found are associated with uncertainty. Especially with regards to the crane tip motions, since it is out of the scope of this research to incorporate a specific crane vessel. Therefore, in section 5.4, the results will be subjected to a sensitivity study related to crane tip specific variables. As such, a first exploration of workability of installation is provided.

## 5.4 Sensitivity analysis of the installation limits and extent of exploration into workability

The sections 5.2 and 5.3 provided the installation limits, expressed in maximum allowable mean wind velocity at 10 m above SWL, for WTG tower installation with jack-up and floating vessel characteristics, respectively. The limits were determined for installation using a vertical asymmetric catcher and a conical catcher. Without any WTG tower guidance in installation, the allowable mean wind velocity in installation is limited to between 3 and 7 m/s, corresponding to the values of 2 to 4 on the Beaufort wind force scale, respectively.

Different methods have been assessed to increase the installation limits found. One of the methods was to apply constant force on the bottom of the WTG tower. The force would be applied as soon as the catcher

has surpassed the top of the MP during lowering. The aim of this action was to 'pull' the WTG tower with its catcher against the MP. The simulations indicated that this action did not significantly increase the allowable mean wind velocity in installation. A plausible explanation for this is that constant force does not draw net kinetic energy from the WTG tower (i.e. energy is added when the bottom of the tower moves in the same direction as the force and energy is subtracted if not). Net, the energy balance does not change.

Another method has been assessed that does yield a significant increase in allowable mean wind velocity for installation. This increase has been observed in the simulations where linear damping was applied to the horizontal motions of the WTG tower bottom. Damping, which in nature draws kinetic energy from a system, decreased the motion amplitudes of the WTG tower bottom. As such, also the collision magnitude and risk of axial impact were reduced, and the installation limits increased significantly. The corresponding allowable mean wind velocities in installation are given in Table 6. To put these values into perspective, for installation at the Borssele offshore wind farm off the coast of the Netherlands, they would yield the workability percentages as indicated in Table 6 [48].

The mean wind velocities found for installation with floating vessel are in the same range as for the jack-up vessel characteristics. Floating vessel crane tip motions have a significantly larger amplitude, however the frequency is smaller as indicated in Table 4 and Table 5. The simulations showed that due to the lower frequency, the side-lead angle variations are smaller and therefore, considerably larger crane tip amplitudes are allowed in installation. This explains the higher allowable mean wind velocity in installation with a conical catcher using floating vessel characteristics and the use of a conical catcher. For the vertical asymmetric catcher, the lower side-lead angle variations increased the allowable mean wind velocity. This increase was however limited due to the risk of axial impact between the catcher and the MP. Hence, the lower allowable mean wind velocity for the vertical asymmetric catcher with floating vessel characteristics compared to jack-up vessel characteristics.

| **Allowable mean wind velocity** | *Jack-up vessel characteristics* | *Floating vessel characteristics* |
|---|---|---|
| *Vertical asymmetric catcher* | 10.8 m/s<br>78% Workability at Borssele Wind Farm [48] | 9.7 m/s<br>71% Workability at Borssele Wind Farm [48] |
| *Conical catcher* | 11.9 m/s<br>85% Workability at Borssele Wind Farm [48] | 13.1 m/s<br>90% Workability at Borssele Wind Farm [48] |

*Table 6: Overview of allowable mean wind velocities for different vessel characteristics and catcher types*

It must be noted that it is out of the scope of this research to incorporate specific crane vessels. Therefore, some vessel or crane tip specific variables are associated with uncertainty. Therefore, in order to get a more complete picture of installation limits and a first exploration of workability of installation, a sensitivity analysis has been performed with regards to vessel specific variables. Three variables have been considered in the sensitivity analysis.

- The amplitude of harmonic crane tip motions. Table 4 and Table 5 provided an overview of crane tip motions as used for installation with jack-up vessel and floating vessel characteristics, respectively. These motions are equal to a constant, multiplied the mean wind velocity squared. This constant has been halved, kept equal, and doubled for the sensitivity analysis.
- The allowable side-lead angle is initially set at 3 degrees. This vessel-specific installation requirement is varied analyzed at 2, 3 and 4 degrees for the sensitivity analysis.
- The crane operator induces displacements of the crane tip during installation. This displacement has analyzed with -0.5, 0 or 0.5 m deviation.

The sensitivity analysis based on the three aforementioned variables has been performed for installation with both types of catchers and jack-up vessel as well as floating installation vessel characteristics. Figure 57 and Figure 58 provide the results of this sensitivity analysis for installation with jack-up vessel and floating vessel characteristics, respectively. The allowable mean wind velocity in installation is given in bands in the figure. The lower and upper end are the allowable mean wind velocities with one standard deviation, based on the variations in the vessel-specific variables.

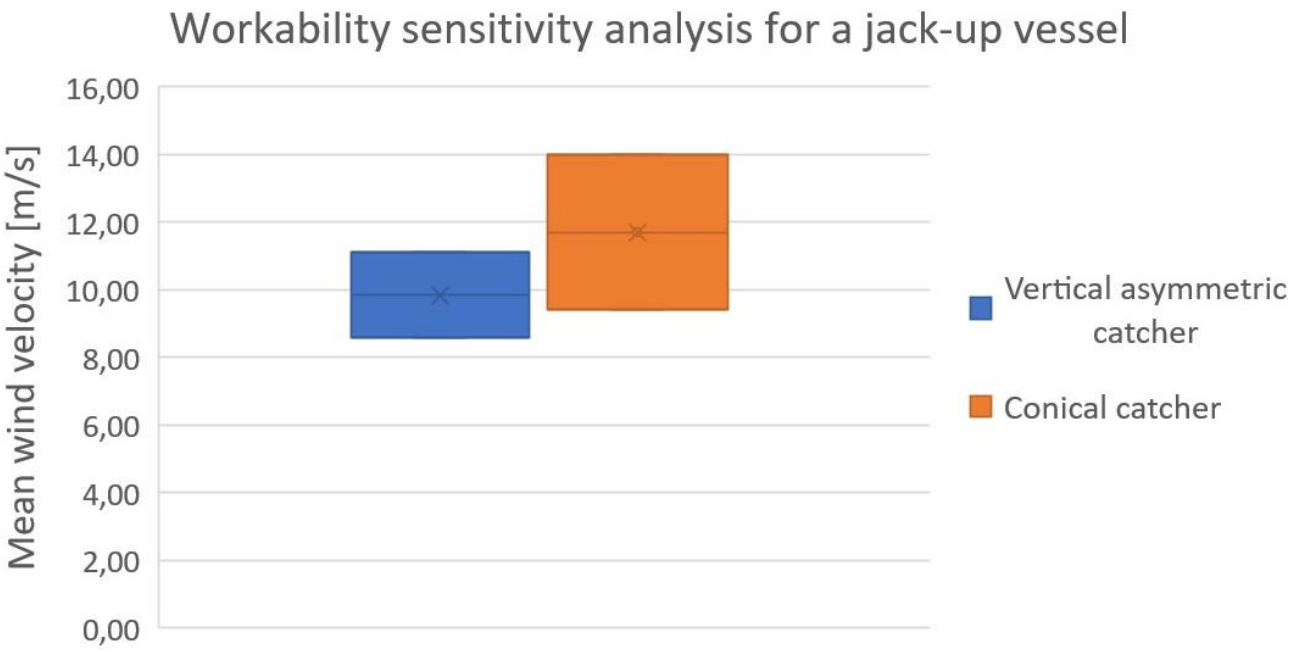


*Figure 57: Sensitivity analysis of the allowable mean wind velocity in installation for jack-up vessel-specific variables*

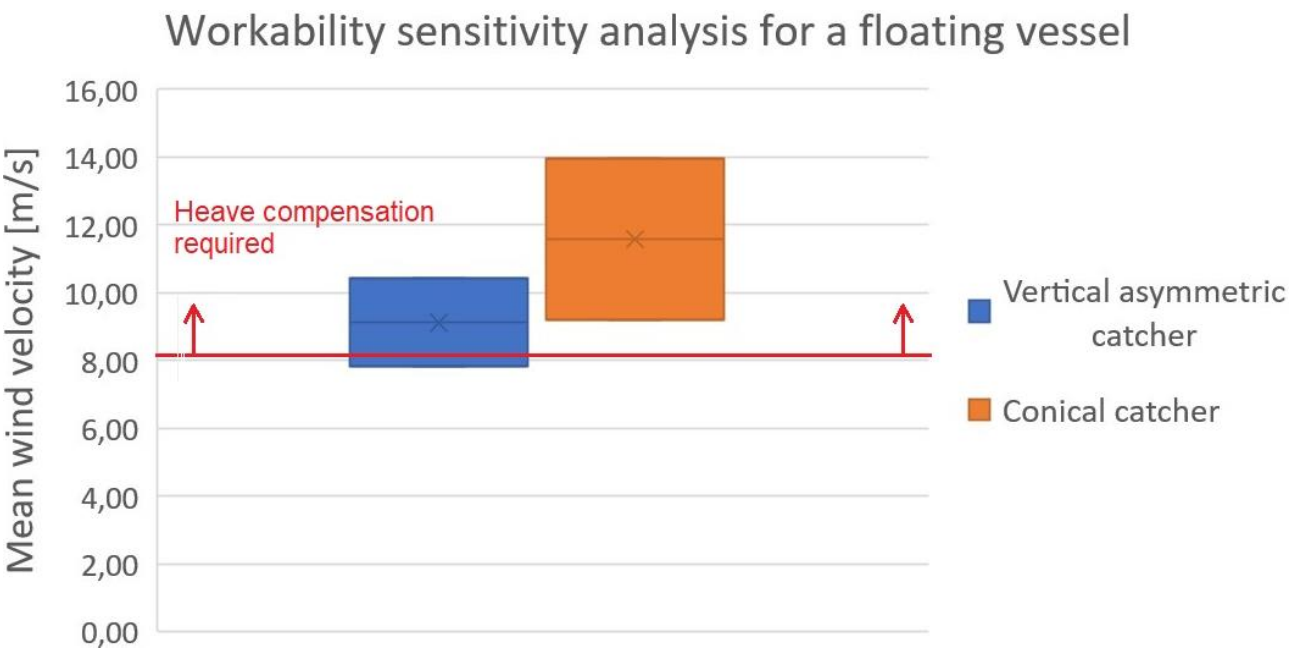


*Figure 58: Sensitivity analysis of the allowable mean wind velocity in installation for floating vessel-specific variables*

Some important observations can be made from the sensitivity analysis performed with respect to vessel-specific variables as seen in Figure 57 and Figure 58.

- The results show that allowable mean wind velocities are in the same range for installation with jack-up vessel and floating vessel characteristics. Simulations indicate that due to the lower frequency of crane tip motions of the floating vessel, the side-lead angle variations are smaller. Therefore, larger crane tip amplitudes are allowed before the side-lead angle limit is reached.

- The conical catcher has a higher variability than the vertical asymmetric catcher related to vessel specific variables. However, the simulations show that the allowable mean wind velocity in installation with the conical catcher is higher than with the vertical asymmetric catcher.
- For the installation with floating vessel characteristics, the vertical crane tip motion amplitudes are significant and could lift the catcher above the top of the MP again after contact has been made. To prevent this event from happening, heave compensation is required to reduce the vertical motions of the crane tip. It should be noted that it is not required for this part of the installation to fully compensate vertical crane tip motions. The catcher is allowed to vertically move along the MP as long as it is not lifted above the MP again after contact is made.

Some notifications on the first exploration into workability of installation have to be made. The results presented in this research are primarily aimed at providing an understanding of motion and collision behavior, installation requirements and the extent to which these requirements limit the installation. The installation limits only serve as a first exploration to workability of installation, because the workability comprises the entire installation operation (i.e. from shore to final landing on foundation). Also, more detailed information on the installation vessel and associated dynamics as well as potential 3D effects are to improve the workability assessment. Regarding 3D, in the next section, potential effects on WTG tower installation and workability are identified. The next section also provides the discussion of this research.

## 5.5 Discussion

In this study, a model is developed to simulate the installation of a WTG tower based on the Double Slip Joint and the use of catchers. The aim is to find the installation limits based on various installation requirements. A first exploration into workability of installation is consequently provided. This section discusses important aspects of this research and the simulation model in subsection 5.5.1. Subsection 5.5.2 discusses a first look at WTG tower installation in 3D. In this subsection, potential 3D motion and collision effects on workability of installation are identified. It is also discussed with the help of an offshore installation operation how potentially negative effects arising in 3D on the workability of installation may be reduced or mitigated.

### 5.5.1 The simulation model, environmental excitation, and non-linear collision modeling

The model, developed in this research, simulates the lowering and catcher mating (i.e. catcher on the bottom of the WTG tower contacts the top of the MP) during installation of a WTG tower on a MP. Regarding the WTG tower and the MP, a rigid body approach is taken. This approach does incorporate the effects of bending and vibrations of the WTG tower and MP in the description of the contact element to describe stiffness and damping in collisions. The values for this stiffness and damping are determined through finite element analysis of collision responses for a flexible WTG tower and MP.

The validity of this modeling approach has been confirmed by comparing the simulation model with this finite element model. The motion behavior of the WTG tower is found to be similar in both models. Also, the collisions and contact forces are well comparable in timing and magnitude and show the same general behavior in both models. Some important modeling aspects require further discussion.

*Environmental excitation of the WTG tower*

Wind is a source of excitation of the WTG tower in installation. The wind velocity increases in height above SWL and changes in time. Modeling the wind shear profile is important as this affects the wind induced force and moment on the WTG tower and as such the motion behavior during installation. Including the time-variations in the wind field is important because low frequency variations, or wind gusts, affect the motion behavior of the WTG tower during installation.

The simulation model also includes aerodynamic damping as a result of the relative motions of the WTG tower in the wind field. Modeling this is important, because it is a source of kinetic energy dissipation and it affects the motion behavior of the WTG tower. Both the rotations and translations of the WTG tower affect the relative wind velocity on the WTG tower. Therefore, both motions have been considered in the aerodynamic damping. Incorporating aerodynamic damping is important because, due to the associated kinetic energy dissipation, it reduces WTG tower oscillations during installation.

Waves are a second and less obvious source of WTG tower excitation. Waves induce vessel motions and consequently, they induce crane tip motions during installation. The crane tip hoists the WTG tower and as such, the wave induced crane tip motions affect the WTG tower motion behavior. This research incorporates harmonic horizontal and vertical crane tip excitation for two different types of installation vessels. First, a relatively high frequency and low amplitude excitation which is typical for a jack-up vessel. Second, a relatively low frequency and high amplitude excitation typical for a floating installation vessel. It must be noted, however, that no specific vessel or corresponding dynamics have been incorporated in the model. Therefore, the results do not provide for a definitive answer on the workability of installation, but rather for a first exploration into workability of installation.

*Non-linear collision modeling*

In this research, special attention has been paid to the collisions between the catcher and the top of the MP. In literature, it was found that it was common practice to assume that contact can be described by a linear spring-damper. This common practice was shown not to be applicable when making use of finite element analysis. It was shown that contact stiffness is in fact non-linear, with the contact stiffness consisting of two sources of stiffness that are connected in series in the contact element (i.e. both sources have the same

contact force that describes their respective deformation). Bending of the WTG tower and MP is the first source of stiffness. An EB beam model in ANSYS was used to quantify this stiffness and showed that this source of stiffness is linear. However, the second source of stiffness, caused by local deflections of the mating parts, is observed to be non-linear and as a result, the overall contact stiffness is non-linear. Finite element analysis showed that as the catcher contacts the top DSJ ring of the MP, the contact starts at a point, but as the contact load increases, also the area of contact increases. The local stiffness therefore contains a stiffening non-linearity (i.e. the stiffness increases with the deflection). The equivalent stiffness, which includes both bending and local deformation, showed that for low contact loads, the total deformation is governed by both bending and local deformation. For high contact loads, the contact area is large and little local deformation occurs. For these high contact loads, the stiffness is governed by bending of the WTG tower and MP and a more linear stiffness behavior is observed.

The description of the non-linear contact stiffness in collisions between the catcher and MP is implemented in the simulation model. The importance of an accurate description of collision behavior is found in assessing installation limits. The importance is supported by the fact that bouncing behavior between the catcher and MP is different for different contact stiffnesses. Also, the magnitude of the contact forces varies. Therefore, an accurate description of the contact element is necessary in order to obtain a reliable assessment of the installation requirements related to the risk of axial impact and the maximum allowable contact force.

This research focused on the local deflection of the DSJ ring in contact with the catcher. Local deformation of the catcher and the part of the MP and WTG tower close to the DSJ ring may also affect the local stiffness. It is not expected that the results of this research would differ significantly if this would have been considered. The final results, described in section 5.4, concern an installation where the horizontal motions of the bottom of the WTG tower are damped. This damping is achievable through (active) tugger winches. The resulting WTG tower bottom motion amplitudes are small, and the collision forces remain well within their limits.

*Assessment of installation limits and exploration of workability*

Installation limits are not solely determined by the maximum contact force in collisions between a catcher and the MP. Rather, a set of requirements applies that should be complied with during an installation in order to facilitate a successful installation. Requirements include prevention of axial impacts between the WTG tower and MP, the prevention of slack wires, and the limitation of the side-lead angle. These criteria have been incorporated in the model to assess the limits for both installation with the conical catcher or installation with the vertical asymmetric catcher. As specific installation vessels and corresponding dynamics are not incorporated in this research, specific requirements related to the capability of the crane vessel to install the WTG tower may be present in practice, but do not surface in this research. These requirements may for example be associated with preventing (excessive) vessel-load interaction, heave compensation of the crane, ensuring the structural integrity of the crane and preventing the load from colliding with the crane or vessel.

The installation limits and first exploration of workability have been assessed for different lifting line lengths, where in all cases, the lifting line was attached in a double pendulum-way to the top of the WTG tower. However, in offshore WTG tower installation campaigns, the WTG tower does not necessarily have to be suspended by a single lifting line connected to the WTG tower top. Also, some installation vessels may allow for the use of multiple cranes with multiple lifting lines. Appendix F shows three examples of installation technologies and configurations that are performed or proposed by the industry that have different installation characteristics.

### 5.5.2 Looking forward to 3D: Identification of potential effects and mitigation measures

This section provides a first look at the installation in 3D and it serves as guidance and a starting point for further research for two reasons. First, potential 3D motion and collision effects are identified that may have an effect on installation limits and workability of installation. Second, it suggests ways to mitigate or reduce

potentially negative effects on workability arising from 3D motion and collision effects. Finally, this section concludes with a note on how damping can be practically applied to the WTG tower bottom motions.

*Identification of potential 3D effects*

A good starting point for understanding 3D motions and collisions of the WTG tower is the double pendulum. The lifting line is the massless upper element of the double pendulum and the WTG tower is the bottom element with a distributed mass. The bottom of a 3D undamped double pendulum, with small angles and without crane tip excitation may show Lissajous-like motion behavior [49], [50]. An example of this periodic motion behavior is provided in Figure 59 (left) [51].

For offshore WTG tower installation, the small angle approach is considered valid, since the angles are not allowed to become large (e.g. side-lead angle is allowed to become around 3 degrees). There is however crane tip excitation, a time and spatially variable wind load and aerodynamic damping. Therefore, the motion behavior of the bottom of the double pendulum does not exhibit regular behavior. [52] Studied the circular out-crossing rate in TP installation and found that the TP bottom displacements are irregular, which is seen in Figure 59 (right).

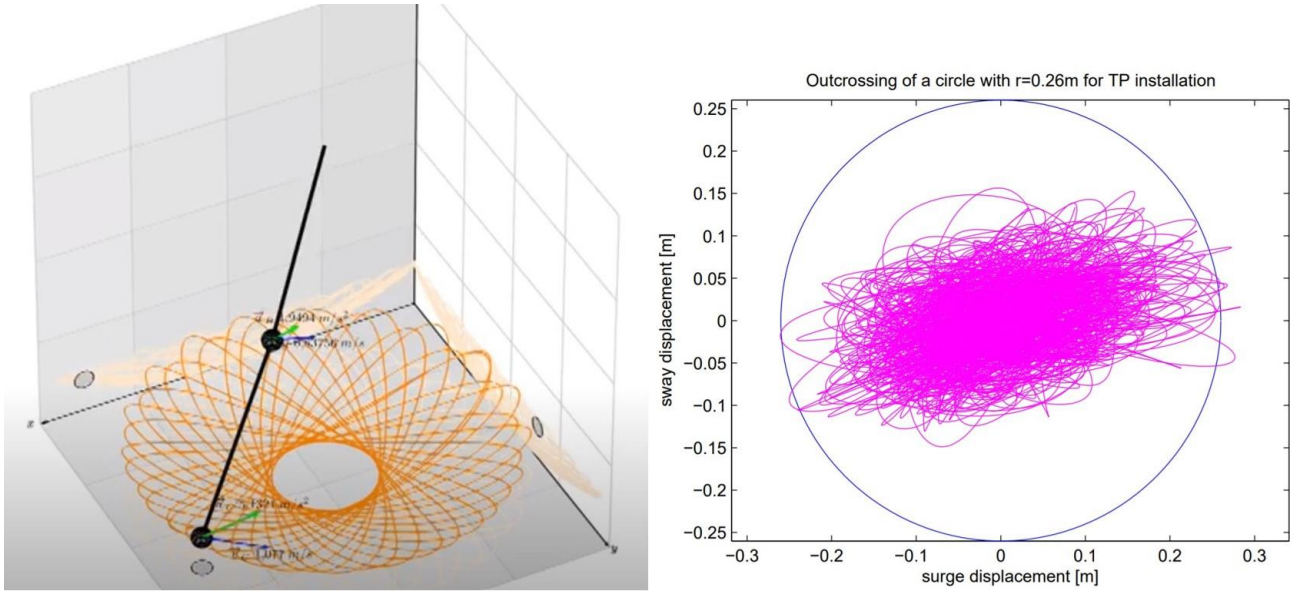


*Figure 59: Motion patterns of the bottom of a 3D double pendulum with small angles exhibiting Lissajous-like motion behavior (left) [51]. Right gives the motion pattern of the bottom of a TP that is excited by crane tip motions and wind [52].*

Two potential 3D effects are identified that may affect the installation limits and the workability of installation:

- Figure 59 (right) shows that the horizontal displacements of the bottom of the TP are moving both in surge and sway directions [52]. This indicates that without using any installation tools (e.g. tugger winches) to limit either the surge or sway displacement, out-crossings may occur in both directions and consequently, the circular out-crossing rate may be higher in 3D and more restrictive in installation limits and workability.
- Figure 59 also shows that when an out-crossing occurs (magenta line crosses the blue circle), the angle between the lines is not necessarily 90 degrees. To be more specific, inclined collisions are possible that may yield motion responses out of the plane of the collision that are not considered in the 2D or in-plane approach. For example, an inclined collision resulting from an incoming surge motion of the WTG tower bottom may induce a contact force component in the sway direction and a corresponding moment around the longitudinal axis of the WTG tower, potentially resulting in sway and yaw (rotation around longitudinal axis) motions of the WTG tower after contact.

*Identification of potential mitigation measures*

A closer look at a real offshore installation operation suggests that the aforementioned potential 3D effects on the circular out-crossing rate and the inclined collision responses may be reduced. Figure 60 shows a WTG tower with a vertical asymmetric catcher on the bottom. On the right in the figure is the installation vessel and tugger lines are connected between the vessel and the WTG tower (indicated by the black arrows). The tugger lines limit the ability of the bottom of the WTG tower to sway and yaw. With reduced sway and yaw motions, out-crossings are reduced in sway direction and out-of-plane motion responses resulting from inclined collisions may be limited in amplitude.


*Figure 60: Installation of a WTG tower using a vertical asymmetric catcher. Tugger lines control the sway motions, suggesting that the WTG tower motions are primarily in the surge direction (source: https://www.youtube.com/watch?v=4f3qkd_oaCs)*

Figure 60 also shows that there are no tugger lines preventing the surge motions (indicated in red) of the WTG tower bottom. This research showed that damping the WTG bottom motions in this direction reduces the risk of axial impact and the magnitude of collision forces between the catcher and MP and it suggests that the workability of installation improves consequently. A potential way to apply this damping is to connect two active tugger winches from the WTG tower bottom to the vessel. One that is connected to the bow and one that is connected to the stern of the vessel. The active winches should be controlled in a way that they serve as linear dampers on the motions of the bottom of the WTG tower.

In [53], the concept of controlling active tugger winches, such that they serve as dampers is studied and it concluded that damping can be introduced by controlling the phase difference between the motion of the vessel and the motion of the load. The motion phase of the load should lag 90 degrees behind the motion phase of the vessel. As such, kinetic energy is extracted from the load motions and a velocity dependent force is acted on the load. However, [53] also noted that for the active tugger winch to serve as a damper, the phase difference of 90 degrees is important for otherwise, the damping will decrease and a stiffness or mass term is added to the load.

# 6

# Conclusions & Recommendations

From the analysis of the results of this study, obtained with the non-linear model to simulate the installation of a WTG tower onto an MP, some conclusions can be drawn, which are presented in this chapter. Also, the recommendations for future research are formulated.

## 6.1 Conclusions

This research provides insight in WTG tower installation with a Double Slip Joint connection using either a conical or vertical asymmetric catcher. Besides the applicability to the Double Slip Joint connection, the approach taken in this research is applicable to installation on any monopile as long as the top of the monopile is circumferential. Note that this research concerns WTG tower lowering and catcher mating and that this approach does not concern the mating of DSJ rings, where specific properties apply to their installation behavior. The focus in this research is placed on obtaining an accurate description of motion and collision behavior of a WTG tower with the aforementioned catchers in lowering and catcher mating during installation. The focus in this research is also placed at obtaining an understanding of installation behavior and defining requirements that the WTG tower installation should comply to. The framework of installation requirements and the model simulations provide for an assessment of limits in installation and serve as a first exploration of workability of installation. Conclusions are drawn with respect to several aspects, which are provided below.

*Collisions between the catcher and MP*

- Contact stiffness in a collision between a catcher and the MP is concluded to be non-linear. With finite element analysis, it is shown that it consists of combined local deflection of the DSJ ring and bending of the WTG tower and MP. The equivalent contact stiffness contains a stiffening non-linearity (i.e. stiffness increases with deflection). This conclusion concerns a contact element where the stiffness in lumped into a single element, instead of a situation where the stiffness is distributed over the contact area.
- The conical catcher can handle significantly higher contact loads than the vertical asymmetric catcher. Finite element analysis showed that even though stiffeners are applied and the edges of the connection of the vertical asymmetric catcher to the WTG tower are rounded, the stresses due to collisions with the MP are concentrated at the edges of the connection of the catcher to the WTG tower. These peak stresses are not observed with the conical catcher whose connection to the tower spans the entire bottom of the tower. The finite element analysis therefore indicates that the

allowable contact forces, for the dimensions used, are close to three times higher for the conical catcher than the vertical asymmetric catcher.

*Installation requirements*

In order to assess whether an installation attempt is successful, a set of installation requirements has been formulated to which the installation should comply. Below, conclusions are formulated regarding these installation requirements for the vertical asymmetric catcher and the conical catcher.

- Finite element analysis proved that the vertical asymmetric catcher has significantly lower allowable contact forces than the conical catcher. Model simulations showed that for installation with the vertical asymmetric catcher, the relatively low contact force limit is reached soon during collisions between the catcher and the MP. This limits the allowable motions of the WTG tower during installation with a vertical asymmetric catcher.
- For installation with the vertical asymmetric catcher, the crane tip must be horizontally displaced during lowering in order to 'lean' the WTG tower with its catcher against the MP. This action is required in order to prevent axial impact between the bottom of the WTG tower and the top of the MP. This 'leaning' is not required to prevent axial impact for installation using a conical catcher. From the perspective of the crane operator, installation using a vertical asymmetric catcher may therefore prove to be more challenging than the conical catcher.
- It is observed in the simulations that during lowering of the WTG tower and collisions between the catcher and the MP, the lifting line tensile force varies at most a few percent around its mean value. Therefore, the risk of slack wires for this part of the installation is confirmed to be low and does not limit this part of the installation.
- For installation vessels, it is commonly required that the side-lead angle is limited to around 3 degrees. During lowering of the WTG tower and collisions between the catcher and the MP, the side-lead angle varies. Model simulations showed that the side-lead angle has larger variations when the WTG tower is lowered to the extent that collisions occur. This phenomenon is observed to a larger extent for the vertical asymmetric catcher compared to the conical catcher. Therefore, for the vertical asymmetric catcher, the side-lead angle requirement limits the WTG tower motions during installation more than it does for the conical catcher.

*Initial exploration into workability*

This study provided a simulation-based assessment of installation limits based on a framework of installation requirements that has been defined. As such, a first exploration to workability of installation is provided. Some conclusions can be drawn with regards to this first exploration to workability of installation.

- The results indicate that the maximum allowable mean wind velocity is higher for installation with a conical catcher than with a vertical asymmetric catcher. This observation is supported by the findings that the side-lead angle variations are smaller, the maximum allowable contact force is higher and there is no active horizontal crane tip displacement required during lowering for the conical catcher. Therefore, this research suggests that the workability of installation is higher overall for the conical catcher than for the vertical asymmetric catcher.
- It is observed in the simulations that for high vertical crane tip motion amplitudes, the catcher can go above the MP again after contact, with the risk of a subsequent axial impact. This research suggests that for installation with floating vessels, heave compensation is required to some extent to prevent the catcher from being lifted above the MP after contact has been made.
- Model simulations showed that applying damping to the horizontal motions of the bottom of the WTG tower significantly reduces the contact forces and the risk of axial impact. It was observed that therefore, the allowable mean wind velocity in installation increases significantly. This research therefore suggests that the workability of installation is improved by horizontally damping the motions of the bottom of the WTG tower.

## 6.2 Recommendations

The focus of this research has been limited to the motion and collision limits, as well as the requirements in installation. To this end, with regards to workability, only a first exploration has been performed. The following is therefore recommended for future research.

- This study has been performed using 2D or in-plane simulations in which there are 3 degrees of freedom. In 3D, there are 6 degrees of freedom, where the sway (out-of-plane) and yaw motions of the WTG tower bottom may increase the circular out-crossing rate and yield inclined collisions that both have a potentially negative effect on the workability of installation, as indicated in section 5.5. This section also suggests that controlling the aforementioned motions and collision responses is relatively straightforward with tugger lines. For future research, it is however recommended to study this tugger line configuration in more detail with the aim of workability optimization. To be more specific, it is recommended to study the effects of different tugger winch characteristics (e.g. constant tension or actively controlled) on the circular out-crossing rate and inclined collision responses resulting from sway and yaw motions and how they affect the workability of installation.
- Simulations indicate that applying linear damping to the horizontal 2D or in-plane motions of the bottom of the WTG tower reduces contact forces and the risk of axial impact. The research suggests that the workability of installation is consequently improved. It was indicated in section 5.5 that active tugger winches can achieve damping characteristics by inducing a 90-degree phase lag between the load and vessel motions. For future research, it is recommended to study the accuracy with which active tugger winches can keep a 90-degree phase lag, especially during the catcher mating phase. In this phase, collisions between the catcher and foundation occur that induce a sudden change in the motion phase of the load relative to the vessel. It is therefore recommended in particular to study the timing with which the actively controlled tugger winch can 'adapt' its characteristics to the new motion phase characteristics.
- For high vertical crane tip amplitudes, the catcher may be lifted above the MP again after contact has been made, with the associated risk of subsequent axial impact. To prevent this event from occurring, heave compensation may be required to reduce the amplitude of vertical motions of the crane tip. Since the dimensions of offshore wind turbines keep increasing, it is recommended for to study how and to which extent heave motions can be compensated for increasingly heavy structures.
- It is recommended for future research to installation workability to perform a case study in 3D, incorporating the entire system of a specific installation vessel, WTG tower, foundation, and installation site. This allows for the use of site-specific wind and wave data and installation vessel motion RAO's and as such, it allows for the use of software packages like OrcaFlex. For an improved understanding of workability, it is recommended to investigate how wind and waves independently excite the foundation, the vessel, and the WTG tower and how (excessive) vessel-load interaction can be prevented. For the latter, it is recommended to investigate vessel-load interaction for different phases in installation. During lowering, there is no contact between the WTG tower and foundation and therefore, the motion behavior and vessel-load interaction may differ from the mating phase, where contact is made between the foundation and WTG tower.
- The Double Slip Joint connection allows for installation underwater. It is recommended for future research to study the effects of the wave splash zone, added mass, hydrodynamic damping and potential other effects have on installation behavior, limits, and workability of installation.
- This research shows that the actions of the crane operator influence the collision behavior between the catcher and the MP. It is recommended to study the timing and accuracy with which the crane operator can displace the crane tip and how this affects the workability.

# Bibliography


[1] C. U. Jensen, T. E. Panduro and T. H. Lundhede, “The Vindication of Don Quixote: The Impact of Noise and Visual Pollution from Wind Turbines,” *Land Economics, University of Wisconsin Press,* vol. November 2015, no. 4, pp. 668-682, 2014.

[2] W. Musial and B. Ram, “Large-Scale Offshore Wind Power in the United States, Executive Summary,” National Renewable Energy Laboratory, Golden, Colorado, September 2010.

[3] R. G. Sullivan, L. B. Kirchler, J. Cothren and S. L. Winters, “Offshore Wind Turbine Visibility and Visual Impact Treshold Distances,” Argonne National Laboratory, Argonne, 2012.

[4] W. Mackenzie, “Foresight 20/20,” Wood Mackenzie, Edinburgh, United Kingdom, 2020.

[5] F. M. Birkeland, “Numerical Simulation of Installation of XL Monopile for Offshore Wind Turbines,” Norwegian University of Science and Technology, Trondheim, 2016.

[6] M. J. Kaiser and B. Snyder, “Offshore Wind Energy Installation and Decommissioning Cost Estimation in the U.S. Outer Continental Shelf,” Energy Research Group, LLC, Louisiana, 2010.

[7] E. M. Dolores, J.-S. López-Gutiérrez and V. Negro, “Gravity-Based Foundation in the Offshore Wind Sector,” Research Group on Marine, Coastal and Port Environment and other Sensitive Areas, Universidad Politécnica de Madrid, Madrid, Spain, 2018.

[8] M. Seynsche, “Mit drei Beinen auf Hoher See,” Repower, Hamburg, 2007.

[9] I.-W. Chen, B.-L. Wong, Y.-H. Lin, S.-W. Chau and H.-H. Huang, “Design and Analysis of Jacket Substructures for Offshore Wind Turbines,” Department of Engineering Science and Ocean Engineering, National Taiwan University, Taipei, 2016.

[10] M. Dähne, J. Züchner and J. Tougaard, “Impact of underwater sound on harbour porpoises,” in *The treshold value from different perspectives*, Stralsund, 2018.

[11] L. Weilgart, “Impact of Noise Pollution on FIsh and Invertebrates with an Emphasis on Pile Driving,” in *Ocean Care*, Halifax, Canada, 2018.

[12] M. Zeilder, “Monitoring of compliance with the treshold value of 160 dB,” in *Federal Maritime and Hydrographic Agency*, Hamburg, Germany, 2018.

[13] E. Rosenauer, “Investment Costs of Offshore Wind Turbines,” Center for Sustainable Systems, University of Michigan, 2014.

[14] B. T. Pereyra, “Design of a Counter Weight Suspension System for the TetraSpar Floating Offshore Wind Turbine,” Delft University of Technology & Norwegian University of Science and Technology, Delft, 2018.

[15] I. Shiklomanov, “Water in Crisis: A Guide to the World's Fresh Water Resources,” Oxford University Press, New York, 1993.

[16] P. Dallyn, A. El-Hamalawi, A. Palmeri and R. Knight, “Experimental Testing of Grouted Connections for Offshore Substructures: A Critical Review,” ESPRC (UK Engineering and Physical Sciences Research), 2016.

[17] I. Lotsberg, A. Serednicki, H. Bertnes and A. Lervik, “On the Capacity of Grouted Connections in Monopile Offshore Wind Turbine Structures,” *Proceedings of the 10th International Conference on Advances in Steel and Concreet Composite Structures,* vol. 2012, no. 10, pp. 646-653, 2012.

[18] N. Müller, D. Leduc, P. Kraemer and F. Schoefs, “Damage detection in offshore wind turbine grouted connection by nonlinear harmonic identification,” in *Offshore Wind R&D Conference 2018*, Bremerhaven, Germany, 2018.

[19] H. Xianlong and S. Tianli, “A New Identification Method for Bolt Looseness in Wind Turbine Towers,” Vibration-Based Health Monitoring of Mechanical Systems - special edition, 2019.

[20] M. L. A. Segeren and K. W. Hermans, “Experimental investigation of the dynamic installation of a slip joint connection between the monopile and tower of an offshore wind turbine,” *Journal of Physics: Conference Series 524,* 2014.

[21] B. Van Gelder, “Windmolen in oogwenk op zijn plek met dubbele slip joint,” *Cobouw,* vol. 2020, no. 1, 2020.

[22] N. Visser, “Experimental set-up of the Double Slip Joint - Investigating the settling behavior,” Delft University of Technology, Delft, 2015.

[23] M. Wittingen, “Offshore Wind Turbine Monopile Foundation Installation with a Dynamic Positioned Vessel,” Delft University of Technology, Delft, 2018.

[24] W. A. Guachamin, Z. Gao and T. Moan, “Methodology for Assessment of the Allowable Sea States during Installation of an Offshore Wind Turbine Transition Piece Structure onto a Monopile Foundation,” *Journal of Offshore Mechanics and Arctic Engineering,* vol. 2017, no. 12, 2017.

[25] J. Woodhouse, J. C. Rene, C. S. Hall, L. W. Smith, F. H. King and J. W. McClenahan, “The Dynamics of a Ringing Church Bell,” Department of Engineering, University of Cambridge, Cambridge, 2012.

[26] K. Hasselmann, E. Bauer and P. Janssen, “The WAM Model - a Third Generation Ocean Wave Prediction Model,” *Journal of Physical Oceanography,* vol. 1988, no. December, pp. 1775-1810, 1988.

[27] L. B. Savenije, T. Ashuri, G. van Bussel and J. W. Staerdahl, “Dynamic Modeling of a Spar-type Floating Offshore Wind Turbine,” *EWEC Scientific Proceedings,* vol. 2010, pp. 283-287, 2010.

[28] R. Bos, “Extreme gusts and their role in wind turbine design,” TU Delft, Delft, 2017.

[29] IEC (2005a), “IEC 61400-1 Wind turbines - Part 1: Design requirements. 3rd edn. Geneva, Switzerland: International Electrotechnical Commission”.

[30] W. Bierbooms, “Module 4: Offshore Wind Climate,” in *DUWIND COURSE OE5662 OFFSHORE WIND FARM DESIGN*, Delft.

[31] DNVGL-ST-0437, “Loads and Site Conditions for Wind Turbines,” Det Norske Veritas, November 2016.

[32] B. Chen, Z. Zhang, X. Hua, B. Basu and S. R. Nielsen, “Identification of aerodynamic damping in wind turbines using time-frequency analysis,” *Mechanical Systems and Signal Processing,* vol. 2017, no. 91, pp. 198-214, 2017.

[33] K. Hasselmann, T. P. Barnett, E. Bouws, H. Carlson, K. Cartwright, J. A. Enke, H. Ewing, D. E. Gienapp, P. Hasselmann, A. Kruseman, P. Meerburg, D. J. Miller, K. Olbers, K. Richter, W. Sell and H. Walden, “Measurements of wind-wave growth and swell decay during the Joint North Sea Wave Project (JONSWAP),” *Ergnzungsheft zur Deutschen Hydrographischen Zeitschrift Reihe,* vol. 1973, no. 12, p. 95, 1973.

[34] H. Mitsuyasu, Y.-Y. Kuo and A. Masuda, “On the dispersion relation of random gravity waves. Part 2. An experiment,” Cambridge University Press, Cambridge, 1979.

[35] O. M. Philips, “The equilibrium range in the spectrum of wind-generated waves,” Cambridge University Press, Cambridge, 1958.

[36] W. E. Cummins, “The impulse Response Function and Ship Motions,” Symposium Ship Theory, Hamburg, Germany, 1962.

[37] J. M. Journee, “Strip theory algorithms,” Delft University of Technology, Ship Hydrodynamics Labaratory, Netherlands, 1992.

[38] T. I. Fossen, Handbook of marine craft hydrodynamics and motion control, John Wiley & Sons, 2011.

[39] J. Ye, “Dynamic Positioning during Heavy Lift Operations,” Delft University of Technology, Delft, 2016.

[40] J. M. Journée and W. W. Massie, “Offshore Hydromechanics,” Delft University of Technology, Delft, 2001.

[41] L. Xiangguo, M. Zhiqian, Z. Denglin and X. Baochun, “Modeling and anti-sway control of ship-mounted crane,” Advances in Mechanical Engineering, 2017.

[42] TU Delft, “Offshore Hydromechanics Part 2 Course,” Delft, 2019.

[43] R. Van der Valk, “Hoist and boom wire dynamics during offshore heavy lifting,” Delft University of Technology, Delft, 2017.

[44] T. J. Davies and M. Raoof, “Simple determination of the axial stiffness for large-diameter independent wire rope core or fibre core wire ropes,” 2003.

[45] H. H. Vanderveldt, B. S. Chung and W. T. Reader, “Some dynamic properties of axially loaded wire ropes,” Experimental Mechanics, 1973.

[46] C. R. Chaplin, “Damping in wire rope,” 1991.

[47] W. Shoubin, S. Xiaogang and L. Chengwei, “Method of Modal Analysis for Wind Turbines Based on Air-Structure Coupling Vibration Model,” *Information Technology Journal,* 2013.

[48] Netherlands Enterprise Agency, “Site Studies Wind Farm Zone Borssele: Metocean Study for the Borssele Wind Farm Zone Site 1,” DNV GL Energy, Utrecht, 2015.

[49] W. J. O'Connor, “Gantry Crane Control of a Double Pendulum, Distributed-Mass Load, Using Mechanical Wave Concept,” University College of Dublin, Dublin, 2013.

[50] W. B. Hales, “Recording Lissajous Figures,” *The Journal of the Acoustical Society of America,* vol. 16, no. 3, pp. 137-146, 1945.

[51] C. Racional, “Double Pendulum 3D Low Energy,” Based on a Computer Algebra System for the Euler-Lagrange Equations, 2014.

[52] W. A. Guachamin, T. Moan and Z. Gao, “Steady State Motion Analysis of an Offshore Wind Turbine Transition Piece During Installation Based on Outcrossing of the Motion Limit State,” in *OMAE2015-41142*, St. John's, Canada, 2015.

[53] H. Lageveen, “Modelling and Steering of Tuggerwinch,” Delft University of Technology, Delft.

[54] T. Hodgson, N. Sampathkumar and I. Cortizo, “Approach to Wind Wave Correlation in Coupled Analysis of Offshore WTG Substructures,” in *WindEurope*, Glasgow (UK), 2016.

[55] M. Reistad, O. Breivik, H. Haakenstad, O. J. Aarnes, B. R. Furevik and J. R. Bidlot, “A High-Resolution Hindcast of Wind and Waves for The North Sea, The Norwegian Sea and The Barents Sea,” *J. Geophys Res,* vol. 2011, no. 116, 2011.

# Appendix A

## The WAM model [26]: A Third Generation Ocean Wave Prediction Model

In an offshore environment, there exists a correlation between significant wave height and mean wind speed. It is pre-requisite for any type of coupled dynamic analysis of offshore wind turbines to establish a simplified but representative correlation between wind and wave conditions, according to [26]. The correlation between wind and waves is stochastic and [55] found that it is difficult to find an estimate of the probability distribution of wind and wave parameters. Therefore, conservatism regarding defining the wind field in a certain sea state is necessary.

Neglecting the stochastic nature of the wind and wave relationship, a mean wind speed at 10 m above the still water level (SWL) can be related to the significant wave height [26]. There are two situations in which this estimation is accurate. These are fetch-limited and fully developed waves. These situations can be described as follows:

1) A fetch-limited sea is one in which the wind has been blowing in a constant direction and it is not limited by time. In this case, the wave growth is determined by the 'fetch'. Fetch is the distance from lee shore.
2) A fully developed sea is a wave condition in which the wind has been blowing in constant direction for sufficient distance and time.

From these two possible wind and wave conditions, it can be concluded that the WAM model [26] is valid under the assumption that the wind direction doesn't vary in time. For fully developed waves the following relationship can be derived:

$$U_{10}^2(1.1 + 0.035U_{10}) = \frac{10gH_{\frac{1}{3}}}{2.115} \tag{A.1}$$

In which $U_{10}$ is the mean wind speed at 10 m above the still water level (SWL), $g$ is the gravitational acceleration and $H_{1/3}$ the significant wave height. For fetch-limited seas, the following relationship can be derived according to the WAM model [26]:

$$\frac{gH_{\frac{1}{3}}}{u_f^2} = 4.13 * 10^{-2}\left(\frac{gX}{u_f}\right)^{\frac{1}{2}} \tag{A.2}$$

Where $X$ is the distance from lee shore and $u_f$ is the friction velocity:

$$u_f^2 = 0.001U_{10}^2(1.1 + 0.035U_{10}) \tag{A.3}$$

Furthermore, it can be determined by the WAM model [26] what distance from lee shore marks the boundary between a fetch-limited and fully developed sea. This distance can be determined by substitution of the significant wave height $H_{1/3}$ for a fully developed sea into equation A.2 for fetch-limited seas:

$$X_{fetch} = \frac{gH_{\frac{1}{3},fd}^2}{(4.13 * 10^{-2})^2 * u_f^2} \tag{A.4}$$

Where $H_{1/3,fd}$ is the significant wave height for a fully developed sea and $X_{fetch}$ is the distance from lee shore at which the fetch-limited sea becomes fully developed.

The WAM model [26] described in Appendix A is valid under the assumption that the wind blows from the same direction for a sufficient period of time. Only then, the mean wind speed at 10 m above SWL can be obtained for fetch-limited and fully developed seas. The WAM model however only correlates the mean wind speed to waves and no relationship to wind velocity variations are provided.

# Appendix B

A simple collision model: Final velocities as a function of mass ratio for different damping coefficients

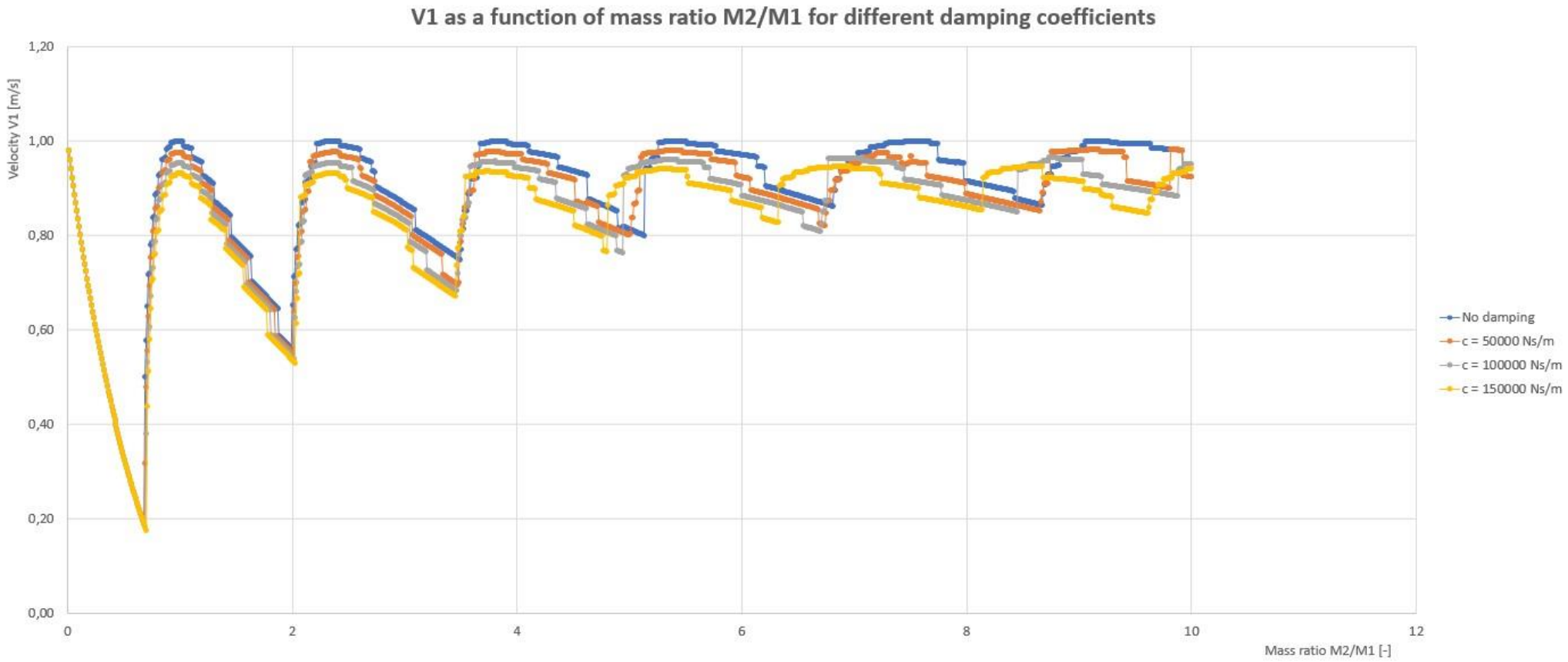


*Figure B. 1: Outgoing velocity of M2 after the first impact with the mass-spring-damper system as a function of the mass ratio. No damping (blue), 50,000 Ns/m damping (orange), 100,000 Ns/m (grey) and 150,000 Ns/m (yellow). Values as in figure are constant for different wall distances.*

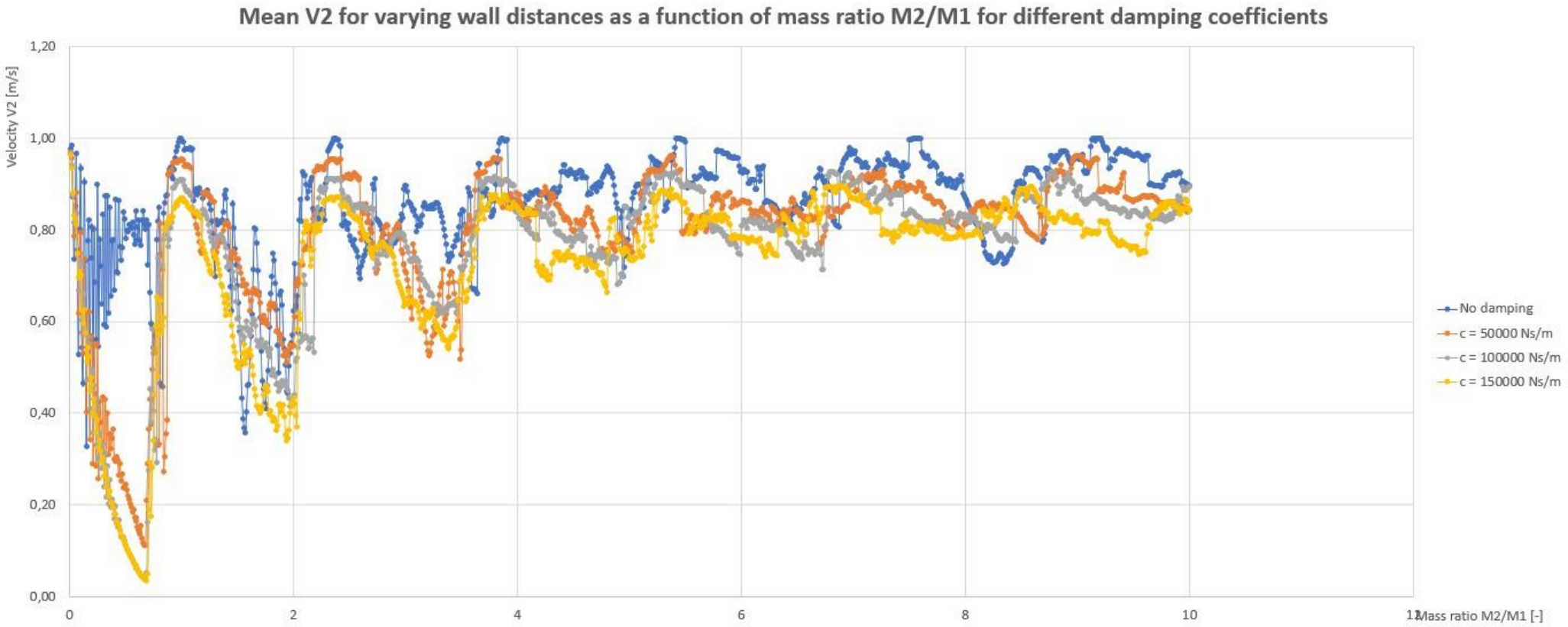


*Figure B. 2: Mean outgoing velocity of M2 after the second impact with the mass-spring-damper system as a function of the mass ratio. No damping (blue), 50,000 Ns/m damping (orange), 100,000 Ns/m (grey) and 150,000 Ns/m (yellow). V2 values in the figure are the mean velocities for a certain damping coefficient averaged over the wall distance as a function of the mass ratio.*

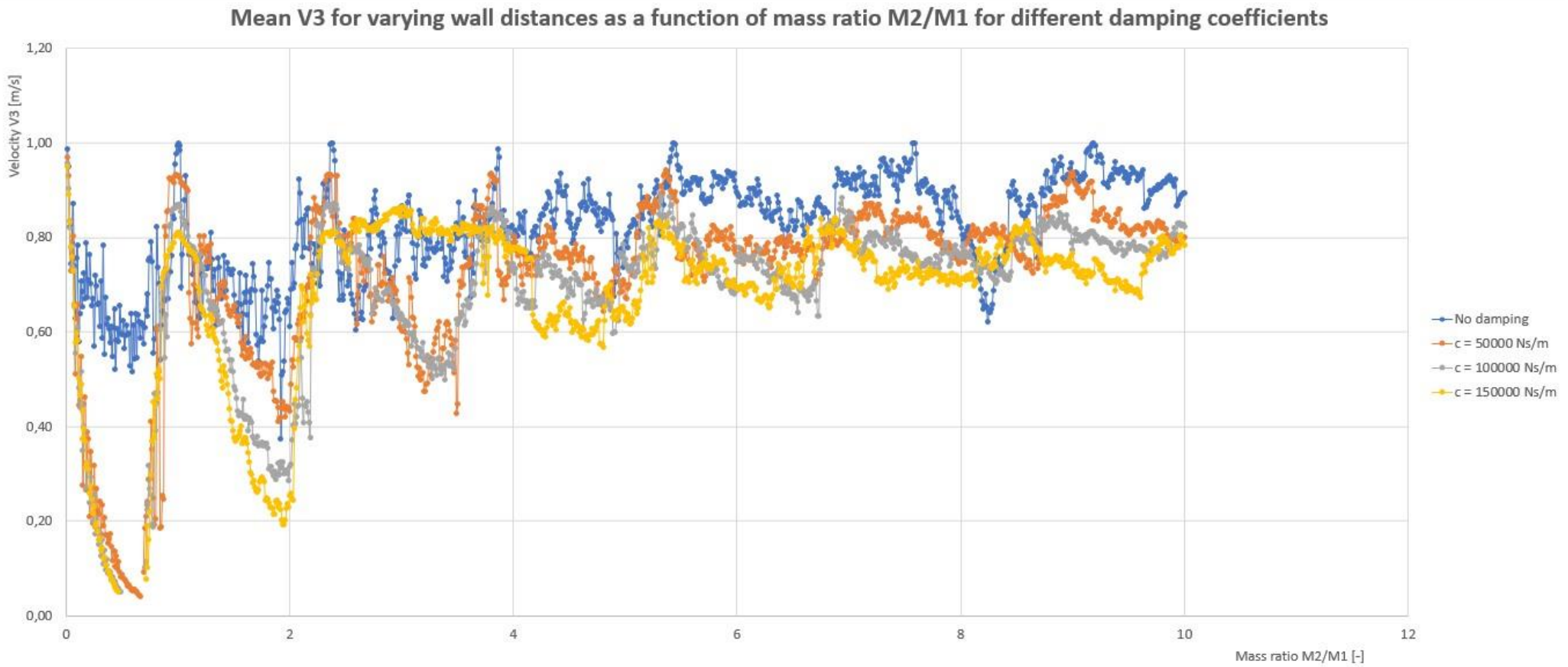


*Figure B. 3: Mean outgoing velocity of M2 after the second impact with the mass-spring-damper system as a function of the mass ratio. No damping (blue), 50,000 Ns/m damping (orange), 100,000 Ns/m (grey) and 150,000 Ns/m (yellow). V2 values in the figure are the mean velocities for a certain damping coefficient averaged over the wall distance as a function of the mass ratio.*

# Appendix C

A simple collision model: Wall distance induced variations on the velocities V2 and V3

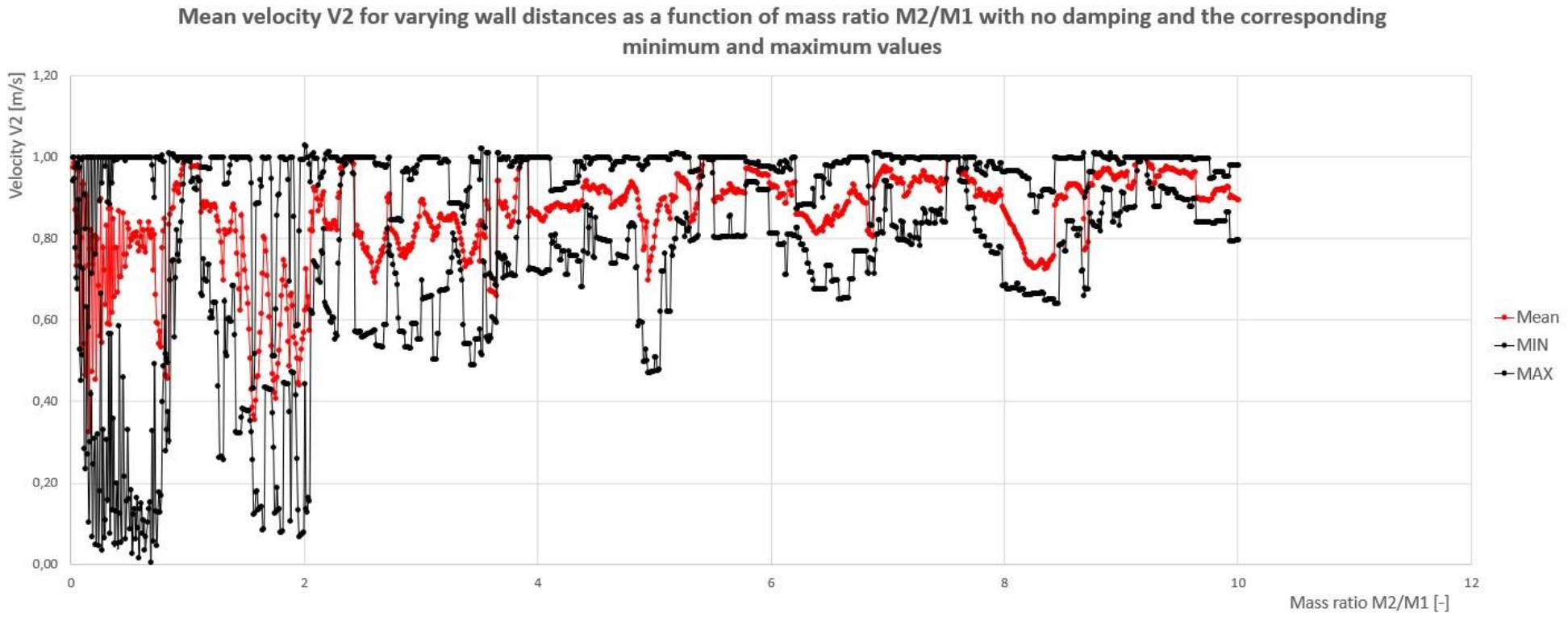


*Figure C. 1: Mean velocity V2 (red) as a function of mass ratio. Vibration-induced irregularities are indicated by the minimum and maximum velocities out of the set of different wall distances (in black). This figure represents the undamped situation.*

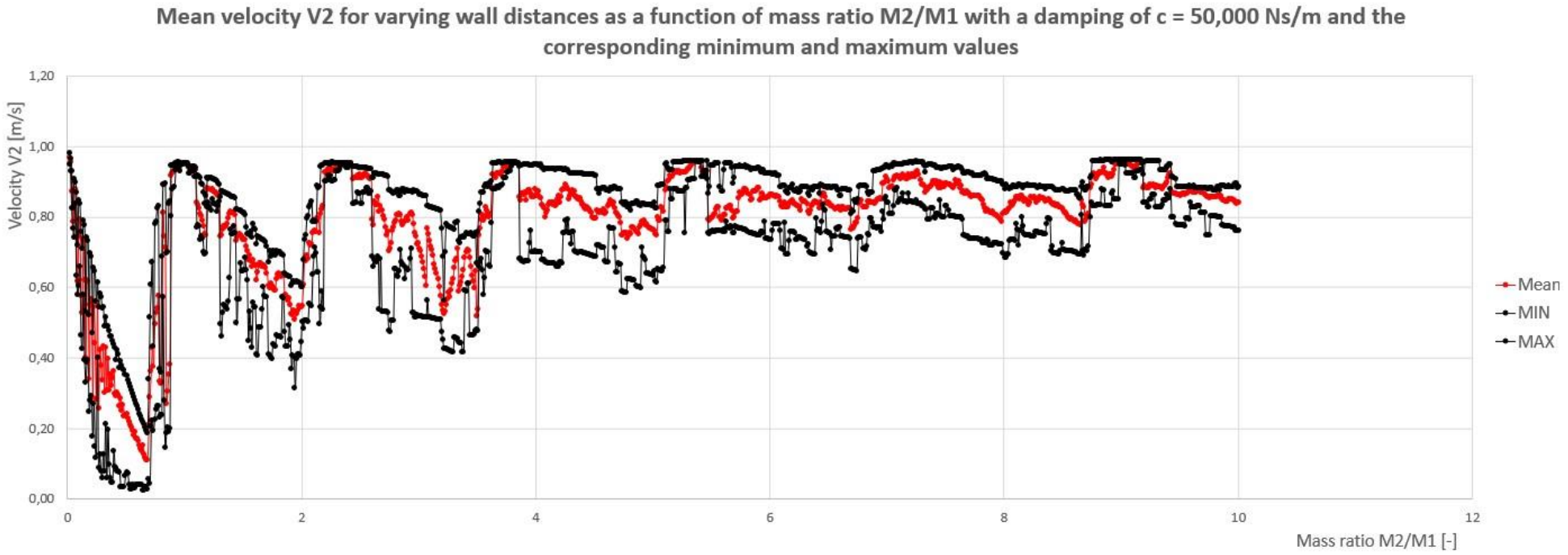


*Figure C. 2: Mean velocity V2 (red) as a function of mass ratio. Vibration-induced irregularities are indicated by the minimum and maximum velocities out of the set of different wall distances (in black). This figure represents the situation with c = 50,000 Ns/m damping.*

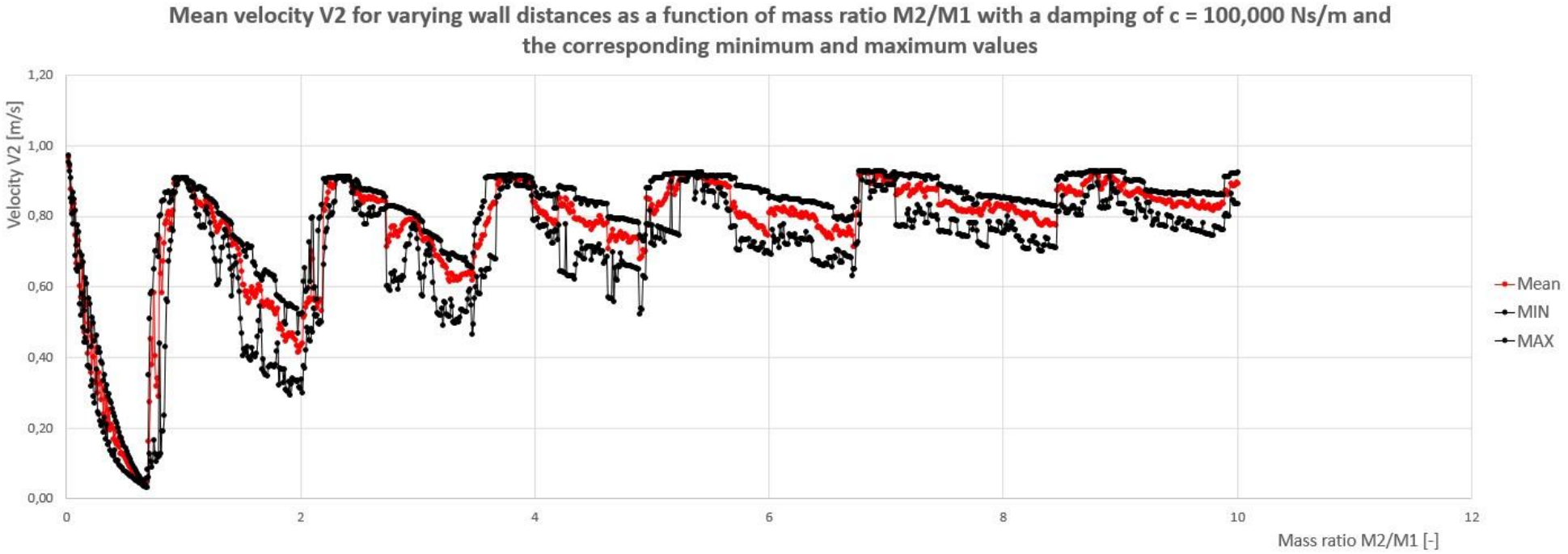


*Figure C. 3: Mean velocity V2 (red) as a function of mass ratio. Vibration-induced irregularities are indicated by the minimum and maximum velocities out of the set of different wall distances (in black). This figure represents the situation with c = 100,000 Ns/m damping.*

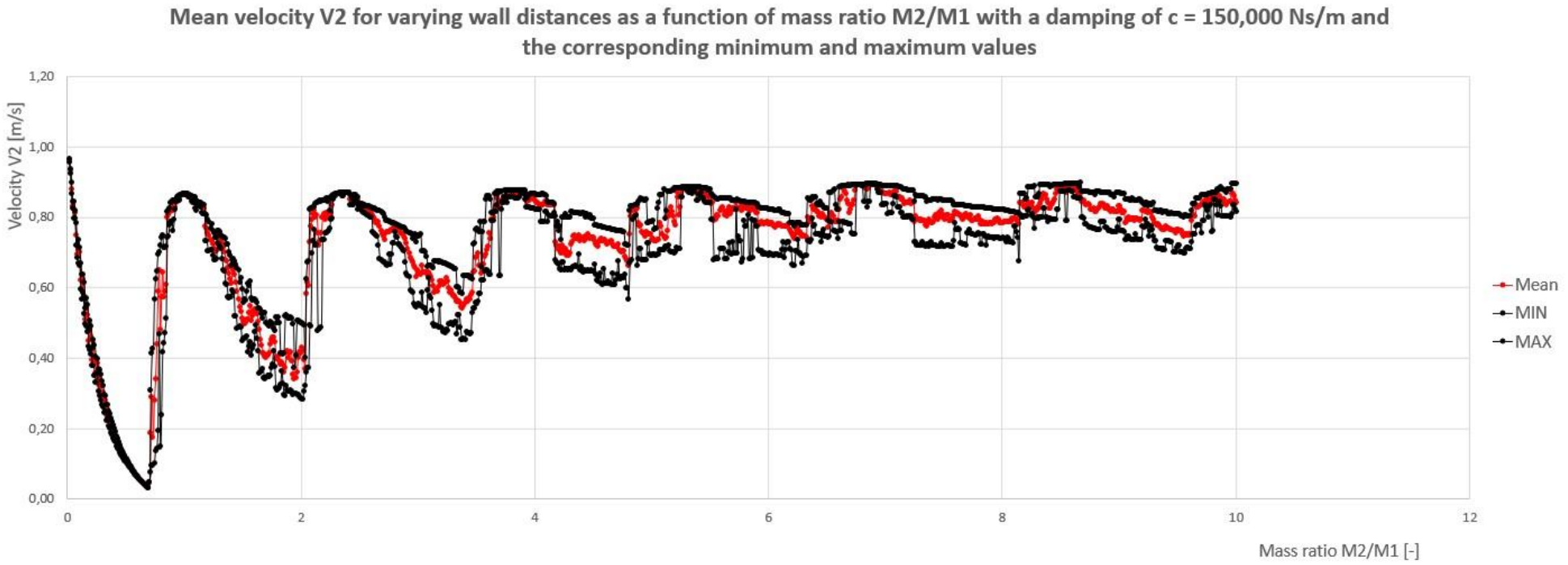


*Figure C. 4: Mean velocity V2 (red) as a function of mass ratio. Vibration-induced irregularities are indicated by the minimum and maximum velocities out of the set of different wall distances (in black). This figure represents the situation with c = 150,000 Ns/m damping.*

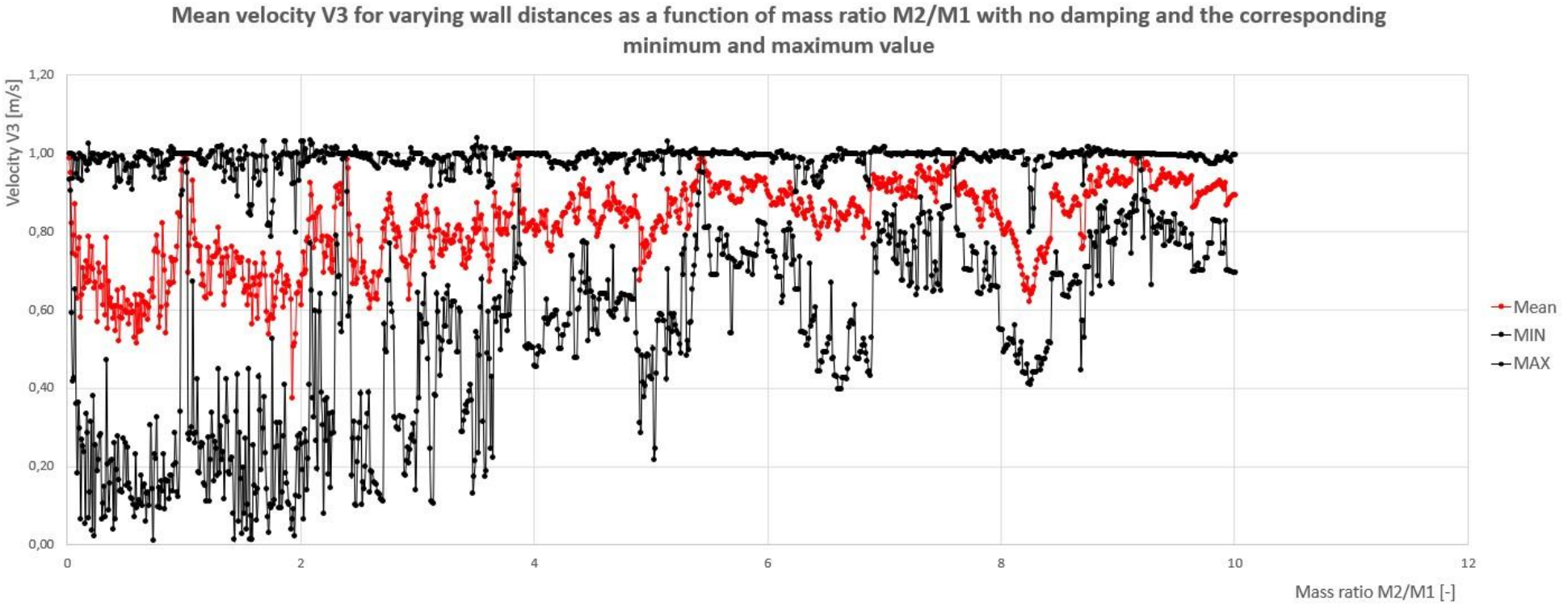


*Figure C. 5: Mean velocity V3 (red) as a function of mass ratio. Vibration-induced irregularities are indicated by the minimum and maximum velocities out of the set of different wall distances (in black). This figure represents the undamped situation.*

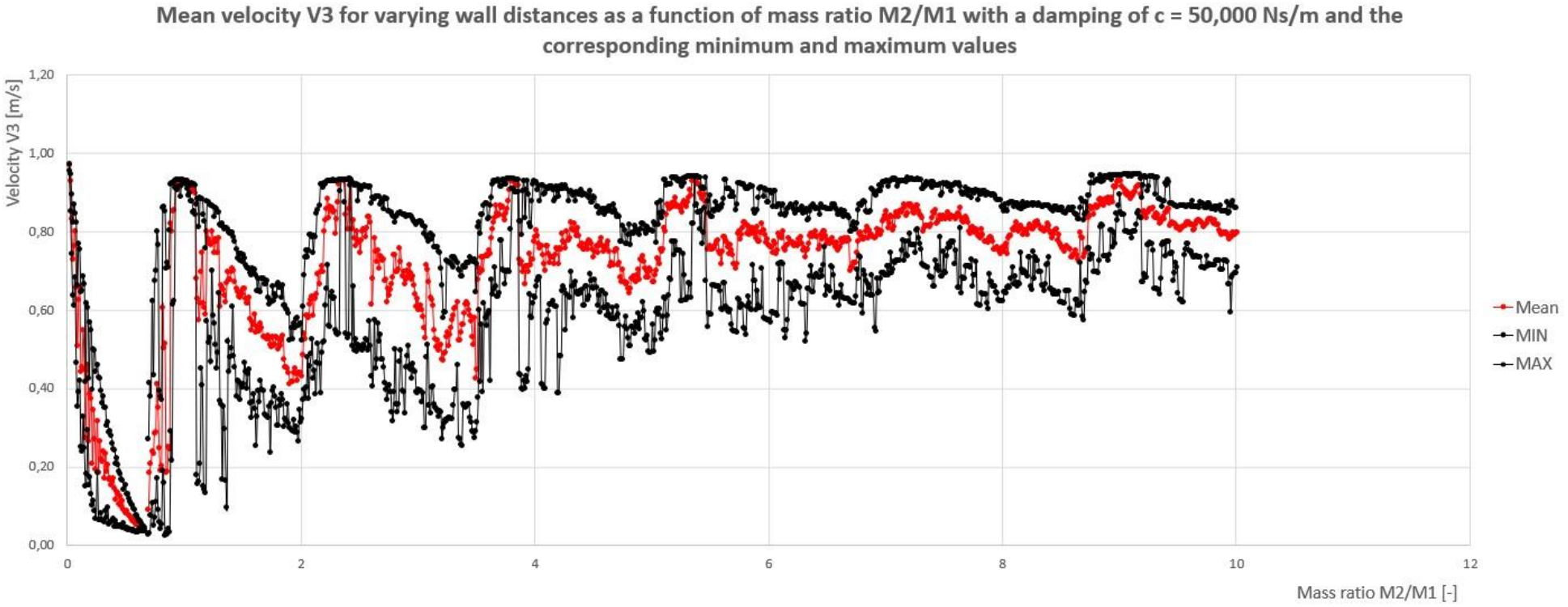


*Figure C. 6: Mean velocity V3 (red) as a function of mass ratio. Vibration-induced irregularities are indicated by the minimum and maximum velocities out of the set of different wall distances (in black). This figure represents the situation with c = 50,000 Ns/m damping.*

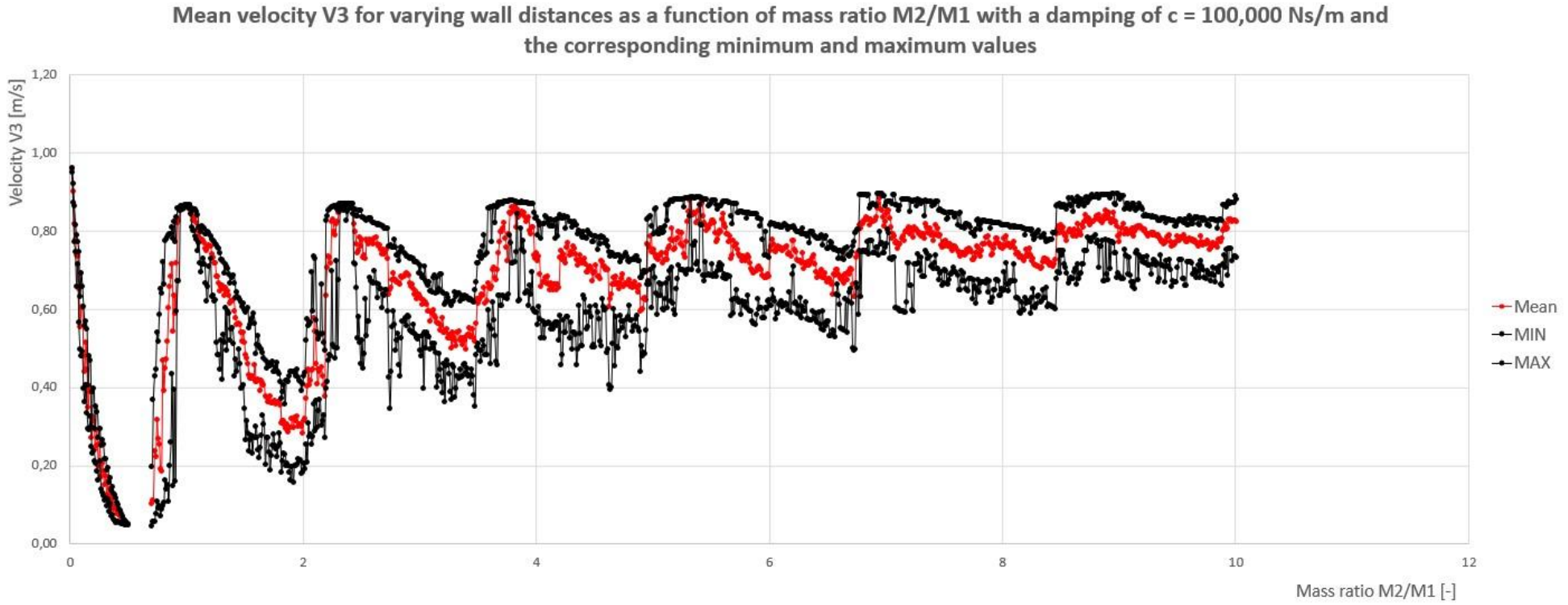


*Figure C. 7: Mean velocity V3 (red) as a function of mass ratio. Vibration-induced irregularities are indicated by the minimum and maximum velocities out of the set of different wall distances (in black). This figure represents the situation with c = 100,000 Ns/m damping.*

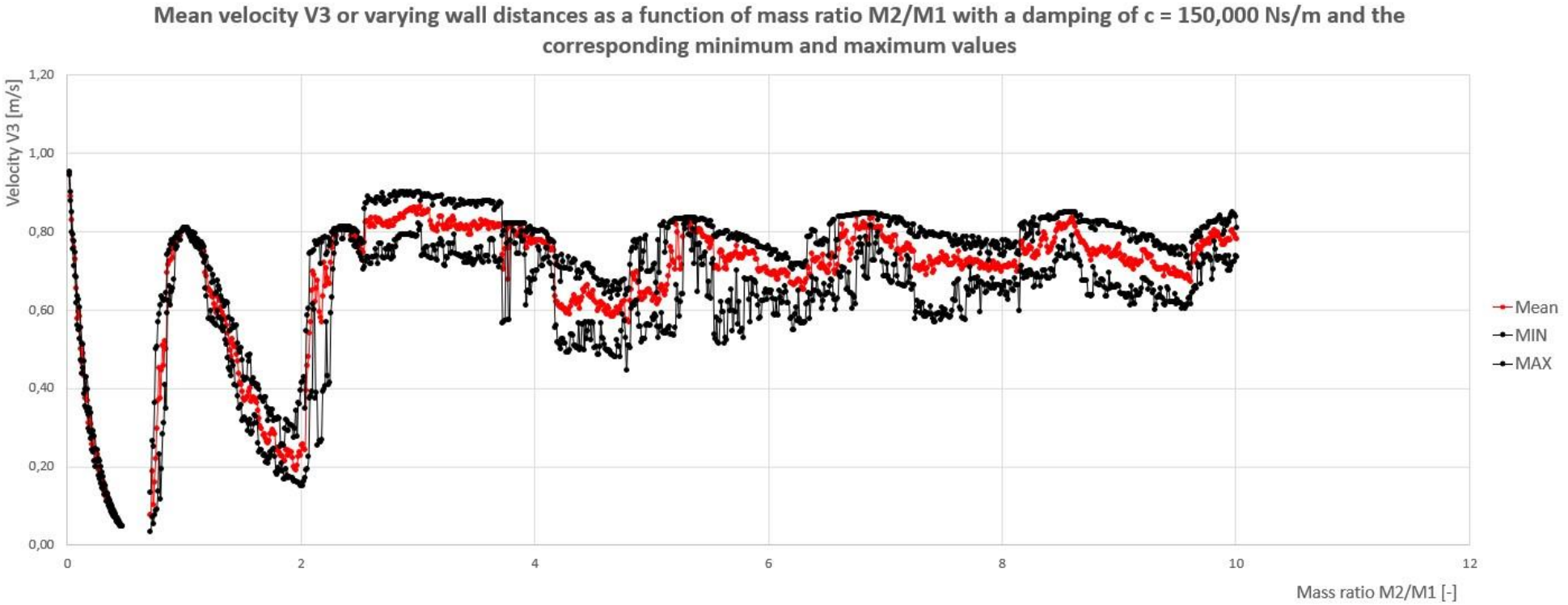


*Figure C. 8: Mean velocity V3 (red) as a function of mass ratio. Vibration-induced irregularities are indicated by the minimum and maximum velocities out of the set of different wall distances (in black). This figure represents the situation with c = 150,000 Ns/m damping.*

# Appendix D: Time-lapse

Rigid WTG tower motions of the simulation model (colored) with the FEM model (ANSYS) for validation

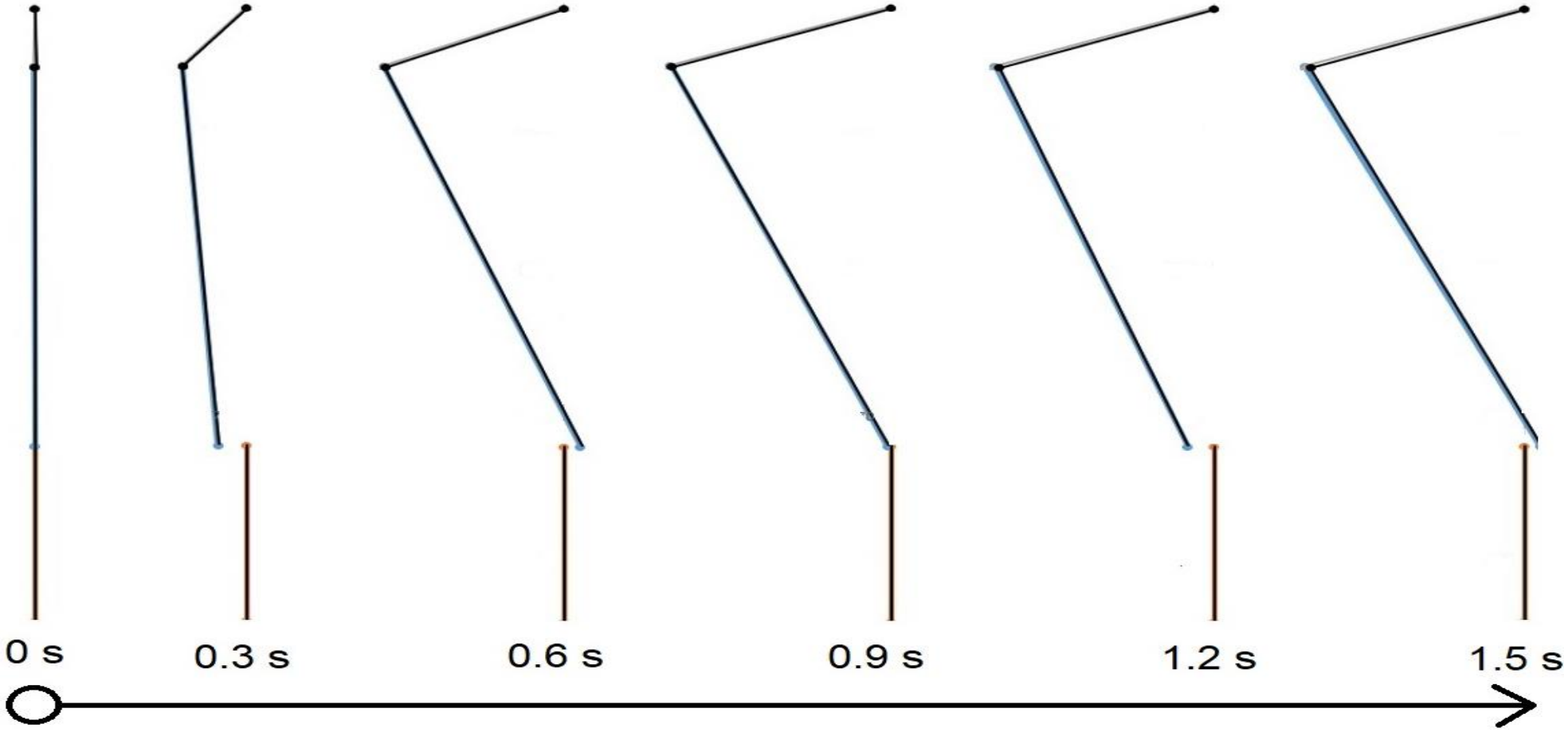


*Figure D. 1: Time-lapse of WTG motions in ANSYS (black) and Excel (colored). The top line is the lifting line, the middle line the WTG tower and the bottom line the MP. From left to right, the simulation progresses by 0.3 s per iteration. Continuing on the next page.*

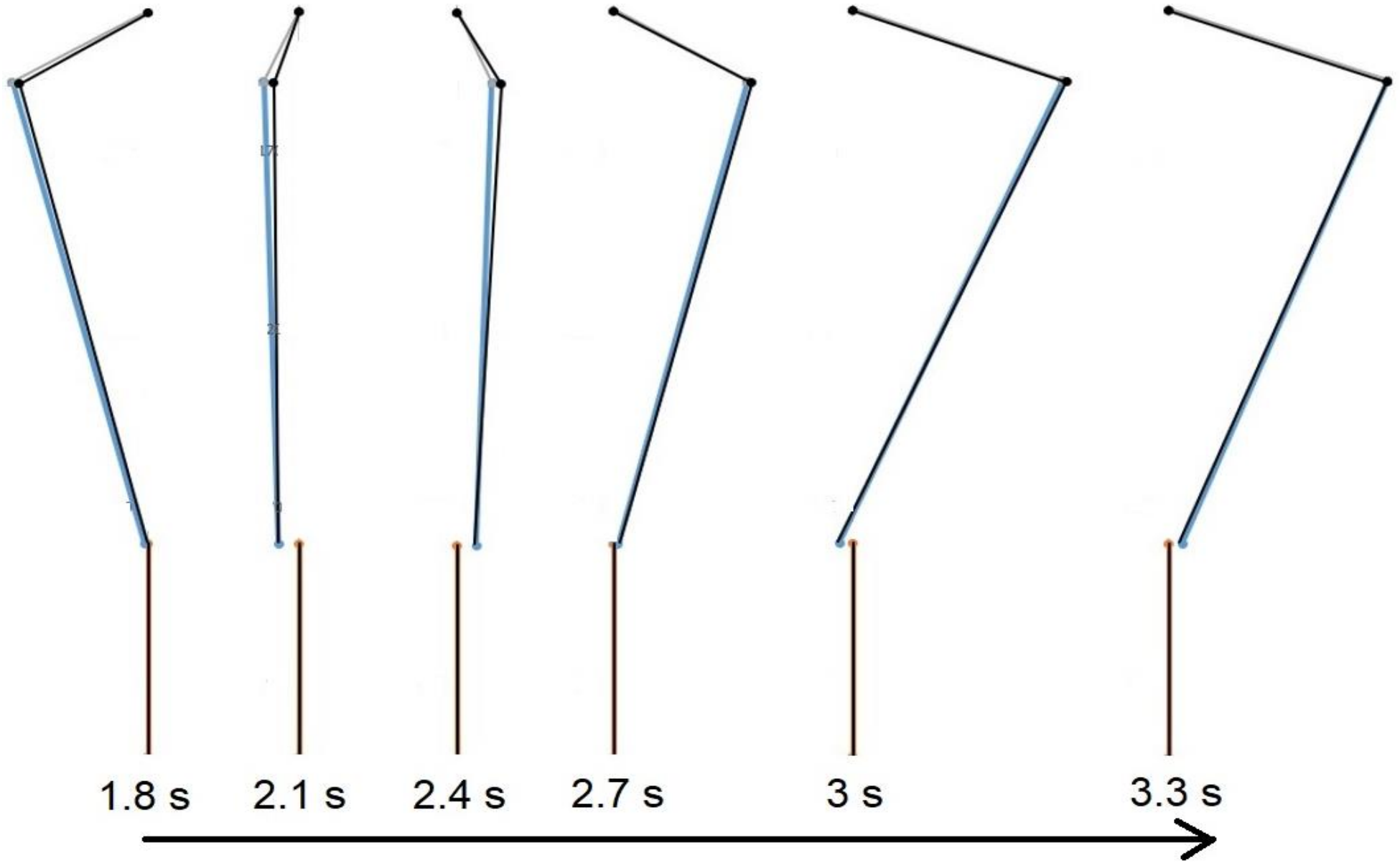


*Figure D. 2: Time-lapse of WTG motions in ANSYS (black) and Excel (colored). The top line is the lifting line, the middle line the WTG tower and the bottom line the MP. From left to right, the simulation progresses by 0.3 s per iteration. Continuing on the next page.*

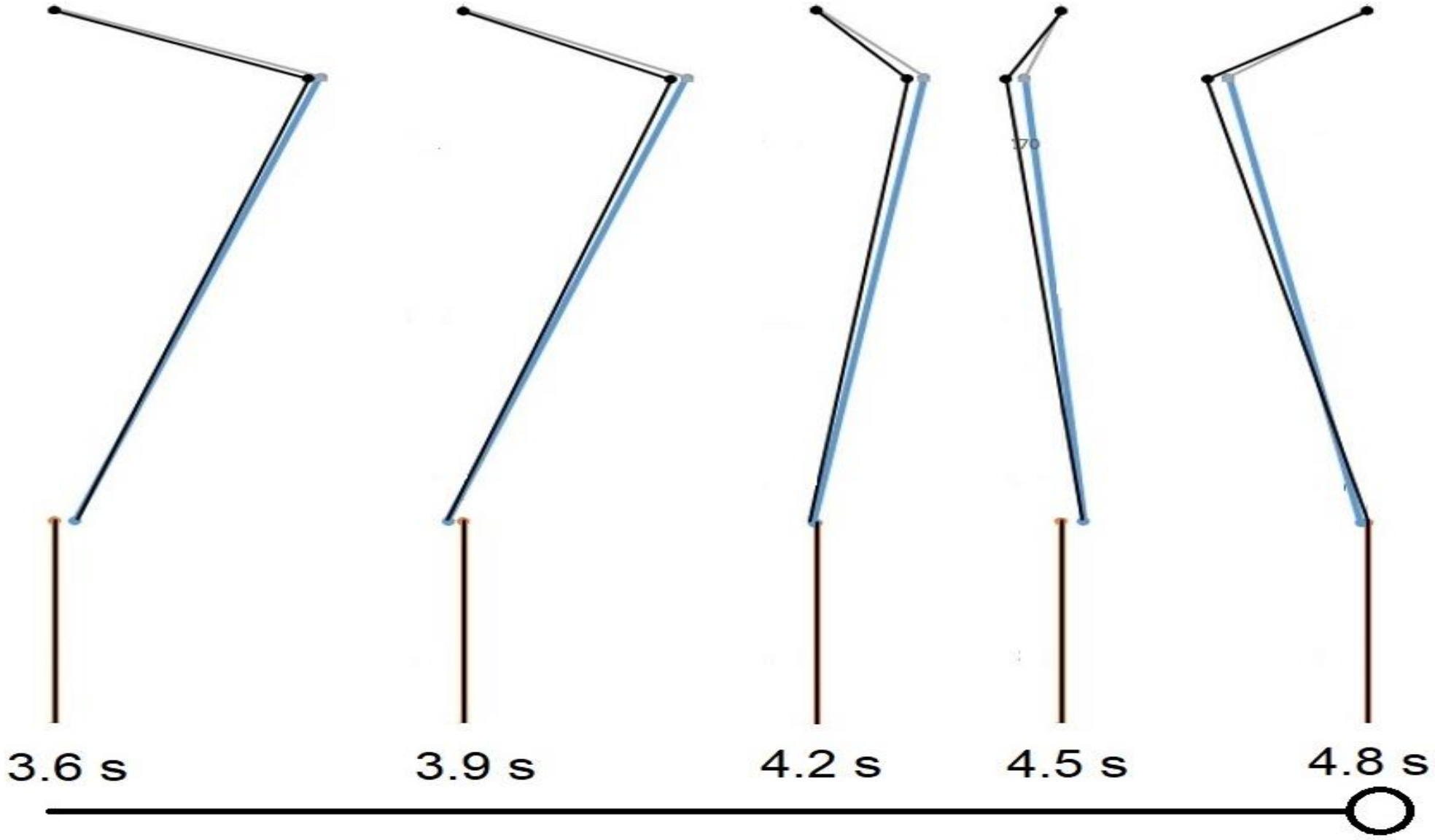


*Figure D. 3: Time-lapse of WTG motions in ANSYS (black) and Excel (colored). The top line is the lifting line, the middle line the WTG tower and the bottom line the MP. From left to right, the simulation progresses by 0.3 s per iteration.*

# Appendix E: Time-lapse

Flexible WTG tower motions of the simulation model (colored) with the FEM model (ANSYS) for validation

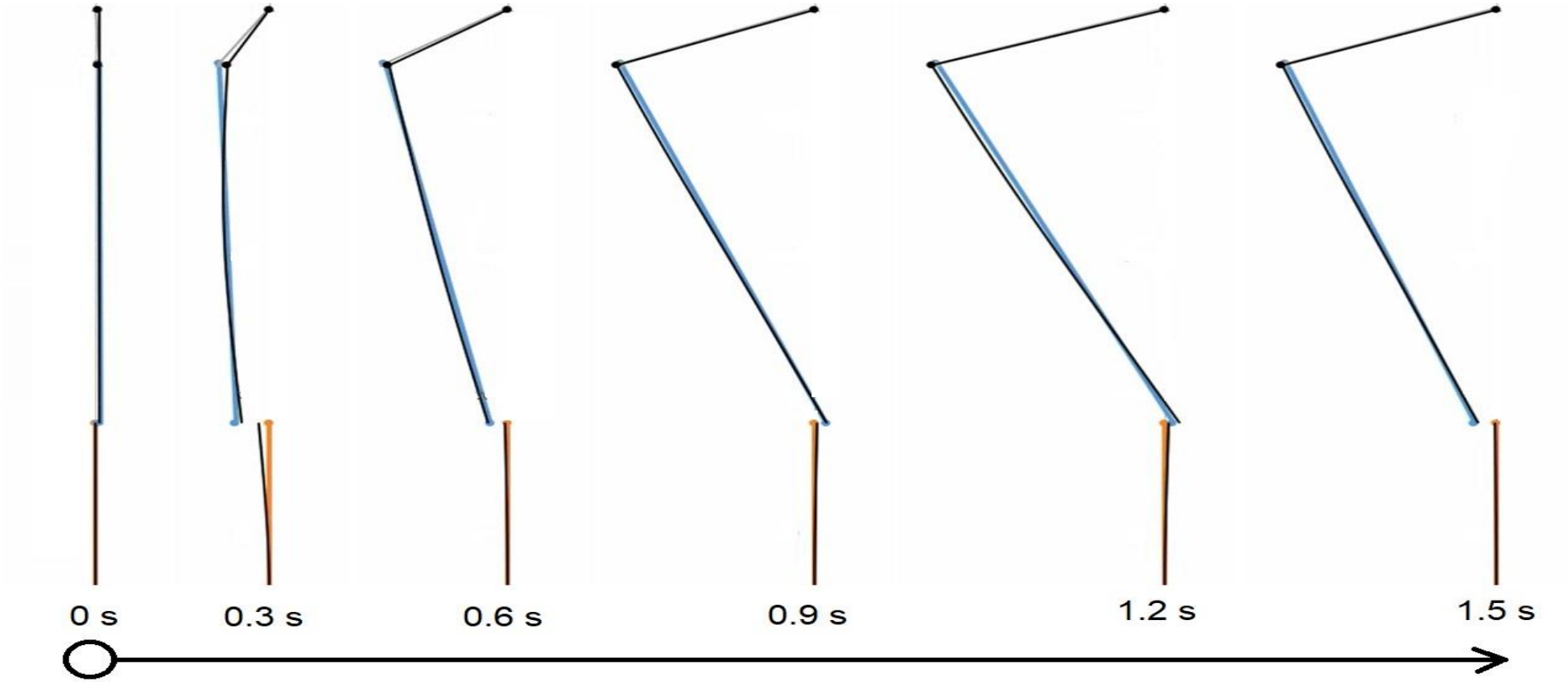


*Figure E. 1: Time-lapse of WTG motions in ANSYS (black) and Excel (colored). The top line is the lifting line, the middle line the WTG tower and the bottom line the MP. From left to right, the simulation progresses by 0.3 s per iteration. Continuing on the next page.*

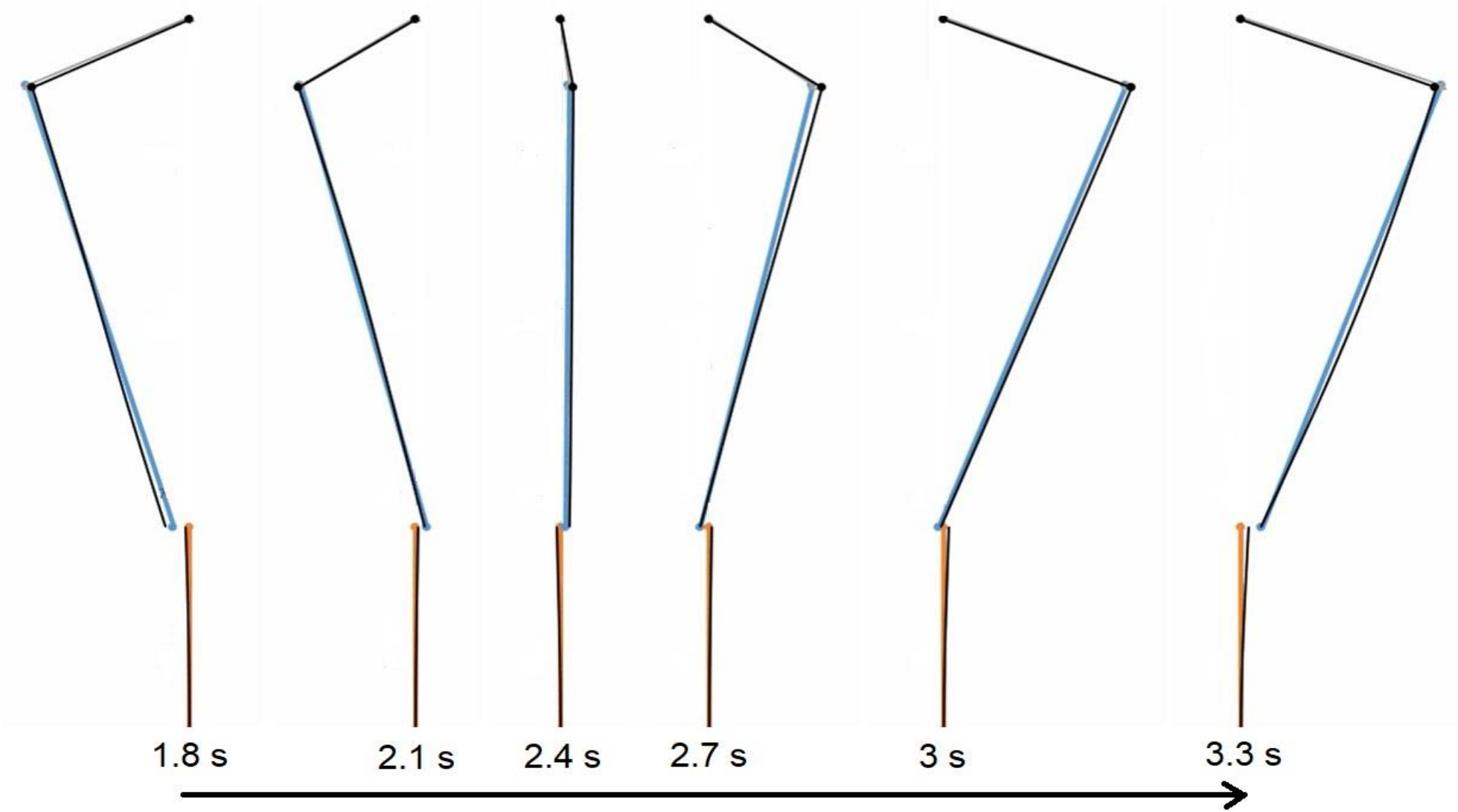


*Figure E. 2: Time-lapse of WTG motions in ANSYS (black) and Excel (colored). The top line is the lifting line, the middle line the WTG tower and the bottom line the MP. From left to right, the simulation progresses by 0.3 s per iteration. Continuing on the next page.*

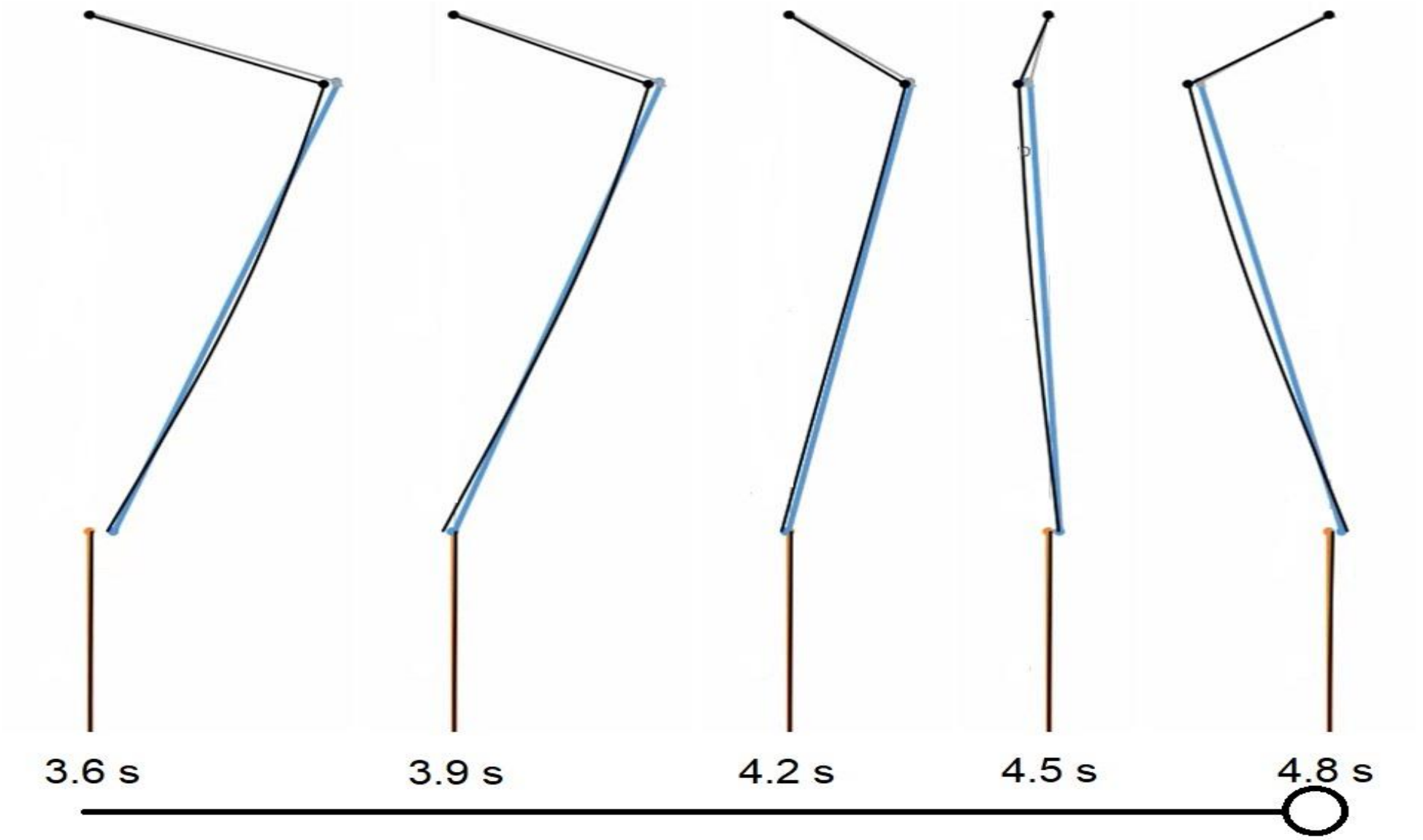


*Figure E. 3: Time-lapse of WTG motions in ANSYS (black) and Excel (colored). The top line is the lifting line, the middle line the WTG tower and the bottom line the MP. From left to right, the simulation progresses by 0.3 s per iteration.*

# Appendix F

## OWT installation technologies and configurations with different installation characteristics

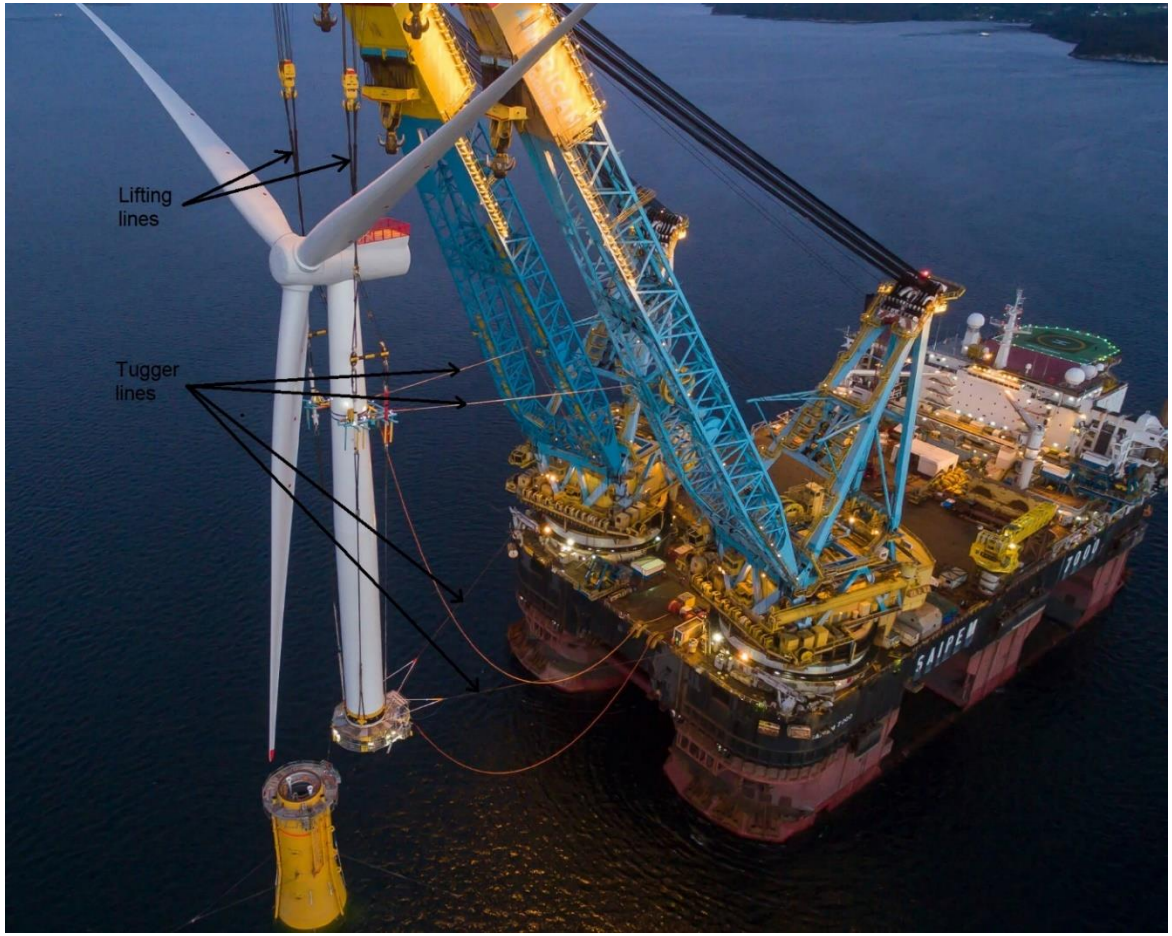


Figure F. 1 shows the installation of a 6 MW offshore wind turbine in the floating Hywind Scotland wind farm. The floating installation vessel, the Saipem 7000, utilizes two cranes to hoist the offshore wind turbine via a yoke connected to the WTG tower below the nacelle. Two tugger lines are attached from the yoke to the cranes. Two other tugger lines are attached from the WTG tower bottom to the deck of the vessel.

*Figure F. 1: Hywind Scotland installation with 2 cranes and lifting lines*

*Figure F. 2: Ulstein Windlifter installation vessel concept*

The Windlifter is a system, designed by Ulstein, to transport and install offshore wind turbines in a single lift. As visualized in Figure F. 2, the system comprises storage and handling systems for multiple turbines for efficient transport. According to Ulstein, a mechanical system skids the turbines safely and controlled from the vessel onto the foundation.

The Wind Turbine Shuttle is a floating installation vessel concept from Huisman. The vessel consists of a small water plane area twin hull and can transport and install two wind turbines in one go. According to Huisman, the vessel is DP controlled, the system allows active compensation of OWT motions and allows for installation on different foundation types.

*Figure F. 3: Huisman Wind Turbine Shuttle concept transporting and installing two wind turbines.*